

Electromagnetic Field Analysis of Lightning Return Stroke Current

by

Md. Faruque Hossain



Department of Electrical & Electronic Engineering
Khulna University of Engineering & Technology (KUET)
Khulna-920300

Electromagnetic Field Analysis of Lightning Return Stroke Current

by

Md. Faruque Hossain

A thesis

Submitted to the Department of Electrical & Electronic Engineering,
Khulna University of Engineering & Technology (KUET) in partial
fulfillment of the requirements for the degree of

Master of Science

in

Electrical & Electronic Engineering

February 2006



Department of Electrical & Electronic Engineering
Khulna University of Engineering & Technology (KUET)
Khulna-920300

The dissertation
“Electromagnetic Field Analysis of Lightning
Return Stroke Current”

by

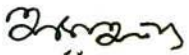
Md. Faruque Hossain

Submitted to Department of Electrical & Electronic Engineering, Khulna University of Engineering & Technology (KUET), in partial fulfillment of the requirements for the degree of **Master of Science** in Engineering is hereby accepted.

Dissertation evaluation committee

Dr. Md. Abul Kalam Azad

Professor, Department of Electrical & Electronic Engineering
Khulna University of Engineering & Technology, Khulna


Chairman 4.2.06
(Supervisor)

Dr. Bashudeb Chandra Ghosh

Professor and Head, Department of Electrical & Electronic Engineering
Khulna University of Engineering & Technology, Khulna


Member 4/2/06

Dr. Md. Osman Goni

Assistant Professor, Department of Electronics & Communication Engineering
Khulna University of Engineering & Technology, Khulna


Member 04.02.06
(Co-Supervisor)

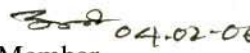
Dr. Md. Abdus Samad

Professor and Dean, Faculty of Electrical & Electronic Engineering
Khulna University of Engineering & Technology, Khulna


Member 04.02.06


Dr. Md. Nurunnabi Mollah

Professor, Department of Electrical & Electronic Engineering
Khulna University of Engineering & Technology, Khulna


Member 04.02.06

Dr. Md. Ruhul Amin

Professor, Department of Electrical & Electronic Engineering
Rajshahi University of Engineering & Technology, Rajshahi


Member
(External) 04/02/06

**Khulna University of Engineering & Technology (KUET),
Khulna-920300, Bangladesh.**

Abstract

Accurate knowledge of the characteristics of lightning electromagnetic fields is needed for studying the effects of the potentially deleterious coupling of lightning fields to various circuits and systems, for achieving an efficient insulation design of electric-power networks and for determining electromagnetic compatibility requirements of telecommunication systems. In the first step, lightning analysis requires the development of return stroke models, which are able to reproduce the electromagnetic field signature similar to that generated by natural return stroke.

In this thesis, the lightning return stroke is, firstly, assumed as a current pulse originating at ground level and propagating along the channel of perfect electrical conductor. Then the effects of channel resistance and inductance both on the current and the electromagnetic fields are investigated. The results show that the inclusion of channel resistance and inductance will change the prediction of the model in such a direction that they will come closer to the experimental observations.

Reviewing different models, electromagnetic model is used in the present study. For the accurate analysis of the transient electromagnetic field around a three-dimensional (3D) conductor system, application of electromagnetic modeling codes are more appropriate. Among many available codes, Numerical Electromagnetic Code (NEC-2) based on the method of moments is chosen for the above purpose since it has been widely and successfully used in analyzing thin-wire antennas.

The effect of ground electrical parameter on the channel current and remote electromagnetic fields is deduced in the present thesis for several grounds. With different methodologies different input data are involved in the lightning analysis: one of them is related to the lightning current itself. The effect of different current wave-shapes is also investigated in this work.

Experimental observations and theoretical investigations have shown that the presence of an elevated strike object (such as a tall tower) could affect lightning current and their radiated electromagnetic fields substantially. Therefore, an analysis of tower current and remote electromagnetic fields radiated by lightning return strokes to tall towers is presented taking two towers of different heights. In the work, both the slow-front and steep-front wave-shapes, corresponding respectively to typical first and subsequent return strokes, are adopted as injected current waveform. Because, the subsequent return strokes that are characterized by lower current peaks but higher front steepness and return stroke speed may result in higher field peaks. It is shown in particular that the presence of a tower tends, in general, to increase substantially the electric and magnetic field peaks and their derivatives. Furthermore, the presented results are shown to be consistent with recent experimental observations of current in lightning strokes to the high stack in Japan and Toronto CN Tower and of the associated electromagnetic fields.

Finally, to show the validity of the model, some results calculated by NEC-2 are compared with the results calculated by Virtual Surge Test Lab (VSTL), which is based on Finite Difference Time Domain (FDTD) method. In such case, reduced scale model is considered because of large computation time of FDTD method.

Acknowledgements

At first, I would like to prostrate in worship to almighty Allah, who give me mercy and power to complete my M. Sc. Engineering program successfully.

I am grateful to Prof. Dr. A. K. Azad for his support, guidance and encouragement in pursuing this opportunity. His advices came always at the right moment, which helped me to keep going during hard times. His good guiding skills and encouraging attitude makes me feel confident to face future challenges in the field of Lightning Research.

All this would not be possible without the guidance of Dr. Md. Osman Goni, a person with a lot of ideas, great imagination and excellent communication skills. Through his presentations, he can take us into very complex subjects in such a way that one can understand every single detail. I am also grateful to him and express my sincere thanks for having given me the opportunity to learn and do research under his able guidance.

I would like to thank the members of the Committee: Dr. M. A. Samad, Dr. B. C. Ghosh, Dr. Md. Nurunnabi Mollah and Dr. Md. Ruhul Amin for there involvement in providing direction for this dissertation and reviewing the work.

I take this opportunity to thank Mr. A. N. M. Enamul Kabir, Dr. Md. Rafiqul Islam and Dr. Md. Ashraful Ghoni Bhuyan for their continuous encouragement. Thanks are due to Mr. Md. Salah Uddin Yusuf for his help and the good times we spent together.

I would also like to thank all the members of the faculty of Electrical & Electronic Engineering of the University for their help whenever it was needed.

Last but not least, I express my sincere gratitude to my family and friends, for their continuing support and encouragement in whatever I do.

AUTHOR
February, 2006

Dedicated to ...

To those who always
supported me.

To my Family, For their love
and support.

To the source of my inspiration,
Subarna, for all the years of sacrifice and
stress that pursuing this degree has entailed.

Contents

Abstract	i
Acknowledgements	iii
List of Figures	vii
List of Tables	xi
Chapter 1: Introduction	1
1.1 Introduction	1
1.2 Lightning Behavior and Characteristics	2
1.2.1 Physics of Lightning	2
1.2.2 Lightning Mechanism	3
1.2.3 Lightning Behavior	4
1.2.4 Lightning Effects	5
1.3 Motivation of the Work	6
1.4 Lightning Return Stroke Models: Literature Review	8
1.5 Electromagnetic Modeling Code	10
1.6 Objectives of the Work	11
1.7 Thesis Organization	12
Chapter 2: Solution Techniques for Electromagnetic Problem	13
2.1 Introduction	13
2.2 Frequency Domain Technique: Method of Moments	14
2.2.1 Electric Field Integral Equation	14
2.2.2 Numerical Solution by the Method of Moments	16
2.3 Numerical Electromagnetic Code-2	22
2.3.1 Structure Modeling Guidelines	23
2.3.2 Program Input and Program Control	27
2.4 Time Domain Technique: Finite Difference Time Domain	32
2.4.1 FDTD Formulation	33

2.4.2	Time Step and Space Step	35
2.5	General Surge Analysis Program: VSTL	35
2.5.1	Thin Wire Representation	36
2.5.2	Boundaries and Earth Plane	37
2.5.3	Localized Voltage and Current Sources	38
2.5.4	Calculation Procedure and Output	39
 Chapter 3: Lightning Return Stroke to Ground		 41
3.1	Introduction	41
3.2	Modeling of the Analyzing System	41
3.3	Representing the Leader Channel as a Perfect Conductor	42
3.4	Effect of Channel Resistance	46
3.5	Effect of Channel Inductance	48
3.6	Effect of Different Input Waveforms	51
3.7	Effect of Ground Conductivity	54
3.8	Effect of Subsequent Return Strokes	57
3.9	Computation Time	60
3.10	Summary	60
 Chapter 4: Lightning Return Stroke to Tall Structures		 61
4.1	Introduction	61
4.2	Model of Tall Structures Struck by Lightning	62
4.3	Current and Current Derivative along the Tower	63
4.4	Electromagnetic Fields	65
4.5	First Versus Subsequent Stroke	68
4.6	Comparison with Measured Waveforms	73
4.7	Computation Time	78
4.8	Summary	79

Chapter 5: Simulation by FDTD Method and Comparison with the NEC-2 results	80
5.1 Introduction	80
5.2 Simulation by FDTD Method	80
5.2.1 Lightning Return Stroke to Ground	81
5.2.2 Lightning Return Stroke to Tall Structures	83
5.2.3 Computation Time	86
5.3 NEC-2 Results of Reduced Scale Model	86
5.3.1 Lightning Return Stroke to Ground	86
5.3.2 Lightning Return Stroke to Tall Structures	88
5.3.3 Computation Time	90
5.4 Comparison of the FDTD and NEC-2 Results	90
5.5 Summary	91
Chapter 6: Discussions and Conclusions	92
6.1 Discussions	92
6.2 Conclusions	93
6.3 Scope for Future Work	93
Bibliography	95
Appendix	102
A. Electric Field Integral Equation	102
B. History and Availability of NEC-2	104
C. FDTD Formulation	106
D. Sample Input Data to NEC-2 for Stroke to Ground	112
E. Sample Input Data to NEC-2 for Stroke to Tall Tower	116
F. Sample Input Data to FDTD for Reduced Scale Model	120
G. Magnetic Field Distributions	124

List of Figures

Fig. 2.1.	Current filament geometry for thin-wire kernel.	20
Fig. 2.2.	Flow diagram of NEC-2 main program input section.	27
Fig. 2.3.	Flow diagram of NEC-2 main program computation section.	28
Fig. 2.4.	An impulse voltage measuring system subjected to analysis as example.	29
Fig. 2.5.	Flow of the solution using NEC-2.	31
Fig. 2.6.	Configuration of electric and magnetic fields in cell.	34
Fig. 2.7.	Thin wire and configuration of adjacent electric and magnetic fields.	37
Fig. 2.8.	Calculation of current by Ampere's Law.	39
Fig. 2.9.	Calculation procedure of program VSTL.	40
Fig. 3.1.	Model for the analysis of lightning return stroke to ground.	42
Fig. 3.2.	Waveform of voltage source to simulate the first return stroke.	42
Fig. 3.3.	Current along the lightning channel of perfect conductor.	43
Fig. 3.4.	Vertical electric field for different channel resistances at (a) 50 m (b) 2 km and (c) 100 km from the lightning channel in case of ground stroke.	44
Fig. 3.5.	Azimuthal magnetic field for different channel resistances at (a) 50 m (b) 2 km and (c) 100 km from lightning channel in case of ground stroke.	44
Fig. 3.6.	Typical example of (a) electric field and (b) magnetic field at 2 km for first (solid line) and subsequent (dotted line) return strokes in case of stroke at ground level [53].	45
Fig. 3.7.	Typical example of radiation electric fields due to (a) first return stroke (b) subsequent return strokes [56]. The waveforms are normalized to a distance of 100 km.	46
Fig. 3.8.	Current along the lightning channel for channel resistance of (a) 1 Ω/m and (b) 3 Ω/m .	47
Fig. 3.9.	Current along the lightning channel for channel inductance of (a) 1 $\mu H/m$ (b) 3 $\mu H/m$ and the resistance of 1 Ω/m .	49
Fig. 3.10.	Vertical electric field for different channel inductance at (a) 50 m (b) 2 km and (c) 100 km from the lightning channel in case of stroke at	50

	ground level.	
Fig. 3.11.	Azimuthal magnetic field for different channel inductance at (a) 50 m (b) 2 km and (c) 100 km from lightning channel in case of stroke at ground level.	50
Fig. 3.12.	Static electric fields at different height in case of ground stroke.	51
Fig. 3.13.	Double exponential, ramp and concave waveforms of injected current.	51
Fig. 3.14.	Computed current along the lightning channel for (a) double exponential (b) ramp and (c) concave waveforms.	52
Fig. 3.15.	Vertical electric field at (a) 50 m (b) 2 km and (c) 50 km from the lightning channel for different input waveforms.	53
Fig. 3.16.	Azimuthal magnetic field at (a) 50 m (b) 2 km and (c) 50 km from the channel for different input waveforms.	53
Fig. 3.17.	Computed current along the lightning channel for different ground in case of stroke at ground level. The ground conductivity is taken as (a) 0.01 S/m for stone (b) 0.001 S/m for soil (sandy).	55
Fig. 3.18.	Vertical electric field at (a) 50 m (b) 2 km and (c) 100 km from the channel in case of lightning strike to ground of perfect conductor (copper), stone and sandy soil.	56
Fig. 3.19.	Azimuthal magnetic field at (a) 50 m (b) 2 km and (c) 100 km from the channel in case of lightning strike to ground of perfect conductor (copper), stone and sandy soil.	56
Fig. 3.20.	Injected steep-front waveform to simulate the subsequent return stroke.	57
Fig. 3.21.	Computed current along the channel for steep-front injection.	57
Fig. 3.22.	Vertical electric field at (a) 50 m (b) 2 km and (c) 100 km from the lightning channel for first and subsequent stroke in case of lightning return stroke to ground.	58
Fig. 3.23.	Azimuthal magnetic field at (a) 50 m (b) 2 km and (c) 100 km from the channel for first and subsequent stroke in case of lightning return stroke to ground.	58
Fig. 4.1.	Model for the analysis of lightning return stroke to tall structures of height H (200 m and 550 m).	62
Fig. 4.2.	(a) Current (b) current derivative along the 200 m tall strike object for	64

	a typical first return stroke.	
Fig. 4.3.	(a) Current (b) current derivative along the 550 m tall strike object for a typical first return stroke.	64
Fig. 4.4.	Vertical electric field at (a) 50 m (b) 2 km and (c) 100 km from the elevated structure of height 200 m and 550 m for a typical first return stroke.	66
Fig. 4.5.	Azimuthal magnetic field at (a) 50 m (b) 2 km and (c) 100 km from the elevated structure of height 200 m and 550 m for a typical first return stroke.	66
Fig. 4.6.	Static electric field at different height in case of lightning strike to 550 m tall tower.	67
Fig. 4.7.	(a) Current; and (b) current derivative along the 550 m tall strike object for a typical subsequent return stroke.	69
Fig. 4.8.	Vertical electric field at (a) 50 m (b) 2 km and (c) 100 km from the 550 m tall structure for first and subsequent return stroke.	70
Fig. 4.9.	Azimuthal magnetic field at (a) 50 m (b) 2 km and (c) 100 km from the 550 m tall structure for first and subsequent return stroke.	70
Fig. 4.10.	Measured [64] waveforms of lightning current and electromagnetic fields at or around a 200 m high stack.	73
Fig. 4.11.	Computed waveforms of lightning current and electromagnetic fields at or around a 200 m high stack.	73
Fig. 4.12.	Waveform of voltage source for the computation that produced Fig. 4.11.	74
Fig. 4.13.	Observation result for slow rise wavefront current of a CN Tower lightning flash recorded on August 17, 1991.	76
Fig. 4.14.	Observation result for fast rise wavefront current of a CN Tower lightning flash recorded on August 17, 1991.	76
Fig. 4.15.	Computed waveforms for slow-front injected current at the CN Tower.	77
Fig. 4.16.	Computed waveforms for steep-front injected current at the CN Tower.	77
Fig. 5.1.	Injected voltage waveforms for the reduced scale model.	81
Fig. 5.2.	(a) Slow-front (b) steep-front current along the channel. Computed	82

	by the FDTD method on reduced scale model.	
Fig. 5.3.	Vertical electric field at (a) 2 m and (b) 20 m from the channel for the current shown in Fig. 5.2. Computed by the FDTD method.	82
Fig. 5.4.	Current along the channel for ground conductivity (a) 0.01 S/m and (b) 0.001 S/m. Computed by the FDTD method on reduced scale model.	83
Fig. 5.5.	Vertical electric field for different ground conductivities at (a) 2 m and (b) 20 m from the channel. Computed by the FDTD method.	83
Fig. 5.6.	(a) Slow-front (b) steep-front current along the tower. Computed by the FDTD method on reduced scale model.	84
Fig. 5.7.	Vertical electric field at (a) 2 m (b) 20 m from the tower for different input current. Computed by the FDTD method on reduced scale model.	84
Fig. 5.8.	Vertical electric field at 35 m for slow-front injection.	85
Fig. 5.9.	Tower top current for different ground parameters. Computed by the FDTD method. Computed by NEC-2.	85
Fig. 5.10.	(a) Slow-front (b) steep-front current along the channel. Computed by NEC-2 on reduced scale model.	87
Fig. 5.11.	Vertical electric field at (a) 2 m and (b) 20 m from the channel for the current shown in Fig. 5.10.	87
Fig. 5.12.	Current along the channel for ground conductivity (a) 0.01 S/m and (b) 0.001 S/m. Computed by NEC-2 on reduced scale model.	87
Fig. 5.13.	Vertical electric field for different ground conductivities at (a) 2 m and (b) 20 m from the channel. Computed by NEC-2 on reduced scale model.	88
Fig. 5.14.	(a) Slow-front (b) steep-front current along the tower. Computed by NEC-2 on reduced scale model.	88
Fig. 5.15.	Vertical electric field at (a) 2 m (b) 20 m for different input current. Computed by NEC-2 on reduced scale model.	89
Fig. 5.16.	Vertical electric field at 35 m for slow-front injection. Computed by NEC-2 on reduced scale model.	89
Fig. 5.17.	Tower top current for different ground parameters. Computed by NEC-2 on reduced scale model.	90

List of Tables

Table 1.1	Sample input data to NEC-2	29
Table 3.1	Peak value and maximum steepness of E-field at 100 km for different channel parameters.	48
Table 3.2	Effects of ground electrical parameter on the remote electric field.	55
Table 3.3	Parameters of lightning return stroke channel base current and the corresponding electric and magnetic field in case of lightning strike to ground.	59
Table 4.1	Parameters of lightning current along the tower of height 200 m and 550 m for a typical first return stroke.	65
Table 4.2	Parameters of lightning (a) electric (b) magnetic fields for a typical first return stroke. at 2 km and 100 km. Lightning strike to tall structures of height 200 m and 550 m.	68
Table 4.3	Parameters of lightning current along the 550 m tall tower for a typical first and subsequent return stroke.	69
Table 4.4	Parameters of lightning return stroke channel base current and the corresponding electric and magnetic field when lightning strike to 550 m tower.	71
Table 4.5	Ratio of subsequent-to-first magnetic field peak H_S / H_f to subsequent-to-first current peak I_s / I_f for the field at 2 km.	72

Chapter 1

Introduction

1.1 Introduction

Lightning is one of the natural phenomena that have amazed the human beings since the beginning of the civilization. In the history of almost all societies there are records that relate lightning to a punishment from The Almighty. But with time, people started questioning the techniques of it and started wondering whether this phenomenon arising in the sky was an act of The Almighty or a natural phenomenon.

It was in 1750 that Benjamin Franklin suggested an experiment that later proved lightning is an electrical discharge. Two years later the experiment was first successfully performed in France, followed by England and Belgium. Since then, the scientific community has tried to understand the physical mechanism and the consequences of lightning flashes.

Telecommunications facilities continue to play an increasingly important role in the modern infrastructure of today's information society. However, owing to the steady use and development of new technologies, electrical and telecommunication equipments are becoming more and more complex. Today, modern electronic devices that operate at a higher switching rate and work at lower voltages are used. As a consequence, the sensitivity of these devices to transients and electromagnetic interference (EMI) is also high. Of the threats from the electromagnetic environment, lightning discharges that can cause micro-interruptions of the power supply, or disruption in the telecommunication or data-transmission networks during thunderstorms are the most important. This, in turn, creates a need for more advanced studies and modeling of lightning and the effects of transients on power and telecommunication system.

The analysis of lightning effects requires the following stages:

1. Development of lightning return stroke models, which means the modeling of the spatial-temporal distribution of the current in the lightning channel that are

able to reproduce the electromagnetic field signature similar to that generated by natural return stroke.

2. Calculation of the electromagnetic field radiated by such a current distribution, including propagation effects on soil with finite conductivity.
3. Evaluation of the voltages resulting from the coupling between the electromagnetic field and the various circuits and systems.

A brief explanation of the lightning phenomenon and important research questions are given below, which are necessary to proceed in this work.

1.2 Lightning Behavior and Characteristics

1.2.1 Physics of Lightning

Lightning is a transient electrical discharge in the atmosphere. The conditions needed to produce lightning have been known for some time. However, exactly how lightning forms have never been verified. Leading theories focus around separation of electric charge and generation of an electric field within a thunderstorm. Recent studies also indicate that ice, hail, and semi-frozen water drops known as graupel are essential to lightning development.

Thunderstorms have very turbulent environments. Strong updrafts and downdrafts occur with regularity and within close proximity to each other. The updrafts transport small liquid water droplets from the lower regions of the storm to heights between 35,000 and 70,000 feet above the freezing level. Meanwhile, downdrafts transport hails and ice from the frozen upper regions of the storm. When these collide, the water droplets freeze and release heat. This heat in turn keeps the surface of the hail and ice slightly warmer than its surrounding environment, and a "soft hail", or "graupel" forms. As the ice particles within a cloud (called hydrometers) grow and interact, they collide, fracture and break apart. It is thought that the smaller particles tend to acquire positive charge, while the larger particles acquire more negative charge. These particles tend to separate under the influences of updrafts and gravity until the upper portion of the cloud acquires a net positive charge and the lower portion of the cloud becomes negatively charged. This separation of charge

produces enormous electrical potential both within the cloud and between the cloud and ground. This can accumulate to millions of volts, and eventually the electrical resistance in the air breaks down and a flash begins. How may the lightning be classified and the most important one are described below.

1.2.2 Lightning Mechanism

Lightning classification are based on the following criteria:

1. The initial and the terminal points across which the electrical discharge takes place. The main subdivisions are: intra-cloud (within the cloud), inter-cloud (within two clouds) and cloud to ground discharges.
2. The polarity of the charges transported to ground. This can be subdivided as positive- and negative- flashes

Cloud to ground lightning is the most damaging and dangerous form of lightning. Although not the most common type, it is the one, which is best understood. Let us describe in more details the mechanism of the cloud to ground flashes.

Ground lightning discharges start high in the thundercloud in the region of high electric fields, several miles above the ground. Most flashes originate near the lower negative charge center and deliver negative charge to earth. The discharge develops both upward and downward until the downward branches eventually exit the cloud and move toward the ground. The initial or leader stage of the downward flash is characterized by a stepped movement, with pauses between each step, and heavy branching. The leader and its branches carry large amounts of electric charge from the cloud, which causes the breakdown of the air. As the leader approaches within a few hundred feet of the ground, the increasing high electric fields at the earth's surface induced by the descending charge causes upward leaders to be triggered from objects on the earth. One of these upward or connecting leaders meets a branch of the descending flash, establishing a path between cloud and ground. The charge on the flash then dumps rapidly into the ground, giving rise to a very large short-duration pulse of current into the ground or struck object. This pulse starts at the ground and moves upward into the cloud, and is known as the return stroke. Once a path is established between cloud and ground, many subsequent discharges can

follow it, resulting in a multiple-stroke lightning flash. These large return stroke currents cause most damage to structures and their contents.

There is not much information available on the mechanism of the positive flashes. However, available information indicates that its mechanism is similar to the negative with some differences. For instance, observations show that the positive stepped leader propagates more or less continuously towards the ground [1]. Moreover, positive flashes may contain a single return stroke while the negatives may contain several.

1.2.3 Lightning Behavior

The return stroke carries currents of about 10 kA to 500 kA and flows for a time of up to one thousandth of a second. Up to 25 strokes have been recorded in a single lightning flash, although the average is two or three. Approximately one-third of all flashes are single stroke. Leader currents are quite low, usually just a few hundred amperes, and may also be very short in duration, just a few microseconds. Return stroke currents, on the other hand, can be very large. Ninety-five percent of return strokes have peak currents between 5 kA and 100 kA, although rarely currents as high as 500 kA have been measured. First strokes generally carry three to five times as much charge and current as the subsequent strokes of a multiple-stroke flash. Return stroke current rises quickly in from one to ten microseconds and decays in a few hundred microseconds. Over 90% of ground flashes carry negative charge to earth. However, the 10% of positive flashes tend to carry higher currents and charges and are therefore more damaging.

The following table gives data for normal cloud to ground lightning discharges bringing negative charge to earth. Representative values are given, as well as a range of typical values. Data is taken from Uman [2], which in turn takes the data from a variety of sources.

Summary of lightning parameters

	<u>Representative</u>	<u>Range</u>
Stepped Leader		
Average velocity of propagation of stepped leader	150 km/sec	100 - 2600 km/sec
Charge deposited on stepped-leader channel	5 C	3 - 20 C
Dart Leader		
Velocity of propagation	2000 km/sec	1000 - 21,000 km/sec
Charge deposited on dart-leader channel	1 C	0.2 - 6 C
Return Stroke		
Velocity of propagation	80,000 km/sec	20,000 - 160,000 km/sec
Current rate of increase	10 kA/ μ sec	1 - 80 kA/ μ sec
Time to peak current	2 μ sec	1 - 30 μ sec
Peak current	10-20 kA	-110 kA
Charge transferred (excluding continuing current)	2.5 C	0.2 - 20 C
Energy dissipated	100 kJ/meter	
Lightning Flash		
Number of strokes per flash	3-4	1 - 26
Time interval between strokes	40 msec	3 - 100 msec
Time duration of flash	0.2 sec	0.01 - 0.2 sec

1.2.4 Lightning Effects

Lightning is a dangerous and destructive atmospheric phenomenon. At any time some 2,000 on-going thunderstorms generate about 50-100 lightning strikes to earth per second, causing the majority of forest fires and, in the U.S. alone, hundreds of millions of dollars in property losses. The strong currents associated with the lightning discharge cause severe damages in the stroked object (direct strike) and also in its close vicinity (indirect strike).

- 1. Direct Lightning Effects:** When lightning strikes a structure directly, the rapid rising impulse return stroke currents of tens or hundreds of kilo amperes are injected directly into it. These currents will distribute throughout the building, using the building steel, reinforced concrete, electrical conduit, and its services, including electric power, data and telephone lines as a path to earth. These lightning currents commonly cause damage to electronic equipment, including computers and peripherals, telephone switches and data interface equipment. This is the case even in structures equipped with a lightning protection system. Objects on the roof of a structure are particularly vulnerable to direct strikes. These include antennas, satellite receiving systems, air-conditioning plant, security cameras, elevator systems and lights.
- 2. Indirect Lightning Effects:** Even when lightning does not directly strike a structure, there may be severe damaging indirect effects. Lightning may strike a power line some distance away from the facility, injecting surge currents into the building through the electrical service entrance. Sags and momentary outages of the ac power service are frequent during storms, and nearby lightning induce huge damaging voltages into unshielded data and communication cables. The lightning flash also acts as an extremely powerful radio transmitter, particularly during the return stroke phase, and can induce extremely high voltages in electrical conductors up to a mile or more away. These induced voltages can be particularly severe in data communication, signaling and local area network cables, and commonly cause damage to interface equipment.

1.3 Motivation of the Work

In the last 15-20 years, the widespread use of sensitive electronic devices in data transmission networks, in power system equipment (circuit breakers, control and protection circuits), and in household appliances has increased the interest in transients. From this point of view, transients caused by lightning (direct and/or indirect) can be one of the major causes of malfunction, or even destruction, of electrical equipment. In particular, lightning-induced voltages, which can cause micro-interruptions of the power

supply, or disruption in the telecommunication or data-transmission networks during thunderstorms, have been seriously reconsidered, due to the increasing demand by customers for good quality in the power supply, and for reliability in the transmission of information. The opening of the telecommunication market, followed now by that of electrical power, is only accelerating this trend.

Modern society in this information technology era takes it for granted the complex chain of telecommunication systems to have 100 % integrity. Failure is considered to be totally unacceptable in the view of the significant implications in most aspects of modern life. However, the interconnection of electrical equipment to different networks for power distribution, telecommunications, cable-TV, computer LAN or WAN, etc., electromagnetic disturbance is increasing the risk of transients entering into these sensitive systems. This, in turn, creates a need for more advanced studies to understand the characteristics and the consequences of over-voltages and transients on power and telecommunications systems.

Furthermore, experimental observations and theoretical investigations have shown that the presence of an elevated strike object, such as a tall tower, could affect substantially lightning current and their radiated electromagnetic fields. Most of the studies about lightning transient have concentrated on extracting information concerning the variation of the current signature along the tower taking the return stroke channel as a perfect conductor and only a few have presented the remote electromagnetic fields predicted by the models. Even in the cases where remote electric fields are given, no attempt was made to analyze the effects of various transmission line parameters on the return stroke current and remote electromagnetic fields.

Accurate knowledge of the characteristics of electric and magnetic fields produced by lightning discharges is needed for studying the effects of the potentially deleterious coupling of lightning fields to various circuits and systems, for achieving an efficient insulation design of electric power networks and for determining electromagnetic compatibility requirements of telecommunication systems.

1.4 Lightning Return Stroke Models: Literature Review

Of all the lightning processes, the return stroke is the most energetic and so needs more investigation. There are several classes of models for the lightning return stroke, depending on the purpose of the model. However, there is no comprehensive model of the lightning return stroke that could reconcile most of the observed characteristics of the return stroke. As proposed by Rakov [3], they can be classified as follow:

1. Gas dynamic or “physical” models which are primarily concerned with the radial evolution of a short segment of the lightning channel and its associated shock wave.
2. Electromagnetic models that are usually based on a lossy, thin-wire antenna approximation to the lightning channel. These models involve a numerical solution of Maxwell’s equations to find the current distribution along the channel from which the remote electric and magnetic fields can be computed.
3. Distributed-circuit models that can be viewed as an approximation to the electromagnetic models described above and that represent the lightning discharge as a transient process on a vertical transmission line characterized by resistance (R), inductance (L), and capacitance (C), per unit length.
4. Engineering models in which a spatial and temporal distribution of the channel current (or the channel line charge density) is specified based on such observed lightning return stroke characteristics as current at the channel base, the speed of the upward-propagating front, and the channel luminosity profile.

Model which belongs to first category are primarily used to reproduce physical parameters (temperature, pressure, mass density etc.) of the return stroke. Models in second, third and fourth categories are mainly used to reproduce the electromagnetic field from a return stroke.

Distributed-circuit models consider the lightning channel to be an R-L-C transmission line for which voltage V and current I are solutions of the telegrapher’s equations. In general, each of the transmission line parameters representing a return stroke channel is a function of time and space; that is, the transmission line is non linear and non uniform [4]. Even if R, L, and C were constant, the application of the R-L-C transmission line model to

lightning is an approximation. Indeed, for a vertical lightning channel with the current equivalent return path being the vertical channel image (assuming a perfectly conducting ground) the validity of the transverse electromagnetic mode (TEM) assumption is questionable, in particular near the return stroke tip where a relatively large longitudinal component of electric field is present. Usually, a distributed circuit model of the lightning return stroke is postulated without proper analysis of its applicability.

The Transmission-Line (TL) model [5], the Traveling Current Source (TCS) model [6], the Modified TL (MTL) model [7]-[9], and the Diendorfer-Uman (DU) and Diendorfer-Uman Modified (MDU) models [10], [11], all of these engineering models are popular for their simplicity, which permits relating the return stroke current to a channel-base current known from measurements in a straightforward way [3]. The analysis of lightning currents or electromagnetic fields around a tower struck by lightning have mostly been made through modeling the structures by single or cascaded lossless transmission lines, specifying surge impedance or reflection and refraction coefficients at their ends [12]-[16]. The modeling such conductor systems by transmission lines is correct if the electromagnetic field around a conductor is in the TEM mode and their parameters need to be determined experimentally or hypothetically. But the transient electromagnetic field around a vertical structure is different from that of the TEM mode, which is the basis of the equivalent-circuit approach.

To analyze such transient electromagnetic field around a three-dimensional (3D) conductor system, application of electromagnetic model are more appropriate than approaches based on the circuit theory because they can compute fields at any point around the structures without postulating an equivalent circuit. Electromagnetic return stroke models based on the representation of the lightning channel as a lossy antenna have been proposed by Podgorski and Landt [17] and Moini *et al.* [18]. These models involve a numerical solution of Maxwell's equations using the method of moments (MoM) (e.g., Sadiku [19]), which yields the complete solution for channel current including both the antenna-mode current and the transmission-line-mode current (e.g., Paul [20]). Very recently M. Ishii and Y. Baba applied Electromagnetic model for the analysis of tower surge response and show reasonably accepted results [21].

1.5 Electromagnetic Modeling Code

Lightning is an electromagnetic problem. Due to their unpredictable behavior the only way we can measure their behavior mathematically is through the use of numerical estimation techniques. For the accurate analysis of such transient electromagnetic field of lightning, application of electromagnetic modeling codes are more appropriate. Of many available codes, those based on the MoM [22] are probably best suitable for the electromagnetic analysis of a tower system. Podgorski and Landt [17], Moini *et al.* [18] used Thin-Wire Time-Domain (TWTD) code [23], which is based on the method of moments, to analyze lightning current and the resultant electric and magnetic fields. The accuracy of the results when TWTD is applied to this kind analyzes has not been well investigated.

Numerical Electromagnetic Code-2 (NEC-2) [24] developed at the Lawrence Livermore National Laboratory is another MoM-based electromagnetic modeling code. This code is more widely used than TWTD and has been applied to analyze electromagnetic fields around antennas. There have been several studies related to lightning employing NEC-2. Heidler *et al.* [25] used this code to analyze the induced voltages on conductor loops illuminated by lightning electromagnetic pulse (EMP). Cristina *et al.* [26] employed it to evaluate the electromagnetic field inside of a building struck by lightning. Chai *et al.* [27] employed this code to study the electromagnetic field inside of a wire-array lightning protection system for a launch vehicle when it is struck by lightning. Recently Y. Baba and M. Ishii [28] used this code to reproduce the measured current and electromagnetic field at CN Tower postulating source voltage waveforms and found a reasonably good agreement between computed and experimental results. The effectiveness of NEC-2 in the analysis of surge response on vertical conductor model was also verified in many works comparing with the experimental results [29]-[34].

In order to solve the very fast surge phenomena in a 3D structure as an electromagnetic field problem, the FDTD method [35] is also currently available as practical choice. Furthermore, an imperfectly conducting medium is required to be accurately modeled to represent currents in the earth. Comparing the theories of FDTD and MoM, the former is more advantageous to handle 3D currents in an imperfectly conducting medium such as

earth soil without any difficulty, even if the medium is nonhomogeneous [36]. On the other hand, the latter is more advantageous to accurately represent the thin wire.

The MoM needs to model only the metal structure of interest, and does not need to model the space around it. Long wires are, therefore, easily modeled. This is the advantage compared with the FDTD method that may also be applicable to this problem. The MoM allows discrete circuit elements to be inserted into a model by simply defining the impedance desired on any given wire segment.

1.6 Objectives of the Work

The main objective of the work is to increase the knowledge of the characteristics of electric and magnetic fields produced by lightning discharges which is needed for studying the effects of the potentially deleterious coupling of lightning fields to various circuits and systems. This will include the following sub-objectives, but not limited to them.

1. The understanding of the dynamic electromagnetic behavior of lightning.
2. To reproduce the current and electromagnetic field as like observed in the natural return stroke.
3. To understand the characteristics of current and electromagnetic field produced by lightning discharge.
4. Analysis of the characteristics of electromagnetic field at different distances.
5. To show the effect of ground conductivity on currents and electromagnetic fields.
6. Analysis of the effects of different lightning current waveform.
7. To explain the effects of lightning stroke to tall structures.
8. To understand the characteristics of electromagnetic fields for first and subsequent stroke.

Reviewing different models, electromagnetic model is chosen for the work and for the more accurate result simulation is carried out by electromagnetic modeling codes NEC-2 based on MoM and the surge analysis program named VSTL (Virtual Surge Test Lab.) based on FDTD method. Because of more computation time, a reduced scale model is

considered for FDTD simulation. To examine the validity of our computed result, comparison against two experimental results and FDTD simulation on reduced scale model are shown.

1.7 Thesis Organization

All the items listed in the previous section are considered in this thesis. The contents of the entire work can be divided into four different parts. First, there is a description of the frequency domain and time domain numerical solution techniques of electromagnetic problem. This is covered in Chapter 2, with special attention being given to the electromagnetic modeling codes: NEC-2 (frequency domain) and VSTL (time domain).

Assuming that the representation of the lightning return stroke as a current pulse propagating along a vertical conductor channel is valid, the effects of different channel parameters both on the current and the electromagnetic fields are investigated in Chapter 3. Here, the effect of different ground electrical parameters, different injected current waveforms as well as the effect of subsequent return strokes on the electromagnetic fields is considered.

Chapter 4 presents the analysis of lightning current along the elevated structures and their radiated electromagnetic fields at different distances for both the lightning first stroke and the subsequent stroke to tall structures. Characteristics of some experimental observation and comparison of simulation result with two experimental results are given in this chapter.

Chapter 5 is intended to the FDTD simulation on reduced scale model and to validate the accuracy, the comparison is made between the NEC-2 and FDTD results.

Finally, the conclusions and the scopes of the work required in the future are presented in Chapter 6.

Chapter 2

Solution Techniques for Electromagnetic Problem

2.1 Introduction

Lightning is an electromagnetic problem. Fairly, simple electromagnetic problems can be solved by Maxwell's equations of electromagnetism analytically [37]. For more complicated electromagnetic problems, numerical techniques are more convenient than analytical solutions [38]. The advancement of digital computers' processing power and storage capacity since late 1950s accelerates the development of numerical solutions and increases their practical feasibility [37]. Broad class of complex electromagnetic problems can be handled via a few time and /or frequency domain numerical techniques. Two most widely used numerical techniques: Method of Moments (MoM) and Finite Difference Time Domain (FDTD) method are used in this thesis. MoM is one of the most powerful techniques in frequency domain where complex structure over lossy ground can easily be investigated. FDTD is a popular time domain technique where broad band frequency behaviors can be obtained via a simulation run.

For MoM simulations, NEC-2 code, a standard tool for numerical analysis on electromagnetic field around antennas, can be applied to the analysis of lightning transient. This code solves the electric field integral equation (EFIE) using moment method. On the other hand, this research work employs the surge analysis program named VSTL (Virtual Surge Test Lab.) [39] for FDTD simulation.

The EFIE used in NEC-2, its derivation and the numerical methods are first outlined in this chapter. Guidelines for modeling structures with this code are discussed next to inform the operation of this program. Finally limitations of the program are mentioned. Similarly the FDTD formulations used in VSTL is described and then simulation procedure of VSTL is outlined.

2.2 Frequency Domain Technique: Method of Moments

Method of Moments is a complicated numerical method. The primary formulation of MoM is an appropriate integral equation obtained through the use of Green's functions [22]. The technique is based on solving complex integral equations by reducing them to a system of linear equations and on applying method of weighted residuals. Actually the terms MoM and method of weighted residuals are synonymous. It is Harrington [22], who popularized the term MoM in electrical engineering society. His pioneering efforts first demonstrated the power and flexibility of this numerical technique for solving problems in electromagnetics. The equation solved by MoM technique is generally a form of the electric field integral equation (EFIE) or the magnetic field integral equation (MFIE). Both of these equations can be derived from Maxwell's equations.

2.2.1 Electric Field Integral Equation

NEC-2 allows using both the electric field integral equation (EFIE) and the magnetic field integral equation (MFIE). The former is suited for analysis of thin-wire structures, while the latter is suitable for structures having large smooth surfaces. The former can be used to analyze voluminous structures by representing surface with wire grids. The derivation of EFIE from Maxwell's equation is given in Appendix A.

The form of EFIE used in NEC-2 follows an integral representation of the electric field for a volume current distribution J_v [24],

$$E(r) = \frac{-j\eta}{4\pi k} \int_v J_v(r') \cdot \overline{\overline{G}}(r, r') dV', \quad (2.1)$$

$$\text{where } \overline{\overline{G}}(r, r') = (k^2 \overline{\overline{I}} + \nabla \nabla) g(r, r'),$$

$$g(r, r') = \exp(-jk|r - r'|) / |r - r'|,$$

$$k = \omega \sqrt{\mu_0 \epsilon_0},$$

$$\eta = \sqrt{\mu_0 / \epsilon_0}$$

and the time convention is $\exp(j\omega t)$, \bar{I} is the identity dyad ($\hat{x}\hat{x} + \hat{y}\hat{y} + \hat{z}\hat{z}$), μ_0 and ϵ_0 are the permeability and permittivity of the free space respectively, k is the wave number, η is the intrinsic impedance which has a value of 120π in the free space and ω is the angular frequency. When the current distribution is limited to the plane of a perfectly conducting body, equation (2.1) becomes

$$E(r) = \frac{-j\eta}{4\pi k} \int_S J_S(r') \cdot \bar{G}(r, r') dS', \quad (2.2)$$

with J_S the surface current density. The observation point r is restricted to be off the surface S so that $r \neq r'$. If r approaches S as a limit, equation (2.2) becomes

$$E(r) = \frac{-j\eta}{4\pi k} \oint_S J_S(r') \cdot \bar{G}(r, r') dS', \quad (2.3)$$

where the principal value \oint is indicated since $g(r, r')$ is now unbounded.

An integral equation for the current induced on S by an incident field E_{inc} can be obtained from equation (2.3) and the boundary condition for $r \in S$,

$$n(r) \times [E_{scat}(r) + E_{inc}(r)] = 0, \quad (2.4)$$

where $n(r)$ is the unit normal vector of the surface at r and E_{scat} is the field due to induced current J_S . Substituting equation (2.3) for E_{scat} yields the integral equation,

$$-n(r) \times E_{inc}(r) = \frac{-j\eta}{4\pi k} n(r) \times \int_S J_S(r') \cdot (k^2 \bar{I} + \nabla \nabla) g(r, r') dS' \quad (2.5)$$

The vector integral in equation (2.5) can be reduced to a scalar integral equation when the conducting surface S is the surface of a cylindrical thin wire, thereby making the solution much easier. The assumptions applied to a thin-wire, known as thin-wire approximation, are as follows:

1. Transverse currents relative to axial currents on the wire can be neglected.
2. The circumferential variation in the axial current can be neglected.
3. The current can be represented by a filament on the wire axis.
4. The boundary conditions on the electric field need to be enforced in the axial direction only.

These assumptions are valid as far as the wire radius is much less than the wavelength and much less than the wire length. From 1st, 2nd and 3rd assumptions, the surface current density J_S on a wire of a radius 'a' can be replaced by a filamentary current I ,

$$I(s)\hat{s} = 2\pi a J_s(r),$$

where s is the distance parameter along the wire axis at r and \hat{s} is the unit vector tangent to the wire axis at r . Equation (2.5) then becomes

$$-n(r) \times E_{inc}(r) = \frac{-j\eta}{4\pi k} n(r) \times \int_L I(s')(k^2 \hat{s}' - \nabla \frac{\partial}{\partial s'}) g(r, r') ds', \quad (2.6)$$

where the integration is over the length of the wire. Enforcing the boundary condition in the axial direction reduces equation (2.6) to a scalar equation,

$$-\hat{s} \cdot E_{inc}(r) = \frac{-j\eta}{4\pi k} \int_L I(s')(k^2 \hat{s} \cdot \hat{s}' - \frac{\partial^2}{\partial s \partial s'}) g(r, r') ds' \quad (2.7)$$

Since r' is now the point at s' on the wire axis while r is a point at s on the wire surface $|r - r'| \geq a$ and the integrand is bounded.

This is the basic electric field integral equation at the surface of a thin conducting wire in the axial direction reduced to the scalar equation under the restriction of the boundary condition given by equation (2.4) in the axial direction.

The electric field integral equation is easily extended to imperfect conductors by modifying the boundary condition from equation (2.4) to

$$n(r) \times [E_{scat}(r) + E_{inc}(r)] = Z_s(r) [n(r) \times J_s(r)], \quad (2.8)$$

where the $Z_s(r)$ is the surface impedance at r on the conducting surface. For a wire, the boundary condition is

$$\hat{s} \cdot [E_{scat}(r) + E_{inc}(r)] = Z_L(s) I(s), \quad (2.9)$$

where $Z_L(s)$ is the impedance per unit length at s .

2.2.2 Numerical Solution by the Method of Moments

Method of Moments is a procedure of reducing integral equations to a system of simultaneous linear algebraic equations. The integral equation (2.7) is solved numerically in NEC-2 by the Method of Moments. This method applies to a general linear-operator equation,

$$Lf = e, \quad (2.10)$$

where f is an unknown response, e is a known excitation, and L is a linear operator (an integral operator in the present case). The unknown function f may be expanded in a sum of basis functions, f_j as

$$f \cong \sum_{j=1}^N \alpha_j \cdot f_j \quad (2.11)$$

A set of equations for the coefficients α_j are then obtained by taking the inner product of equation (2.10) with a set of weighting functions, $\{w_i\}$,

$$\langle w_i, Lf \rangle = \langle w_i, e \rangle \quad i = 1, 2, \dots, N. \quad (2.12)$$

Due to the linearity of L , equation (2.11) substituted for f yields,

$$\sum_{j=1}^N \alpha_j \langle w_i, Lf_j \rangle = \langle w_i, e \rangle \quad i = 1, 2, \dots, N. \quad (2.13)$$

This equation can be written in matrix form as

$$[G][A] = [E], \quad (2.14)$$

where $G_{ij} = \langle w_i, Lf_j \rangle$, $A_j = \alpha_j$, $E_i = \langle w_i, e \rangle$, and is easily solved.

The solution is then $[A] = [G]^{-1}[E]$. The matrix equation is solved in NEC-2 by Gauss elimination technique [40]. The basic step is factorization of the matrix \mathbf{G} into the product of an upper triangular matrix \mathbf{U} and a lower triangular matrix \mathbf{L} where

$$[G] = [L][U]. \quad (2.15)$$

The matrix equation is then

$$[L][U][A] = [E], \quad (2.16)$$

from which the solution, \mathbf{A} , is computed in two steps as

$$[L][F] = [E], \quad (2.17)$$

and

$$[U][A] = [F] \quad (2.18)$$

Equation (2.17) is first solved for \mathbf{F} by forward substitution, and equation (2.18) is then solved for \mathbf{A} by backward substitution. For the solution of equation (2.7), the inner product is defined as

$$\langle f, g \rangle = \int_S f(r)g(r)dS,$$

where the integration is over the structure surface. Various choices are possible for the weighting function $\{w_i\}$ and basis functions $\{f_i\}$. When $w_i = f_i$, the procedure is known as Galerkin's method.

In NEC-2, the basis and weighting functions are different, and $\{w_i\}$ are chosen as a set of delta functions

$$w_i(r) = \delta(r - r_i),$$

with $\{r_i\}$ a set of points on the conducting surface. The result is a point sampling of the integral equations known as the collocation method of solution. Wires are divided into short straight segments with a sample point at the center of each segment.

The choice of basis functions is very important for an efficient and accurate solution. In NEC-2, the support of f_i is restricted to a localized subsection of the surface near $\{r_i\}$. This choice simplifies the evaluation of the inner-product integral and ensures that the matrix G will be well conditioned. For finite N , the sum of f_i cannot be exactly equal to a general current distribution. So, the function f_i should be chosen as close as possible to the actual current distribution. Some calculations in NEC-2 which are also related to this work are as follows:

1. Current Expansion on Wires

Wires in NEC-2 are modeled by short straight segments with current on each segment represented by three terms a constant sine function and a cosine function. This expansion has been shown to provide rapid solution convergence. It has the added advantage that the fields of the sinusoidal currents are easily evaluated in a closed form. The amplitudes of the constant, sine and cosine terms are related such that their sum satisfies physical conditions on the local behavior of current and charge at the segment ends.

The total current on segment number j in NEC-2 has the form or the current expansion functions in NEC-2 have the form

$$I_j = A_j + B_j \sin k(s - s_j) + C_j \cos k(s - s_j), \quad |s - s_j| < \frac{\Delta_j}{2}, \quad (2.19)$$

where, $k = \omega\sqrt{\mu_0\epsilon_0}$, where s_j is the value of s at the center of segment j and Δ_j is the length of segment j . Of the three unknown constants A_j , B_j and C_j , two are eliminated by local conditions on the current leaving one constant, related to the current amplitude, to be determined by the matrix equation. The local equations are applied to the current and to the linear charge density, q which is related to the current by the equation of continuity

$$\frac{\partial I}{\partial s} = -j\omega q . \quad (2.20)$$

At a junction of two segments with uniform radius, the obvious condition is that the current and charge are continuous at the junction. At a junction of two or more segments with unequal radii, the continuity of current is generalized to Kirchhoff's current law that the algebraic sum of current into the junction is zero. The total charge in the vicinity of the junction is assumed to distribute itself on individual wires according to the wire radii, neglecting local coupling effects.

2. Evaluation of the Fields

The solution requires the evaluation of electric field at each segment due to this current. Three approximations of the integral equation kernel are used:

1. a thin-wire form for most cases
2. an extended thin-wire form for thick wires and
3. a current element approximation for large interaction distance

In each case the evaluation of the field is greatly simplified by the use of formulae for the fields of the constant and sinusoidal current components. Studies have been carried out considering the thin-wire kernel.

The accuracy of the thin-wire kernel approximation for a wire of radius ' a ' and length ' ΔL ' depends on ka and $\Delta L/a$. Studies have shown that the thin-wire approximation leads to error of less than 1% for $\Delta L/a$ greater than 8. Furthermore, in the numerical solution of electric field integral equation, the wire is divided into segments less than about 0.1λ in length to obtain the adequate representation of current distribution thus restricting ka to be less than about 0.08.

For the thin-wire kernel, the source current is approximated by a filament on the segment axis while the observation point is on the surface of the observation segment. The fields are evaluated with the segment on the axis of a local cylindrical co-ordinate system as illustrated in Fig. 2.1 below:

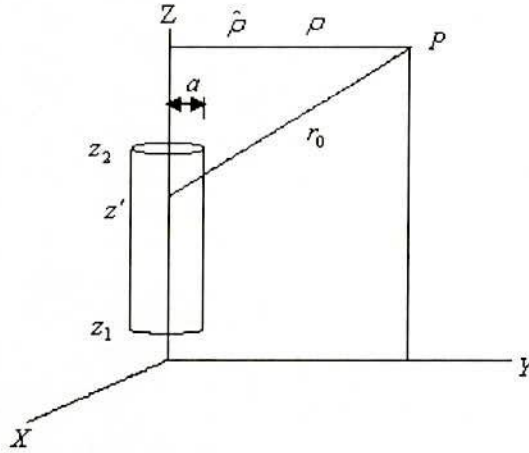


Fig. 2.1. Current filament geometry for thin-wire kernel.

Then with

$$G_0 = \exp(-jkr_0)/r_0 \text{ and } r_0 = [\rho^2 + (z - z')^2]^{1/2},$$

the ρ and z components of the electric field at P due to a sinusoidal current filament of arbitrary phase,

$$I = \sin(kz' - t_0), \quad z_1 < z' < z_2,$$

$$\text{are } E_\rho^f(\rho, z) = \frac{-jn}{2k^2\lambda\rho} \left[(z' - z)I \frac{\partial G_0}{\partial z'} + IG_0 - (z' - z)G_0 \frac{\partial I}{\partial z'} \right]_{z_1}^{z_2}, \quad (2.21)$$

$$E_z^f(\rho, z) = \frac{jn}{2k^2\lambda} \left[G_0 \frac{\partial I}{\partial z'} - I \frac{\partial G_0}{\partial z'} \right]_{z_1}^{z_2}. \quad (2.22)$$

For a current that is constant over the length of the segment with strength I , the fields are

$$E_\rho^f(\rho, z) = \frac{I}{\lambda} \frac{jn}{2k^2} \left[\frac{\partial G_0}{\partial \rho} \right]_{z_1}^{z_2}, \quad (2.23)$$

$$E_z^f(\rho, z) = \frac{I}{\lambda} \frac{jn}{2k^2} \left\{ \left[\frac{\partial G_0}{\partial z'} \right]_{z_1}^{z_2} + k^2 \int_{z_1}^z G_0 dz' \right\}. \quad (2.24)$$

These field expressions are exact for the specified currents. The integral over z' of G_0 is evaluated numerically in NEC-2. Substituting sine and cosine currents and evaluating the derivatives yields the following equation for the fields. For

$$I = I_0 \begin{pmatrix} \sin kz' \\ \cos kz' \end{pmatrix},$$

$$E_\rho^f(\rho, z) = \frac{-I_0}{\lambda} \frac{j\eta}{2k^2\rho} G_0 \left\{ k(z-z') \begin{pmatrix} \cos kz' \\ -\sin kz' \end{pmatrix} + \left[1 - (z-z')^2 (1 + jkr_0) \frac{1}{r_0^2} \right] \begin{pmatrix} \sin kz' \\ \cos kz' \end{pmatrix} \right\}_{z_1}^{z_2},$$

$$E_z^f(\rho, z) = \frac{I_0}{\lambda} \frac{j\eta}{2k^2} G_0 \left\{ k \begin{pmatrix} \cos kz' \\ -\sin kz' \end{pmatrix} + \left[(1 + jkr_0)(z-z') \frac{1}{r_0^2} \right] \begin{pmatrix} \sin kz' \\ \cos kz' \end{pmatrix} \right\}_{z_1}^{z_2}$$

For a constant current of strength I_0 ,

$$E_\rho^f(\rho, z) = \frac{-I_0}{\lambda} \frac{j\eta\rho}{2k^2} \left[(1 + jkr_0) \frac{G_0}{r_0^2} \right]_{z_1}^{z_2}, \quad (2.25)$$

$$E_z^f(\rho, z) = \frac{-I_0}{\lambda} \frac{j\eta}{2k^2} \left[(1 + jkr_0)(z-z') \frac{G_0}{r_0^2} \right]_{z_1}^{z_2} - \frac{I_0}{\lambda} \frac{j\eta}{2k^2} k^2 \int_{z_1}^{z_2} G_0 dz'. \quad (2.26)$$

Despite the seemingly crude approximation, the thin wire kernel does accurately represent the effect of wire radius for wires that are sufficiently thin.

3. Effect of Ground Plane

The NEC-2 code has three options for grounds. The most accurate for lossy grounds uses the Sommerfeld solution of interaction distances less than one wavelength and asymptotic expansion for larger distances. To keep the solution time reasonable, a grid of values of the Sommerfeld solution is generated and interpolation is used to find specific values. This method is presently implemented only for wires in NEC. The solution for a perfectly conducting ground is much simpler since the ground may be replaced by the image of the currents above it. The third option models a lossy ground by a modified image method using the Fresnel plane-wave reflection coefficients. Although this is far from exact for a finite ground, it has been shown to provide useful results for structures that are not too near to the ground.

When the Sommerfeld option is used for an antenna over ground the electric field at \bar{r} due to the current on a segment is evaluated in three terms as

$$\bar{E}(\bar{r}) = \bar{E}_D(\bar{r}) + \frac{k_1^2 - k_2^2}{k_1^2 + k_2^2} \bar{E}_I(\bar{r}) + \bar{E}_S(\bar{r}) \quad (2.27)$$

where $k_1^2 = \omega^2 \mu_0 \epsilon_0 \left(\frac{\epsilon_1}{\epsilon_0} - \frac{j\sigma_1}{\omega\epsilon_0} \right)$, and $k_2^2 = \omega^2 \mu_0 \epsilon_0$,

μ_0, ϵ_0 are the permeability and permittivity of free space, respectively, μ_1, ϵ_1 are that of ground and σ_1 is the conductivity of ground. \bar{E}_D is the direct field of the segment in the absence of ground, and \bar{E}_I is the field of the image of the segment reflected in a perfectly conducting ground. The field \bar{E}_S is due to the Sommerfeld integrals. The detail of the analysis is given in ref. [24].

2.3 Numerical Electromagnetic Code-2 (NEC-2)

The Numerical Electromagnetic Code (NEC-2) is a program written in FORTRAN for the analysis of the electromagnetic response of metal structures particularly antennas by employing Method of Moments. The code needs to model the metal structure of interest. A model may include non-radiating networks and transmission lines connecting parts of the structure, perfect or imperfect conductors, and lumped-element loading. A structure may also be modeled over a ground plane that may be either a perfect or imperfect conductor.

Any metallic object is assumed to be a superposition of small segments on which the current distributions are of interest. The excitation may be either voltage sources on the structure or an incident plane wave. The MoM is to determine the current on every segment due to the source and all the other current by numerically solving the integral equation. This approach avoids many of the simplifying assumptions required by other solution methods and provides a highly accurate and versatile tool for electromagnetic analysis. Once the currents are known, the fields at any point in space are determined from the sum of the contributions of all the wire segments. The output may include induced currents and charges, near electric or magnetic fields, and radiated fields.

NEC-2 is the latest release of the program which is run in Linux operating system and is compiled by Gnu Fortran 77 compiler. This code was developed at the Lawrence Livermore National Laboratory, California, under the sponsorship of the Naval Ocean Systems Center and the Air Force Weapons Laboratory. Although the latest version is NEC-4 [41], it is available only to the citizens of the United States and Canada, or to the users who are licensed from Lawrence Livermore National Laboratory.

Therefore, the author employs NEC-2 developed in 1980 that is now available. The information on the history and availability of the NEC-2 codes is found in Appendix B.

2.3.1 Structure Modeling Guidelines

The basic devices for modeling structures with the NEC code are short, straight segments for modeling wires and flat patches for modeling surfaces. An antenna and any other conducting objects in its vicinity that affect its performance must be modeled with strings of segments following the paths of wires and with patches covering surfaces. Proper choice of the segments and patches for a model is the most critical step to obtaining accurate results. The number of segments and patches should be the minimum required for accuracy; however, since MoM is based on the calculation of currents on small segments and since it is formulated as a matrix system, the memory and the computation time requirements drastically increase as the number of segment increases. Guidelines for choosing segments and patches are given below and should be followed carefully by anyone using the NEC code. Experience gained by using the code will also aid the user in developing models.

A wire segment is defined by the coordinates of its two end points and its radius. Modeling a wire structure with segments involves both geometrical and electrical factors. Geometrically, the segments should follow the paths of conductors as closely as possible, using a piece-wise linear fit on curves.

The main electrical consideration is segment length ΔL relative to the wavelength λ . Generally, ΔL should be less than about 0.1λ at the desired frequency. Somewhat longer segments may be acceptable on long wires with no abrupt changes while shorter segments,

0.05λ or less, may be needed in modeling critical regions of an antenna. The size of the segments determines the resolution in solving for the current on the model since the current is computed at the center of each segment. Extremely short segments, less than about $10^{-3}\lambda$, should also be avoided since the similarity of the constant and cosine components of the current expansion leads to numerical inaccuracy.

The wire radius, a , relative to λ is limited by the approximations used in the kernel of the electric field integral equation. Two approximation options are available in NEC-2: the thin-wire kernel and the extended thin-wire kernel. In the thin-wire kernel, the current on the surface of a segment is reduced to a filament of current on the segment axis. In the extended thin-wire kernel, a current uniformly distributed around the segment surface is assumed. The field of the current is approximated by the first two terms in a series expansion of the exact field in powers of a^2 . The first term in the series, which is independent of a , is identical to the thin-wire kernel while the second term extends the accuracy for larger values of a . Higher order approximations are not used because they would require excessive computation time.

In either of these approximations, only currents in the axial direction on a segment are considered, and there is no allowance for variation of the current around the wire circumference. The acceptability of these approximations depends on both the value of a/λ and the tendency of the excitation to produce circumferential current or current variation. Unless $2\pi a/\lambda$ is much less than 1, the validity of these approximations should be considered.

The accuracy of the numerical solution for the dominant axial current is also dependent on $\Delta L/a$. It must be greater than about 8 to limit errors less than 1%, since small values of $\Delta L/a$ may result in extraneous oscillations in the computed current near free wire ends, voltage sources, or lumped loads. Use of the extended thin-wire kernel will extend the limit on $\Delta L/a$ to smaller values than are permissible with the normal thin-wire kernel. Studies of the computed field on a segment due to its own current have shown that with the thin-wire kernel, with the extended thin-wire kernel, $\Delta L/a$ may be as small as 2 for the same accuracy. In the current solution with either of these kernels, the error tends to be

less than for a single field evaluation. Reasonable current solutions have been obtained with the thin-wire kernel for $\Delta L/a$ down to about 2 and with the extended thin-wire kernel for $\Delta L/a$ down to 0.5. When a model includes segments with $\Delta L/a$ less than about 2, the extended thin-wire kernel option should be used. When the extended thin-wire kernel option is selected, it is used at free wire ends and between parallel, connected segments. The normal thin-wire kernel is always used at bends in wires, however. Hence, segments with small $\Delta L/a$ should be avoided at bends. Use of a small $\Delta L/a$ at a bend, which results in the center of one segment falling within the radius of the other segment, generally leads to severe error.

The current expansion used in NEC enforces conditions on the current and charge density along wires, at junctions, and at wire ends. For these conditions to be applied properly, segments that are electrically connected must have coincident end points. If segments intersect other than at their ends, the NEC-2 code will not allow current to flow from one segment to the other. Segments will be treated as connected if the separation of their ends is less than about 10^{-3} times the length of the shortest segment. When possible, however, identical coordinates should be used for connected segment ends.

The angle of the intersection of wire segments in NEC-2 is not restricted in any manner. In fact, the acute angle may be so small as to place the observation point on one wire segment within the volume of another wire segment. Numerical studies have shown that such overlapping leads to meaningless results; thus, as a minimum, one must ensure that the angle is large enough to prevent overlaps. Even with such care, the details of the current distribution near the intersection may not be reliable even though the results for the current may be accurate at distances from this region.

Wire-grid modeling of conducting surfaces has been used with varying success. The earliest applications to the computation of radar cross sections and radiation patterns provided reasonably accurate results. Even computations for the input impedance of antennas driven against grid models of surfaces have oftentimes exhibited good agreement with experiments.

However, broad and generalized guidelines for near-field quantities have not been developed, and the use of wire-grid modeling for near-field parameters should be approached with caution. A single wire grid, however, may represent both surfaces of a thin conducting plate. The current on the grid will be the sum of the currents that would flow on opposite sites of the plate. While information on the currents on the individual surfaces is lost the grid will yield the correct radiated fields.

Other rules for the segment model are as follows:

1. Segments (or patches) may not overlap since the division of current between two overlapping segments is indeterminate. Overlapping segments may result in a singular matrix equation.
2. A large radius change between connected segments may decrease accuracy; particularly, with small $\Delta L/a$. The problem may be reduced by making the radius change in steps over several segments.
3. A segment is required at each point where a network connection or voltage source will be located. This may seem contrary to the idea of an excitation gap as a break in a wire. A continuous wire across the gap is needed, however, so that the required voltage drop can be specified as a boundary condition.
4. The two segments on each side of a charge density discontinuity voltage source should be parallel and have the same length and radius. When this source is at the base of a segment connected to a ground plane, the segment should be vertical.
5. The number of wires joined at a single junction cannot exceed 30 because of a dimension limitation in the code.
6. When wires are parallel and very close together, the segments should be aligned to avoid incorrect current perturbation from offset match point and segment junctions.
7. Although extensive tests have not been conducted, it is safe to specify that wires should be several radii apart.

2.3.2 Program Input and Program Control

The structure of the main program is shown in the flow charts of Figs. 2.2 and 2.3 where Fig. 2.2 represents the first half of the code as input section. Any of the types of data cards (CP, EN, EX, FR, GN, NE, PT, XQ etc.) may be read at this section to set parameters or to request execution of the solution part (Fig. 2.3) of the code.

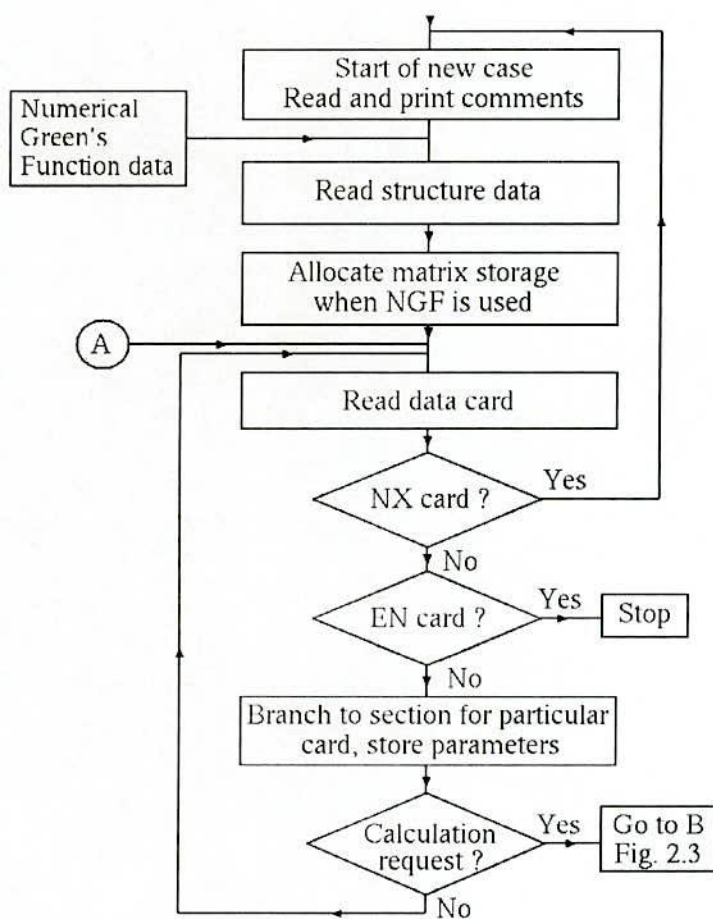


Fig. 2.2. Flow diagram of NEC-2 main program input section.

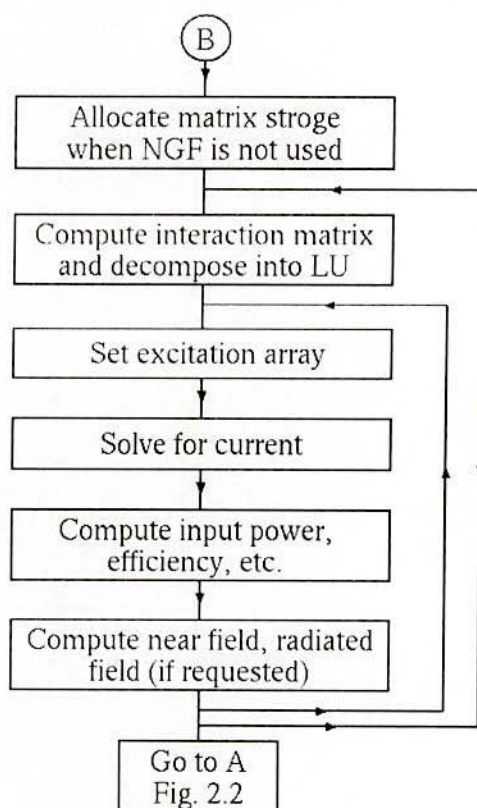


Fig. 2.3. Flow diagram of NEC-2 main program computation section.

Input data files can be written by any text editor. An input data file has several lines. Each line represents either input data or program control. The sample input data deck to NEC-2, which is for an impulse voltage measuring system as illustrated in Fig. 2.4, is shown in Table 1.1. For this example, the resistance divider of 3.3 m in height is divided into 6 segments of 0.55 m.

The input data deck must begin with comment lines 'CM'. The comment lines are terminated by 'CE'. A line starting with 'GW' represents a cylindrical straight wire. The number next to 'GW' is a tag number assigned to all segments of wire. The one next to it is the number of segments into which the wire is divided. The decimal numbers next to them are the coordinates of the wire ends and the radius of the wire $(x_1, y_1, z_1, x_2, y_2, z_2, a)$. Note that the unit is in meters.

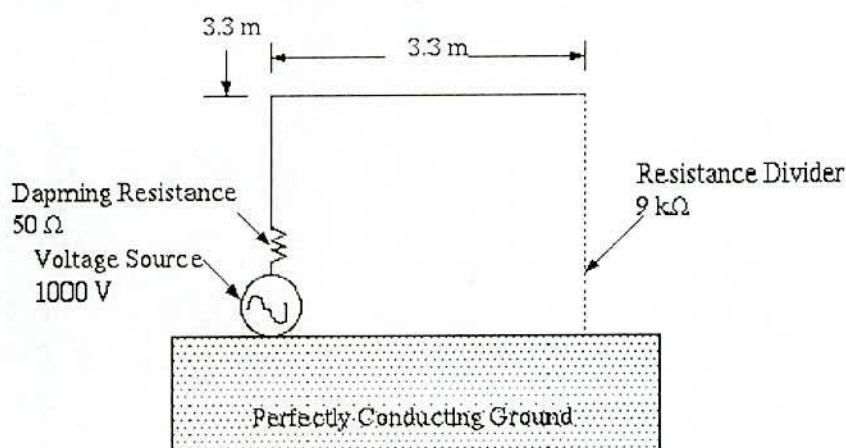


Fig. 2.4. An impulse voltage measuring system subjected to analysis as example.

Table 1.1

Sample input data to NEC-2

```

CM IMPULSE VOLTAGE MEASURING SYSTEM
CM N=512 ΔT= 2.5E-09 SEC
CE PERFECTLY CONDUCTING GROUND IS USED
GW 1 6 0.0 0.0 0.0 0.0 0.0 3.3 0.0025
GW 2 6 0.0 0.0 3.3 3.3 0.0 3.3 0.0025
GW 3 6 3.3 0.0 3.3 3.3 0.0 0.0 0.0025
GE 1
GN 1
LD 4 1 2 2 50.0
LD 4 3 1 6 1500.0
FR 0 257 0 0 7.813E-01 7.813E-01
EX 0 1 1 00 1000.0 0.0
PT 0 3 6
XQ
EN

```

The following two lines, 'GE 1' and 'GN 1', indicate a perfectly conducting ground exists at $z = 0$, i.e. by this commands, images below ground are generated. The 9th and 10th lines beginning with 'LD' specify the impedance loading. The 9th line indicates that the second

segment of the set of segments whose tag number is 1 is loaded by resistance of 50Ω . Similarly, the 10th line indicates that each of the 1st segments through 6th segments of the set of segments having tag number of 3 is loaded by 1500Ω , respectively.

In the line starting with 'FR', the frequency range is specified as 0.7813 MHz to 200 MHz with the linear increment step of 0.7813 MHz. In the line of 'EX', the excitation for the structure is specified. In this case, a voltage source generating 1000 volts is inserted into the 1st segment of the set of segments having tag number of 1. By the line beginning with 'PT', currents for the 6th segment of the set of segments whose tag number is 3 are printed. The last two commands: 'XQ' and 'EN' are commands of program execution and end, respectively.

For the present analysis the author uses $\Delta t = 0.1 \mu\text{s}$, and the corresponding frequency will be as follows:

$$\text{Frequency } f = \frac{1}{512 \times \Delta t} \text{ Hz} = \frac{1}{512 \times 0.1 \times 10^{-6}} \text{ Hz} = 19.53 \text{ kHz}$$

Now the wavelength $\lambda = \frac{c}{f}$, where c is the velocity of light and f is the frequency.

$$\text{So, the wavelength } \lambda = \frac{3 \times 10^8}{19.53 \times 10^3} \text{ meter} = 15360.98 \text{ meter}$$

Now the value of ΔL must be within $10^{-3}\lambda \leq \Delta L \leq 0.1\lambda$. Here, the limiting range for ΔL becomes $15.36 \text{ m} \leq \Delta L \leq 1536 \text{ m}$. Conventionally, the author uses $\Delta L = 25 \text{ m}$, which is within the limit.

When modeling complex structures with features not previously encountered, accuracy may be checked by comparison with reliable experimental data if available. Alternatively, it may be possible to develop an idealized model for which the correct results can be estimated while retaining the critical features of the desired model. The optimum model for a class of structures can be estimated by varying the segment and patch density and observing the effect on the results. Some dependence of results on segmentation will always be found. A large dependence, however, would indicate that the solution has not converged and more segments or patches should be used. A model will generally be usable

over a band of frequencies. For frequencies beyond the upper limit of a particular model, a new set of geometry cards must be input with a finer segmentation.

Several options are available in NEC-2 for modeling an antenna over a ground plane. For a perfectly conducting ground, the code generates an image of the structure reflected in the ground surface. The image is exactly equivalent to a perfectly conducting ground and results in solution accuracy comparable to that for a free-space model. Structures may be close to the ground or contacting it in this case. However, for a horizontal wire with radius a , and height h to the wire axis, $[h^2 + a^2]^{1/2}$ should be greater than about 10^6 wavelengths. Furthermore, the height should be at least several times the radius for the thin-wire approximation to be valid.

A finitely conducting ground can be modeled by Sommerfeld-Norton approximation. It should be noted that NEC-2 can model wires over lossy ground but it cannot model wires buried in the ground. Although NEC-4, the latest version of the NEC-MoM codes, can model buried wires.

NEC-2 numerically solves the electric field integral equation in the frequency domain by the moment method. To get the time-varying response, Fourier transform and inverse Fourier transform are used as shown in Fig. 2.5.

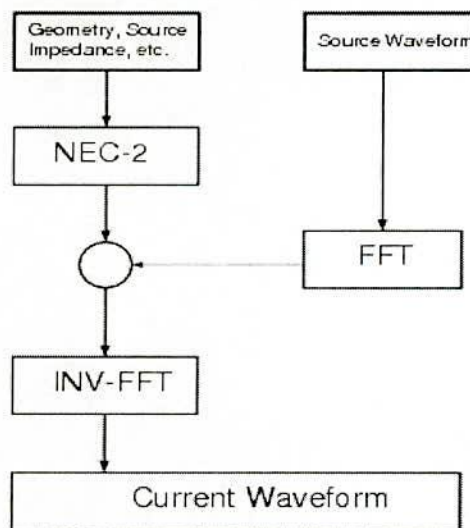


Fig. 2.5. Flow of the solution using NEC-2.

2.4 Time Domain Technique: Finite Difference Time Domain

Finite Difference Time Domain (FDTD) is a popular electromagnetic modeling technique. It is easy to understand, easy to implement in software, and since it is a time domain technique it can cover a wide frequency range with a single run.

The FDTD method belongs in the general class of differential time domain numerical modeling methods. Maxwell's equations (differential form) are simply modified to central-difference equations, discretized, and implemented in software. The equations are solved in a leap-frog manner, that is, the electric field is solved at a given instant in time, then the magnetic field are solved at the next instant in time, and the process is repeated over and over again. The FDTD method divides the space of interest (computational domain) into cubic cells. The E and H fields will be determined at every point within the computational domain. The material of each cell must be specified. Typically, the material will be either free-space (air), metal (perfect electrical conductor (PEC)), or dielectrics, any material can be used, as long as the permeability, permittivity, and conductivity can be specified.

Since FDTD requires that the entire computational domain be gridded, and these grids must be small compared to the smallest wavelength and smaller than the smallest feature in the model, very large computational domain can be developed which result in very long solution times. Models with long, thin features are difficult to model in FDTD because of the excessively large computational domain required.

The processing speed and the memory capacity of computers have rapidly been progressing, and the FDTD method that solves the Maxwell's equations by the method of difference becomes a practical choice in the field of antenna analysis [35], [42]. At present, even a personal computer can be used for the FDTD analysis, and this circumstance occurs to the authors to analyze the lightning electromagnetic fields by the FDTD method.

2.4.1 FDTD Formulation

The Maxwell's equations in the Cartesian coordinates are as follows assuming no anisotropic and/or dispersive medium in the space of interest.

$$\nabla \times \mathbf{E} = -\mu \frac{\partial \mathbf{H}}{\partial t}, \quad \nabla \times \mathbf{H} = \varepsilon \frac{\partial \mathbf{E}}{\partial t} + \sigma \mathbf{E} \quad (2.28)$$

$$\nabla \cdot \mathbf{E} = \frac{\rho}{\varepsilon}, \quad \nabla \cdot \mathbf{H} = 0 \quad (2.29)$$

where \mathbf{E} : electric field, \mathbf{H} : magnetic field, ρ : charge density, ε : permittivity, μ : permeability, σ : conductivity, and all the quantities are in MKSA units. Discretizing the analysis space by a small length Δs in all the directions, the space is filled with cubes of which the sides are Δs , and the cube is called "cell". Assume that the number of divisions of the analysis space along the x coordinate is N_x , along the y coordinate N_y , and along the z coordinate N_z . The analysis space is given by the following range.

$$\begin{aligned} x &= i\Delta s, (0 \leq i \leq N_x), \quad y = j\Delta s, (0 \leq j \leq N_y), \\ z &= k\Delta s, (0 \leq k \leq N_z) \end{aligned} \quad (2.30)$$

Equation (2.28) includes derivatives with respect to position x , y , z , and time t . In the FDTD formulation, representing values of electric and magnetic fields in a cell is configured by turns as shown in Fig. 2.6, and this yields the replacement of the derivatives with respect to x , y , and z in (2.28) with the following central difference.

$$\frac{\partial f(x)}{\partial x} \equiv \frac{f(x + \Delta s/2) - f(x - \Delta s/2)}{\Delta s} \quad (2.31)$$

In the above equation, f is a component of \mathbf{E} or \mathbf{H} , and the same equation is valid also to y and z .

The same central difference shown in the following equation replaces the derivatives with respect to time in (2.28), assuming that electric fields are calculated at time steps $t = n\Delta t$ ($n = 0, 1, \dots$) and magnetic fields at $t = (n + 1/2)\Delta t$ ($n = 0, 1, \dots$) by turns.

$$\frac{\partial f(t)}{\partial t} \equiv \frac{f(t + \Delta t/2) - f(t - \Delta t/2)}{\Delta t} \quad (2.32)$$

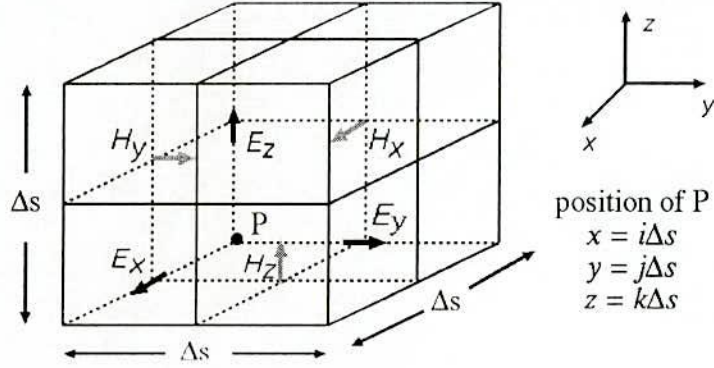


Fig. 2.6. Configuration of electric and magnetic fields in cell.

Applying (2.31) and (2.32) to (2.28) yields the following difference equations (e.g. $E_x^n(i+1/2, j, k)$ represents x component electric field at position $x = (i+1/2)\Delta s$, $y = j\Delta s$, $z = k\Delta s$, and at time $t = n\Delta t$, and the other components are expressed in the same manner). A detail of the FDTD formulation is given in Appendix C.

$$H_{x(i,j,k)}^{n+\frac{1}{2}} = H_{x(i,j,k)}^{n-\frac{1}{2}} - K_3[\{E_{z(i,j,k)}^n - E_{z(i,j,k)}^{n-1}\} - \{E_{y(i,j,k)}^n - E_{y(i,j,k)}^{n-1}\}] \quad (2.33)$$

$$H_{y(i,j,k)}^{n+\frac{1}{2}} = H_{y(i,j,k)}^{n-\frac{1}{2}} - K_3[\{E_{x(i,j,k)}^n - E_{x(i,j,k)}^{n-1}\} - \{E_{z(i,j,k)}^n - E_{z(i,j,k)}^{n-1}\}] \quad (2.34)$$

$$H_{z(i,j,k)}^{n+\frac{1}{2}} = H_{z(i,j,k)}^{n-\frac{1}{2}} - K_3[\{E_{y(i,j,k)}^n - E_{y(i,j,k)}^{n-1}\} - \{E_{x(i,j,k)}^n - E_{x(i,j,k)}^{n-1}\}] \quad (2.35)$$

$$E_{x(i,j,k)}^{n+1} = K_1 E_{x(i,j,k)}^n + K_2[\{H_{z(i,j,k)}^{n+\frac{1}{2}} - H_{z(i,j,k-1)}^{n+\frac{1}{2}}\} - \{H_{y(i,j,k)}^{n+\frac{1}{2}} - H_{y(i,j,k-1)}^{n+\frac{1}{2}}\}] \quad (2.36)$$

$$E_{y(i,j,k)}^{n+1} = K_1 E_{y(i,j,k)}^n + K_2[\{H_{x(i,j,k)}^{n+\frac{1}{2}} - H_{x(i,j,k-1)}^{n+\frac{1}{2}}\} - \{H_{z(i,j,k)}^{n+\frac{1}{2}} - H_{z(i-1,j,k)}^{n+\frac{1}{2}}\}] \quad (2.37)$$

$$E_{z(i,j,k)}^{n+1} = K_1 E_{z(i,j,k)}^n + K_2[\{H_{y(i,j,k)}^{n+\frac{1}{2}} - H_{y(i-1,j,k)}^{n+\frac{1}{2}}\} - \{H_{x(i,j,k)}^{n+\frac{1}{2}} - H_{x(i,j-1,k)}^{n+\frac{1}{2}}\}] \quad (2.38)$$

In the derivation of the above equations, an approximation $\sigma \mathbf{E}^{n-1/2} \cong \sigma \{\mathbf{E}^{n-1} + \mathbf{E}^n\} / 2$ is used, and coefficients K_1 , K_2 , and K_3 are given by the following equations.

$$K_1 = \frac{1 - \frac{\sigma \Delta t}{2\epsilon}}{1 + \frac{\sigma \Delta t}{2\epsilon}}, \quad K_2 = \frac{\Delta t}{\epsilon \Delta s} \frac{1}{1 + \frac{\sigma \Delta t}{2\epsilon}}, \quad K_3 = \frac{\Delta t}{\mu \Delta s} \quad (2.39)$$

Equations (2.33) – (2.38) are the FDTD formulas of the Maxwell's equations, and transient fields are obtained by calculating electric and magnetic fields by turns at time intervals $\Delta t/2$. Although (2.29) is not explicitly formulated, it can be proved that (2.33) – (2.38) automatically satisfies (2.29) [Appendix C].

2.4.2 Time Step and Space Step

Equations (2.33) – (2.38) are considered as numerical integration, and stable integration is performed if the following condition is satisfied (Courant's condition) [36].

$$\Delta t / \sqrt{\mu\epsilon} \leq \Delta s / \sqrt{3} \quad (2.40)$$

On the other hand, the grid dispersion error is minimized when the above relation is equated. Thus, the following formula is used in all calculations in this thesis to determine time step interval Δt from user defined space step Δs .

$$\Delta t = \Delta s \sqrt{\mu\epsilon / 3(1 - \alpha)} \quad (2.41)$$

α is a small positive value specified by a user in order to prevent instability of the numerical integration due to round-off error in (2.33) – (2.41).

2.5 General Surge Analysis Program: VSTL

This research work employs the surge analysis program named VSTL (Virtual Surge Test Lab.) based on the above FDTD method. VSTL has been developed by Noda *et al.* [39] from scratch at Central research institute of electric power industry (CRIEPI) since late 1999, and continuous development is being carried out. VSTL is one of the registered programs of CRIEPI which are available to Japanese electric power utilities and to non-profitable research groups in the world. By use of the FDTD method, the developed program is inherently able to take into account the geometrical features of a simulated structure, unlike electromagnetic transient program (EMTP)-type circuit-based transient programs. Thus, the program is advantageous to solve both the following problem types:

1. Surge propagation on a three-dimensional circuit (3D skeleton structure).
2. Surge propagation inside a three-dimensional imperfectly conducting medium such as earth soil.

The method of moments (MoM) also numerically solves the Maxwell's equations [22], and NEC-2 is a well-known program based on MoM [24]. Although NEC-2 efficiently solves the type (1) problems, it cannot solve the type (2) ones except very simple cases, because the handling of three-dimensional current distribution in the imperfectly conducting medium is complicated [43]. On the other hand, FDTD is inherently able to solve both the problem types efficiently. One weak point of FDTD is the treatment of a thin wire. Thus, a field correction method to accurately treat the radius of the thin wire is proposed in [39] and implemented in VSTL ("thin wire" is defined a wire of which the radius is smaller than the size of a discretized cell).

2.5.1 Thin Wire Representation

If the space step were chosen to be small enough to represent the shape of wire's cross section, an accurate representation would be possible. However, it requires impractical computational resources at this moment. In antenna simulations, the thin wire mainly used to represent an antenna element-the most important part. In surge analysis, it is also important to represent power lines, steel frames, and so on.

Umashankar *et al.* [44] proposed a method to represent the radius of a thin wire with a reasonably large Δs , by correcting adjacent magnetic fields around the wire. It is reported in [45] that this method is valid for the calculation of radiated fields by an antenna. However, Umashankar's method does not give accurate surge impedance [46].

In VSTL, thin wire representation corrects both the adjacent electric and magnetic fields around the wire according to its radius and gives accurate surge impedance [46]. Fig. 2.7(a) shows a wire with radius r placed in the z direction, and the permittivity and permeability of the space are ϵ and μ . Fig. 2.7(b) is the cross section of the wire with the adjacent four electric fields, and Fig 2.7(c) with the adjacent four magnetic fields.

In the FDTD analysis, the basic concept of thin wire representation is forcing the electric field along the center line of the wire to be zero, and E_z components are forced to zero in this case. In order to take into account the effect of the thin-wire radius r , the VSTL uses

the following corrected permittivity to calculate the adjacent four electric fields E_{x1} , E_{x2} , E_{y1} , and E_{y2} in equations (2.33) – (2.35).

$$\epsilon' = m\epsilon, (\epsilon : \text{permittivity of medium}) \quad (2.42)$$

And the following corrected permeability to calculate the adjacent four magnetic fields H_{x1} , H_{x2} , H_{y1} , and H_{y2} in equations (2.36) – (2.38).

$$\mu' = \mu/m, (\mu : \text{permeability of medium}) \quad (2.43)$$

where the correction factor m is given by

$$m = \frac{1.471}{\ln(\Delta s/r)} \quad (2.44)$$

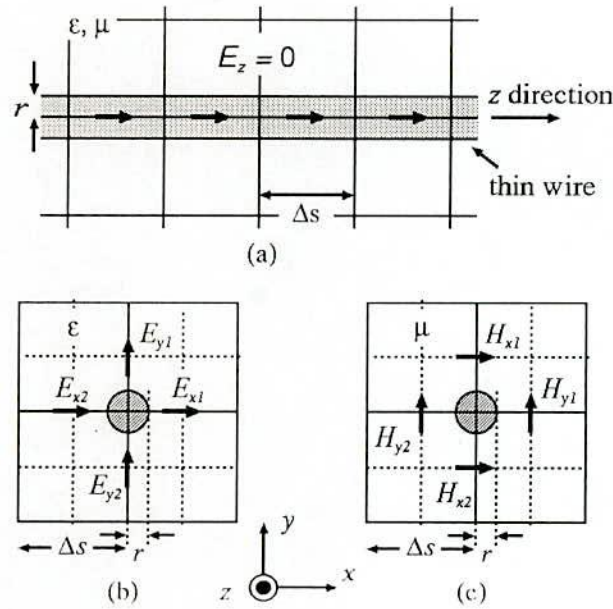


Fig. 2.7. Thin wire and configuration of adjacent electric and magnetic fields.

2.5.2 Boundaries and Earth Plane

Each boundary of the analysis space can independently be defined as a perfectly-conducting plane or an absorbing plane. The perfectly conducting plane can easily be represented by forcing the tangential components of electric fields at the boundary to be zero. The second-order Liao's method [47] is used to represent the absorbing plane, because it is more accurate and requires less memory compared with other methods. An

open space can be assumed by applying the absorbing plane to all the boundaries of the analysis space.

The goal of lightning analysis is usually to find the solution for a 3D skeleton structure above either an imperfectly or perfectly-conducting earth. In the FDTD calculation, the representation of the conducting earth with arbitrary resistivity ρ_e can be accomplished by setting the value of σ in (2.39) to $1/\rho_e$ in the region defined as the earth soil.

The geometrical shape of most power equipments can be represented by a combination of several rectangular-parallelepiped objects, and thus, a rectangular-parallelepiped conductor model is available in VSTL. The rectangular-parallelepiped conductor is simply modeled by forcing the tangential electric fields on its surface to be zero.

2.5.3 Localized Voltage and Current Sources

Unlike the static electric fields, the transient electric fields do not satisfy $\nabla \times \mathbf{E} = 0$. Thus, in the analysis of transient fields, the voltage or the voltage differences do not make sense in general. But, if we take note of an electric field component of a cell, the voltage difference across a side of the cell can reasonably be defined as $V = E\Delta s$, because waves of which the wave length is shorter than $\lambda = 2\Delta s$ do not present in the FDTD calculation due to the bandwidth limitation of Δs . Therefore, we can model a localized voltage source by forcing an electric field component at a specified position in a specified direction to be a specified waveform.

For example, in order to place a voltage source of which the waveform is given by $V^n = V(n\Delta t)$ at $x = i\Delta s$, $y = j\Delta s$, $z = (k + 1/2)\Delta s$ in the z direction, the following equation is used to force the electric field value.

$$E_{z(i,j,k+1/2)}^n = -\{V^n - RI^{n-1/2}\} / \Delta s \quad (2.45)$$

where R is the internal resistance of the voltage source specified by a user (it can be set to zero), and current I is given by the following equation as shown in Fig. 2.8.

$$I^{n-1/2} = \{H_{x(i,j-1/2,k+1/2)}^{n-1/2} - H_{x(i,j+1/2,k+1/2)}^{n-1/2} + H_{y(i+1/2,j,k+1/2)}^{n-1/2} - H_{y(i-1/2,j,k+1/2)}^{n-1/2}\} \Delta s \quad (2.46)$$

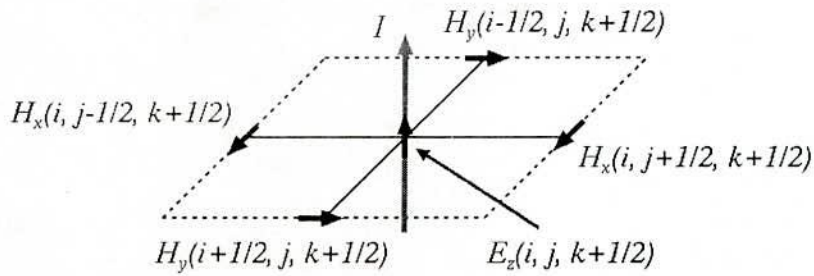


Fig. 2.8. Calculation of current by Ampere's Law.

In the case of a current source, because current itself is a general quantity even in the transient fields, it can be modeled by modifying an electric field component at a specified position in a specified direction as in the following example. In order to place a current source of which the waveform is given by $I^n = I(n\Delta t)$ at $x = i\Delta s$, $y = j\Delta s$, $z = (k + 1/2)\Delta s$ in the z direction, the following term is added to (2.35).

$$-\frac{\Delta t / \epsilon}{1 + \frac{\sigma \Delta t}{2\epsilon}} \frac{I^{n-1/2}}{\Delta s^2}, \quad (2.47)$$

where $\sigma = 1/(R\Delta s)$, and R is the internal resistance of the current source specified by a user (also, it can be set to zero).

2.5.4 Calculation Procedure and Output

The flow chart of the calculation procedure of VSTL is shown in Fig. 2.9. The entire electric field is calculated by the equations (2.36)-(2.38) and the entire magnetic field by equations (2.33)-(2.34). Localized voltage differences and current intensities at a specified position in a specified direction are included in the output of VSTL. The waveform of the localized voltage difference is calculated by $V = E\Delta s$, and that of the current intensity by (2.46). Animation of electric or magnetic field distribution in an arbitrary section is also included in the output. This type of display is extremely useful to understand exactly what is going on in the model, and to help insure that the model is working correctly. Electric field strength is calculated as the root-mean-square value of the two tangential components in the section, and magnetic field strength as the absolute value of the normal component in the section. The visualization is carried out by transferring data to MATLAB.

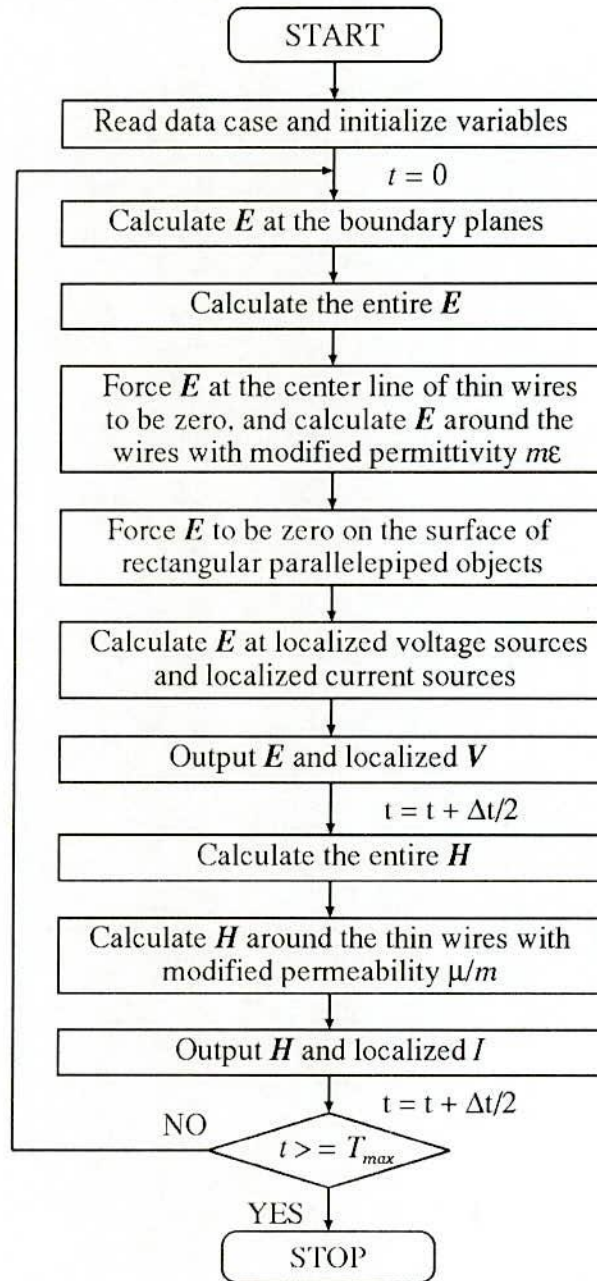


Fig. 2.9. Calculation procedure of program VSTL.

Chapter 3

Lightning Return Stroke to Ground

3.1 Introduction

According to various simple and widely used lightning return stroke models, the lightning return stroke can be treated as a current pulse originating at ground level and traveling along the leader channel with constant velocity without attenuation and dispersion. One would obtain the same result if the return stroke were treated as a current wave propagating along the channel of perfect electrical conductor with the current injection point at ground level. In reality, the leader channel has a certain resistance. Moreover, experimental results show that the propagation velocity of this current wave is less than the light velocity [48], [49]. The main purpose of this chapter is to simulate the return stroke as a current waveform propagating along a perfect channel with current injection at the base of the channel, and to study how the predicted properties of the model vary as the simplifications are removed one by one thus bringing the model closer to the reality. Moreover, how the ground conductivity affects the propagation of current along the channel and the lightning electromagnetic fields are shown.

With different methodologies, different input data are involved in the lightning analysis: one of them is related to the lightning current itself (e.g., peak value, time-to-peak and rate of rise) [50]. The effect of different current waveshapes is also investigated in the present chapter.

3.2 Model of the Analyzing System

In the present section, a model of lightning channel to be used in the following sections is studied. To simulate the lossy channel and the slower propagation velocity of a return stroke current pulse, a vertical conductor loaded uniformly by series resistance and inductance is employed. Fig. 3.1 shows the channel of 1500 m in length which is firstly, taken as perfect electrical conductor and then loaded by series resistance and inductance

step by step. To simulate the source of lightning return stroke current a pulse generator (PG) having internal resistance of 400Ω is placed at the ground level. For the numerical analysis, the conductor is divided into cylindrical segments of 25 m in length and 0.3 m in radius.

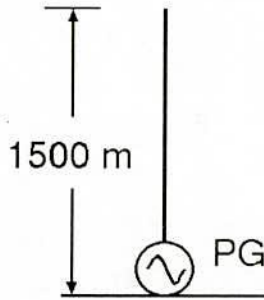


Fig. 3.1. Model for the analysis of lightning return stroke to ground.

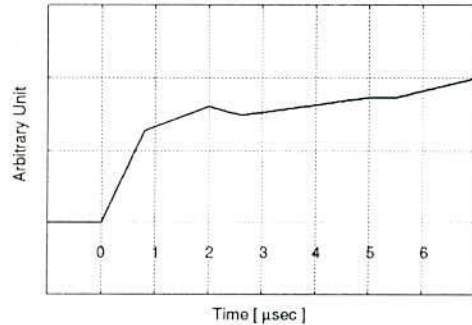


Fig. 3.2. Waveform of voltage source to simulate the first return stroke.

3.3 Representing the Leader Channel as a Perfect Conductor

Assume that the leader channel is a perfect conductor. During the return stroke a current pulse is injected into this conductor from the ground end of the leader channel. This current pulse will propagate along the channel with the speed of light without any distortion or attenuation. The current waveform injected at the base of the channel is assumed to be identical to the current waveform postulated by Y. Baba and M. Ishii [28] which is shown in Fig. 3.2. This waveform is used to simulate the first return stroke.

Fig. 3.3 shows the calculated waveforms of a propagating current wave along the perfect channel. The available experimental data indicate that with increasing height the amplitude of the optical signature decreases and its rise time increases [51]. Since in electrical sparks, the optical signature is strongly correlated to the current waveform [52], both in amplitude and the shape of the rising part, the above observation indicates that the peak current of the return stroke decreases with height while its rise time increases.

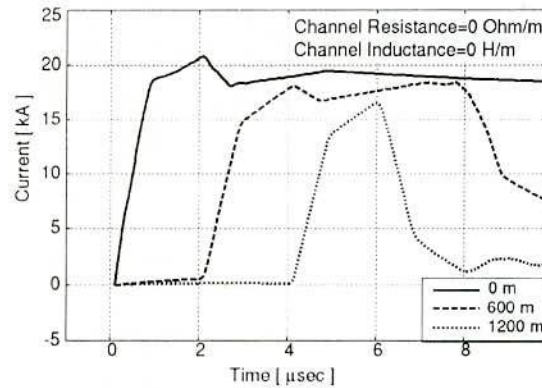


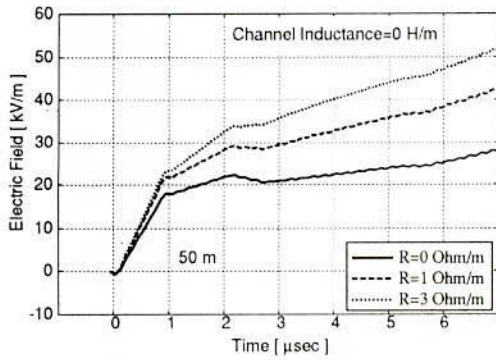
Fig. 3.3. Current along the lightning channel of perfect conductor.

The solid lines of Fig. 3.4 show the computed waveforms of vertical electric fields at distance of 50 m, 2 km, and 100 km from the struck point. The solid lines of Fig. 3.5 show that of azimuthal magnetic field. Downward electric field is defined positive in this work, following the atmospheric field convention. Observe that the electric field at 50 m is mainly electrostatic, the electric field at 100 km is mainly radiation and the electric field at 2 km is a combination of static, induction and radiation. The transient vertical electric field component depends on the return stroke current and the static component depends on the electric charge configuration. The magnetic fields have only the induction and radiation terms rather than the static component. Distant electric and magnetic fields have essentially identical waveshapes.

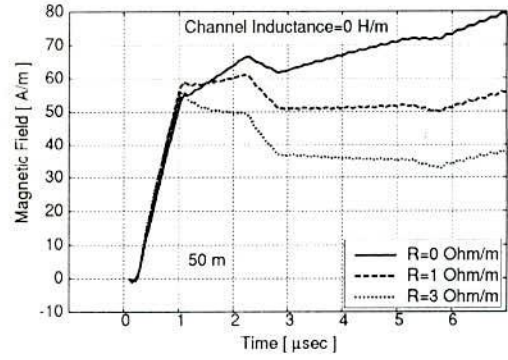
It is worth mentioning that the contribution of the various components of the electric and magnetic fields depends strongly on the distance to the observation point. At closer observation points (less than a few hundred meters), the radiation-term contribution to the field magnitude is small compared to contributions from the static and induction terms. However, at distances beyond some tens of kilometers, the contribution of the radiation term will become predominant and the static and induction terms will have a negligible effect [53].

Let us now consider the features of the model for simulated electric and magnetic fields at 50 m and compare them with the available experimental data. As the work studied, may be no information is available today on the electric fields at 50 m generated by natural return stroke. However, experimental data is available for subsequent return strokes in rocket-

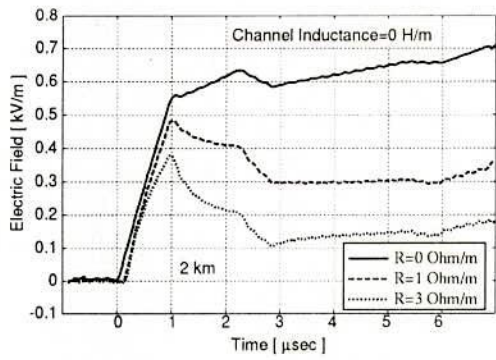
triggered lightning [54]. This experimental data shows that the electric field at 50 m rises to its peak value in a few microseconds and then remains more or less constant with increasing time.



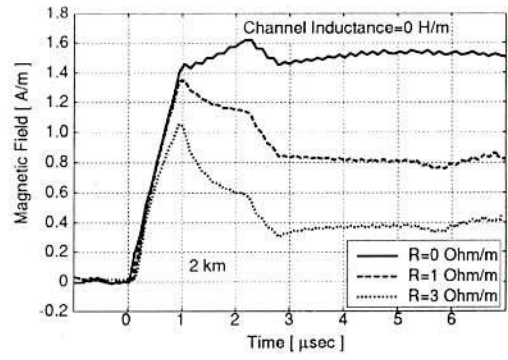
(a)



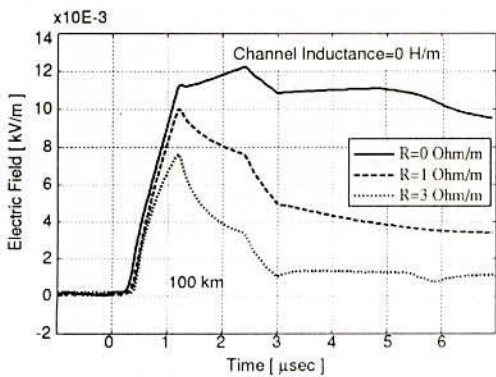
(a)



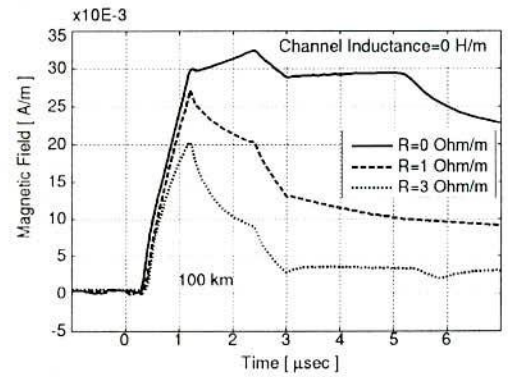
(b)



(b)



(c)



(c)

Fig. 3.4. Vertical electric field for different channel resistance at (a) 50 m (b) 2 km and (c) 100 km from the lightning channel in case of ground stroke.

Fig. 3.5. Azimuthal magnetic field for different channel resistance at (a) 50 m (b) 2 km and (c) 100 km from the lightning channel in case of ground stroke.

In ref. [53] there are examples of the measured electric and magnetic fields at distances from 1 km to 200 km from the lightning channel for both the first and subsequent return strokes. In order to validate the model with the measured electromagnetic fields at intermediate distances this work has presented the simulated electromagnetic fields at 2 km and 100 km and this will be compared with the measurements. A typical example of the measured electric and magnetic fields at 2 km is shown in Fig. 3.6 [53].

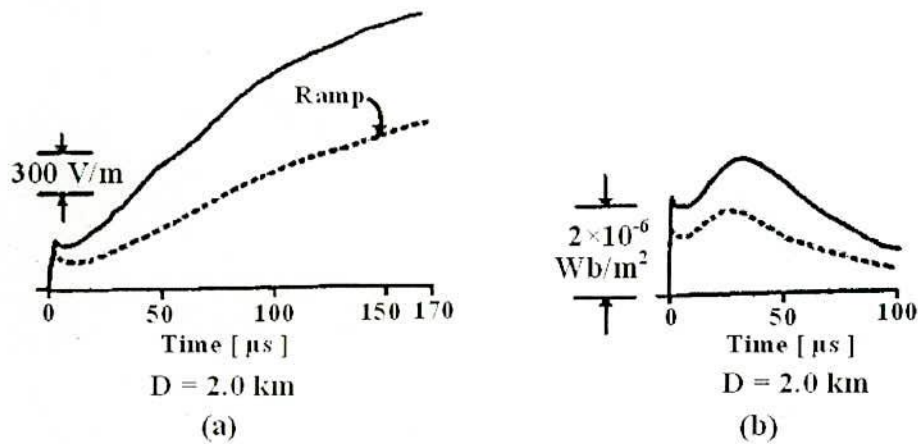


Fig. 3.6. Typical example of (a) electric and (b) magnetic field at 2 km for first (solid line) and subsequent (dotted line) return strokes in case of stroke at ground level [53].

Consider the electric fields at 2 km. From Fig. 3.4 (b) the field at 2 km is characterized by a fast rising part mainly due to the radiation component, one or two subsidiary peaks followed by a ramp increase due to static term. In the case of ideal transmission line, the far field composed of radiation component has the same shape as that of the current waveform [55]. As the initial part of field waveform at 2 km is dominated by the radiation components; therefore by using the relationship of the TL model, the peak value of the current propagating up the vertical conductor can be estimated from the peak field values.

The estimated peak current from the vertical electric field of Fig. 3.4 (b) is 20.7 kA, for $v = c$. This result roughly assures the validity of the numerical analysis with NEC-2. The small difference between the two estimated values may come from that the fields at the distance of 2 km from the lightning channel is not pure radiation fields. Now let us see the magnetic field behavior at 2 km. The main features are that unlike the electric field it has one subsidiary peak after which the field decreases.

Significant amount of information is available on the characteristics of radiation fields generated by lightning flashes [53], [56]. Fig. 3.7 provides example of the radiation fields generated by subsequent return strokes. The radiation field begins with an initial slow ramp followed by a fast transition, which will culminate in an initial peak. After the initial peak the radiation field shows one or two subsidiary peaks located within a few microseconds from the beginning of the waveform. The experimental data also show that the rate of decay of the electric radiation field after the initial peak is faster than that of the corresponding decay of the current waveform [57].

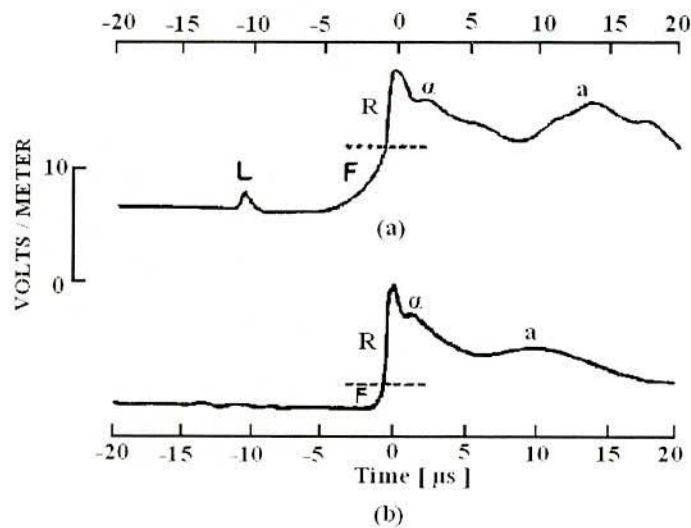


Fig. 3.7. Typical example of radiation electric fields due to (a) first return stroke (b) subsequent return strokes to ground [56]. The waveforms are normalized to a distance of 100 km.

The estimated peak current from the vertical electric field of Fig. 3.4 (c) is 20.5 kA, for $v = c$. For the field at 2 km and 100 km both the electric and magnetic fields resemble the current waveform of channel. However, the simulated result of electromagnetic fields at 2 km and 100 km do not satisfy the each observation of experimental result.

3.4 Effect of Channel Resistance

In reality, neither the leader nor the return stroke channel is a perfect conductor and, therefore, one has to take into account the channel resistance. Figs. 3.3, 3.8 (a) and (b)

show the calculated current along the channel corresponding to the channel resistances of $0 \Omega/\text{m}$, $1 \Omega/\text{m}$ and $3 \Omega/\text{m}$, respectively. If the potential gradient of the dart leader channel is about a few thousands of volts per meter, then the resistance per unit length of the dart leader channel is about a few ohms per meter. The values of the resistances used in our calculation lie in this range.

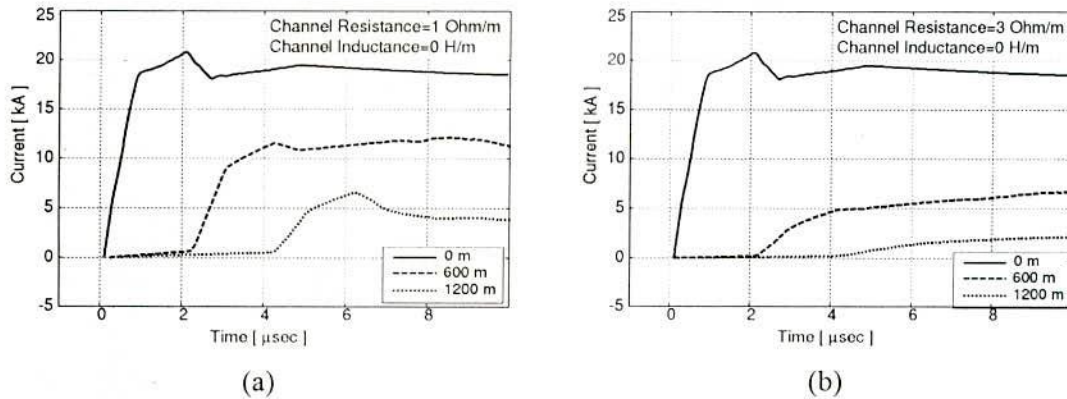


Fig. 3.8. Current along the lightning channel for channel resistance of (a) $1 \Omega/\text{m}$ and (b) $3 \Omega/\text{m}$.

The corresponding electromagnetic fields generated by the return stroke at 50 m, 2 km, and 100 km for different channel resistances are shown in Figs. 3.4 and 3.5. The peak electric field and the peak electric field derivatives of the radiation field at 100 km corresponding to different channel resistances are tabulated in Table 3.1.

The main effect of the channel resistance is a reduction and a lengthening of the peak current with height. The reduction in the current amplitude is significant both at the wave-front and at the wave-tail. Observe that for the increasing channel resistance, peak current decreases with height more rapidly than that of the corresponding decrease of the peak current without resistance. At each height a fraction of the upward propagating current waveform is reflected leading to a decrease in current amplitude. In the case of finite resistance even though the peak current amplitude decreases with height, the total charge flowing along a given channel section is the same. That means the decrease in the peak current with height should be compensated by an increase and lengthening of the current tail. It is shown [Figs. 3.3 and 3.8] that the channel resistance does not affect the propagation velocity of lightning current along the channel.

Table 3.1

Peak value and maximum steepness of E-field at 100 km for different channel parameters.

Channel Resistance (Ω/m)	Channel Inductance ($\mu H/m$)	Maximum E-Field (kV/m)	Maximum Steepness of E-Field (kV/m/ μs)	Effective Speed (m/s)
0	0	12.16e-3	12.78e-3	3.0e8
1	0	10.0e-3	15.14e-3	3.0e8
3	0	7.65e-3	16.32e-3	3.0e8
1	1	8.04e-3	11.88e-3	2.1e8
1	3	5.91e-3	9.81e-3	1.5e8

When the channel resistance is taken into account the electric field at 50 m, instead of decaying, it continues to rise within the time window of calculation [Fig. 3.4(a)]; in disagreement with the experiment in ref. [54]. But the peak of magnetic field decreases as the current along the channel decreases [Fig. 3.5(a)]. At 2 km with constant channel resistance [Figs. 3.4(b) and 3.5(b)] it is seen that both the electric and the magnetic field decreases after the first peak and remains constant which is again in disagreement with experimental result shown in Fig. 3.6. The fields at 100 km show that introduction of a finite resistance into the channel causes a reduction in the field peak and after which the field decreases more rapidly which satisfy the experimental result shown in Fig. 3.7. It is found in our analysis that the field derivative increases as the channel resistance increases.

3.5 Effect of Channel Inductance

The actual speeds of the return stroke measured the average of which lie in the range of $1.0-2.0 \times 10^8$ m/s [49]. To simulate the lossy and slower propagation velocity of current pulse along the channel, uniformly distributed resistance of $1 \Omega/m$ and inductance of $1 \mu H/m$ and $3 \mu H/m$ is considered in this work. According to transmission line model (TLM) the presence of channel resistance causes attenuation and dispersion of the current waveform, leading to a slower and slower rise time with increasing height shown in Fig. 6 of ref. [58] which is generally not in agreement with the electromagnetic model. No TL model is able to generate the correct return stroke speed [58].

Moini *et al.* [18] represented a lightning channel by a vertical conductor, and the slower propagation velocity of current in the channel, $0.43 c$, was realized by changing the permittivity of the surrounding medium. By this method, the characteristic impedance of the simulated channel becomes lower than the actual case.

Figs. 3.9(a) and (b) show the current waveforms for the inductance of $1 \mu\text{H/m}$ and $3 \mu\text{H/m}$, respectively. Fig. 3.8(a) may be considered here for zero inductance. Observe that the rise time increases with the increasing inductance and also the peak current increases with height exceptionally. From figures it can be shown that the loading of $1 \mu\text{H/m}$ makes the propagation velocity about $2.1 \times 10^8 \text{ m/s}$ and $3 \mu\text{H/m}$ makes the velocity about $1.5 \times 10^8 \text{ m/s}$.

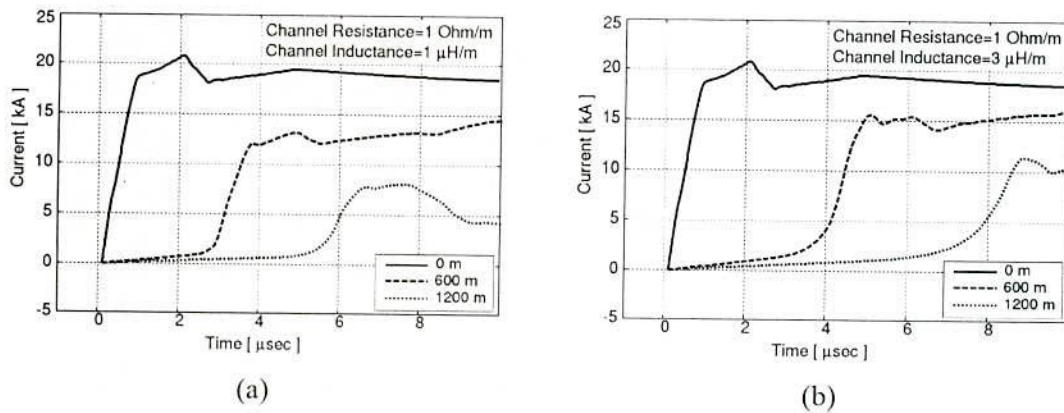
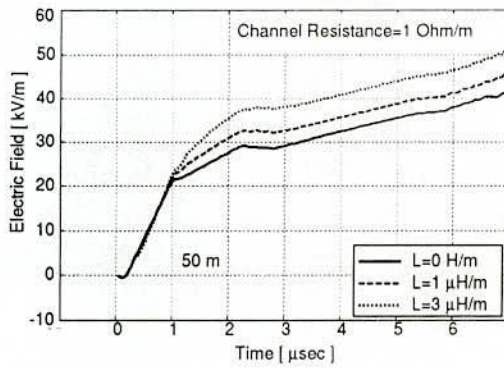
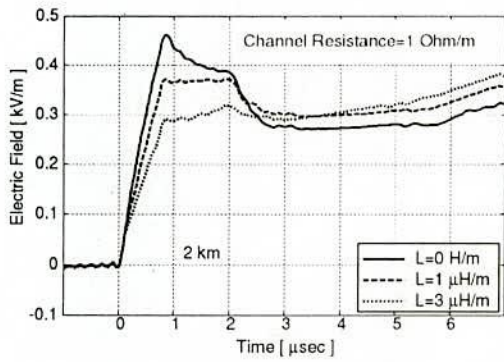


Fig. 3.9. Current along the lightning channel for channel inductance of (a) $1 \mu\text{H/m}$ (b) $3 \mu\text{H/m}$ and the resistance of $1 \Omega/\text{m}$.

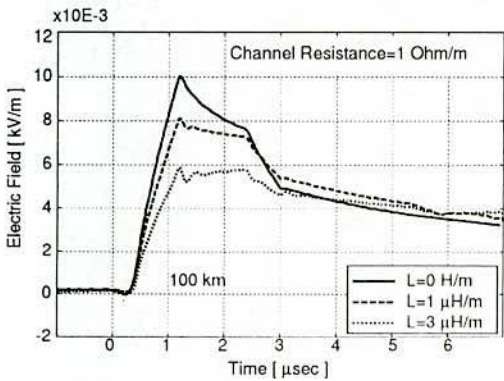
Figs. 3.10 and 3.11 show the electric field and magnetic field, respectively at different distances corresponding to the current in Fig. 3.8(a) and Fig. 3.9. As like constant resistance the electric field at 50 m also increases monotonically with ramp feature. Though the peak of magnetic field at 50 m is not affected by the channel inductance the wave tail increases slowly. However significant changes are observed in the field at 2 km. The peak of both the electric and magnetic field [Figs. 3.10(b) and 3.11(b)] decreases but observe how the tail of the field waveform recovers with increasing inductance and going to closer to the experimental result shown in Fig. 3.6. From Figs. 3.10(c) and 3.11(c) it can be seen the peak value of the fields decreases with increasing inductance and their derivative also decreases which are shown in Table 3.1.



(a)

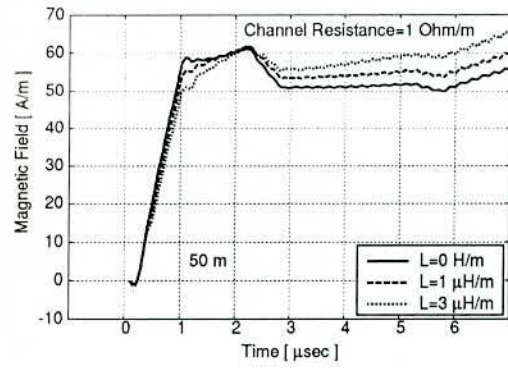


(b)

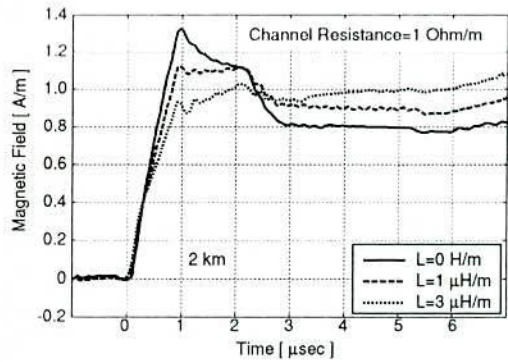


(c)

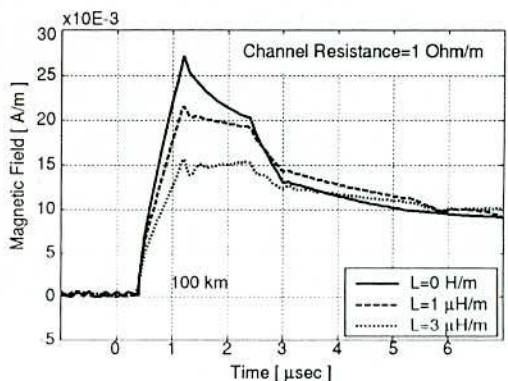
Fig. 3.10. Vertical electric field for different channel inductance at (a) 50 m (b) 2 km and (c) 100 km from the lightning channel in case of ground stroke.



(a)



(b)



(c)

Fig. 3.11. Azimuthal magnetic field for different channel inductance at (a) 50 m (b) 2 km and (c) 100 km from the lightning channel in case of ground stroke.

It is necessary to mention that all the fields are calculated at the height of 20 m from ground level. As the electric field at the distance of 50 m is static field, it depends on the distance from the source. The variation of static electric field within 10 m to 60 m height

is shown in Fig. 3.12 computing at four different levels. The average height of transmission lines, control buildings, instrumented towers etc. in our country are within this range. The magnetic field and distant electric field are dominated by induction and radiation component, so there is no significant variation of those fields' components with different height from the ground surface.

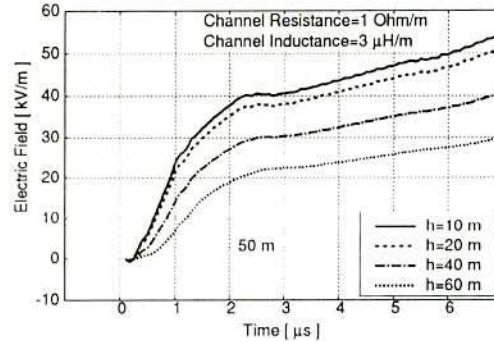


Fig. 3.12. Static electric fields at different height in case of ground stroke.

3.6 Effect of Different Input Waveforms

Although the concave profile more closely represents the front part of measured lightning current waves, the ramp and double exponential fronts are also adopted frequently [59]. Double exponential waveform is frequently used to reproduce the measured current and electromagnetic field for lightning stroke to tall structures. The waveform which is used in the previous analysis also postulated for the lightning stroke to tall structures.

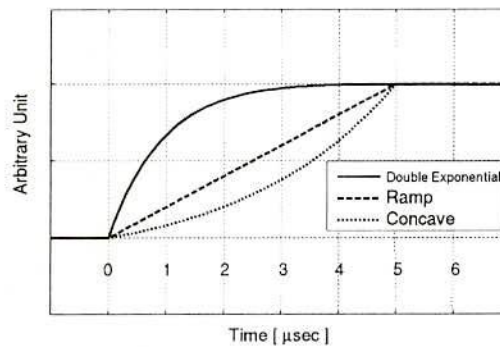


Fig. 3.13. Double exponential, ramp and concave waveforms of injected current.

For the analysis of the effect of different lightning current waveform, these three different current waveshapes, shown in Fig. 3.13, with the previous one [Fig. 3.2] were considered to be injected into the base of the channel under investigation. For comparison purposes, all three waves present the same time to peak ($5 \mu\text{s}$) and same peak value. After current peak, the waves decay linearly, reaching 50% of peak in $50 \mu\text{s}$. To keep the other parameter constant, channel on the perfect ground with resistance of $1 \Omega/\text{m}$ and inductance of $3 \mu\text{H}/\text{m}$ is considered. The source voltage is so chosen that the computed peak current at the channel base will be the same (20.5 kA) for each case.

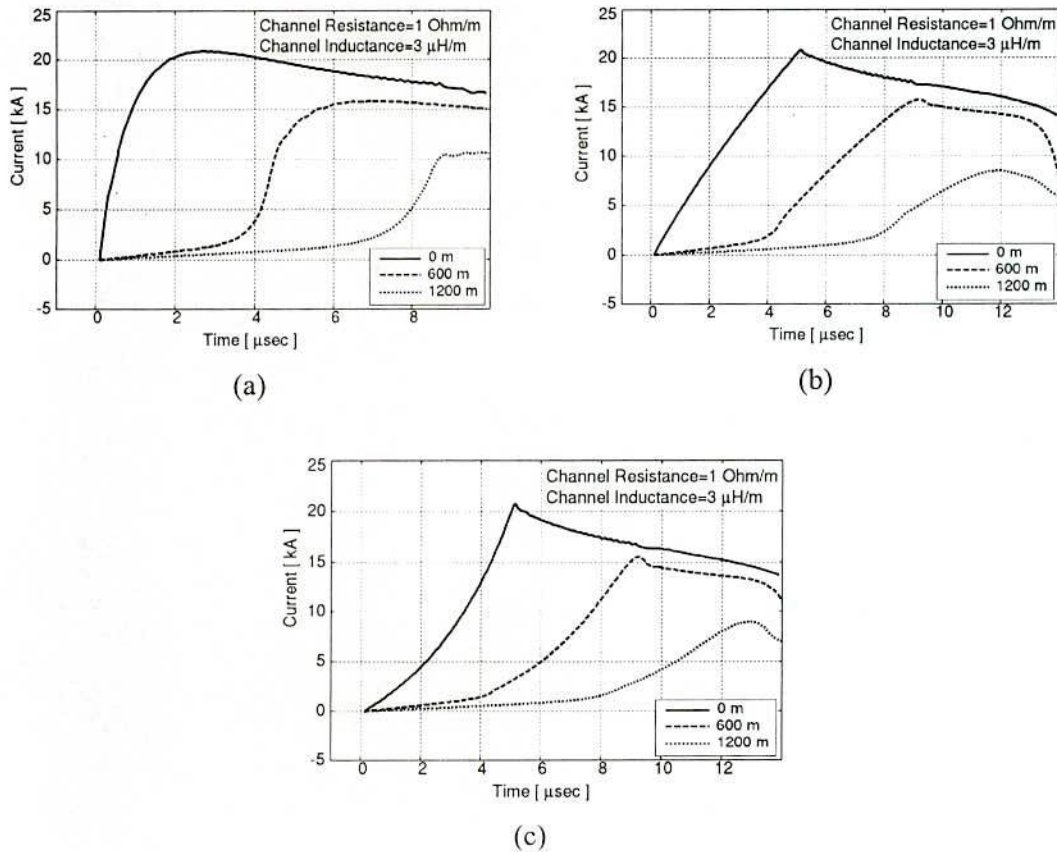
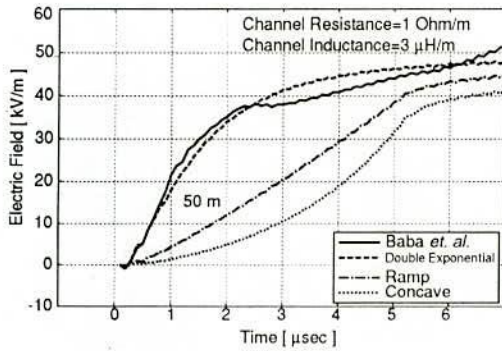


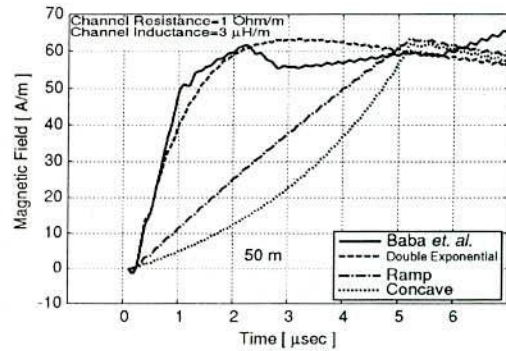
Fig. 3.14. Computed current along the lightning channel for (a) double exponential (b) ramp and (c) concave waveforms.

Fig. 3.14 presents the computed current along the channel, for each injected current wave. Quite different wave profiles and peaks are observed for the double exponential, ramp and concave responses. After $5 \mu\text{s}$, the trend of ramp and concave curves is to reach the same and peak amplitude, once the current waves become similar after this instant of time while

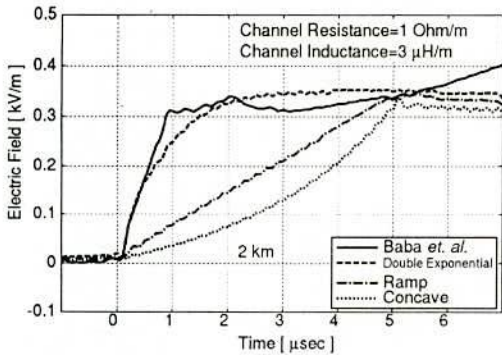
the current for other two waves reaches to peak earlier time than $5 \mu\text{s}$. It is also noticeable from Fig. 3.14 that the current along the channel for ramp and concave input decreases more rapidly than the peak current for double exponential input. The electric and magnetic field corresponding of these current are shown in Figs. 3.15 and 3.16, respectively.



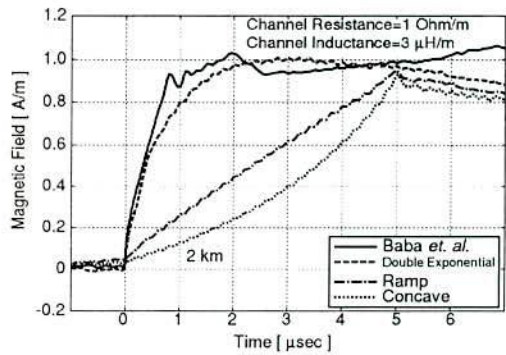
(a)



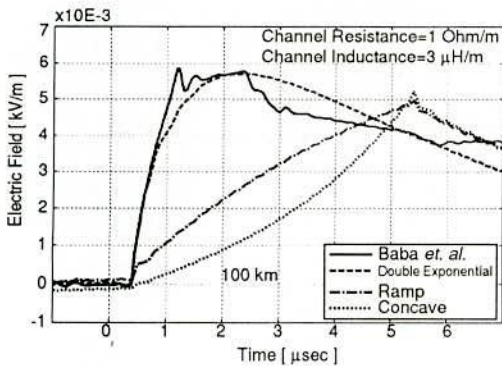
(a)



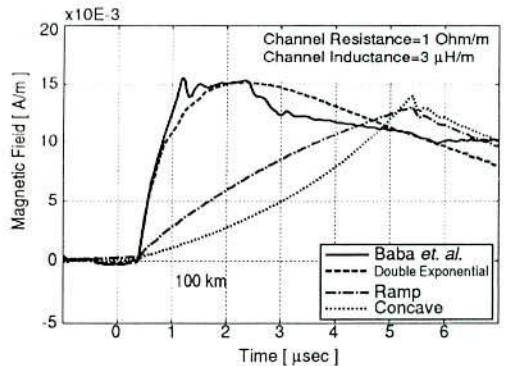
(b)



(b)



(c)



(c)

Fig. 3.15. Vertical electric field at (a) 50 m (b) 2 km and (c) 50 km from the channel for different input waveforms.

Fig. 3.16. Azimuthal magnetic field at (a) 50 m (b) 2 km and (c) 50 km from the channel for different input waveforms.

The fields for double exponential and Y. Baba's postulated waveforms are almost same while the fields for other two waves reach to the peak at larger time. The electric field of ramp and concave wave at 50 m is less than others but same at the 2 km while the magnetic fields have the same peak at 50 m and 2 km. However, at 100 km both electric and the magnetic field is less for the ramp and concave wave and also larger time to peak. Though the numerical value is not shown, it can be clearly understood from Figs. 3.15 and 3.16 that the field derivatives are larger for double exponential and Y. Baba's postulated waveforms than others which may cause larger induced voltage.

Therefore, these results have shown the importance of using representative current wave-shapes for calculation of over-voltages caused by direct strikes or electromagnetic induction. Once the analyses of lightning induced voltage and so the insulation coordination analyses are highly dependent on the resultant electromagnetic field peak and wave-shape, the choice of a nonrepresentative lightning current wave-shape may consequently lead to nonrepresentative results.

3.7 Effect of Ground Conductivity

With the result shown in Fig. 3.9(b) taking the ground as a perfect electrical conductor, two more ground conductivity: 0.01 S/m and 0.001 S/m which represents stone (limestone) and soil (sandy), respectively, are chosen for the analysis. The copper conductivity of 5.8×10^7 S/m is used in the calculation of perfect ground. Fig. 3.17 shows the computed current along the lightning channel for different ground conductivities. As shown in figure, the peak current and its rise time does not change with height for different ground conductivities but significant changes are observed at large times (i.e., in the tail). Observe how the tail of the current waveform decreases with decreasing ground conductivity.

The ground conductivity has a major effect on the waveshapes and magnitudes of the electromagnetic fields. When the electromagnetic field is propagating over a non perfect ground plane, the soil will selectively absorb the high frequency content of the electromagnetic field; causing a change in the field wave-shape.

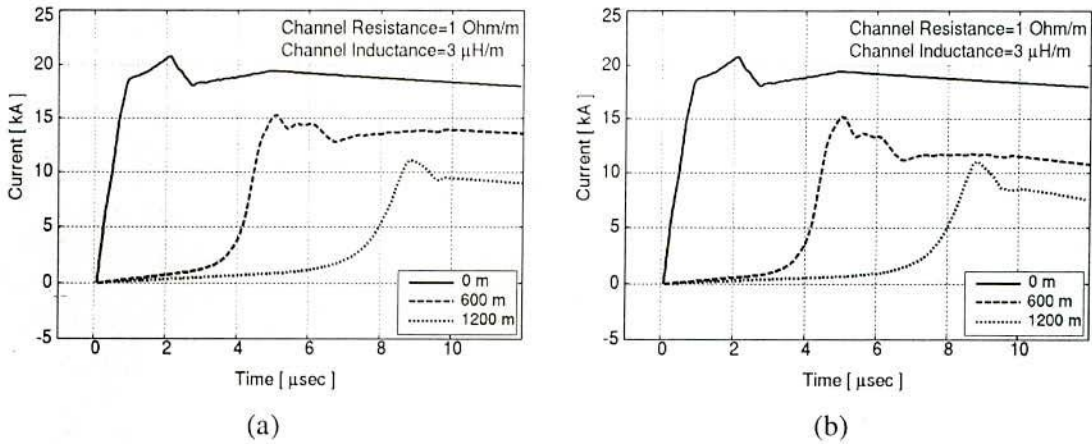
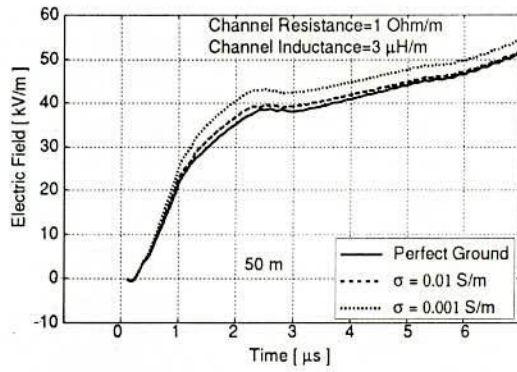


Fig. 3.17. Computed current along the lightning channel for different ground in case of stroke at ground level. The ground conductivities are taken as (a) 0.01 S/m for stone (b) 0.001 S/m for sandy soil.

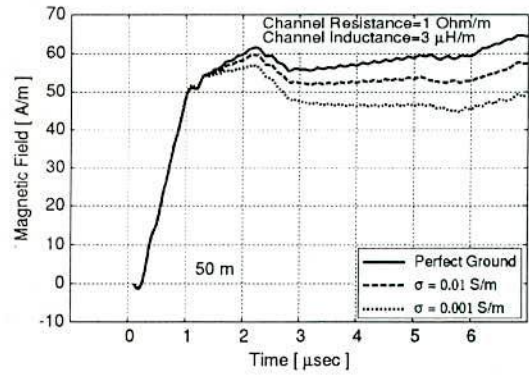
Figs. 3.18 and 3.19 show the electric and magnetic fields respectively, corresponding to the current of Fig. 3.9(b) and Fig. 3.17. In the electric and magnetic field at 50 m, a little but similar effect with the fields of different channel resistance is found. The static electric field increases while the magnetic field decreases with the decreasing ground conductivity. In the case of field at 2 km and 100 km, both the electric and magnetic field peak and their derivatives decrease while their rise time increases. The important parameters of the distant electric field waveforms for different grounds are summarized in Table 3.2.

Table 3.2
Effects of ground electrical parameter on the remote electric field.

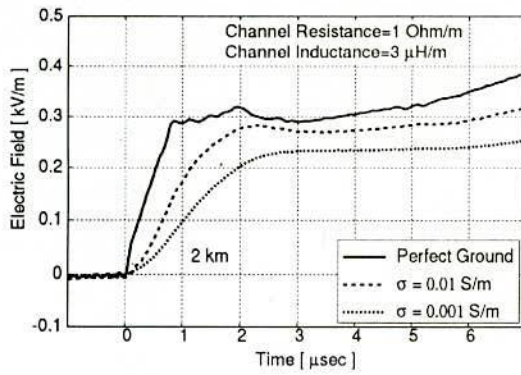
Ground Conductivity (S/m)	At 2 km		At 100 km	
	Maximum E-Field (kV/m)	Maximum Steepness of E-Field (kV/m/μs)	Maximum E-Field (kV/m)	Maximum Steepness of E-Field (kV/m/μs)
5.8×10^7	0.32	0.56	5.91×10^{-3}	9.81×10^{-3}
0.01	0.28	0.24	1.77×10^{-3}	3.48×10^{-4}
0.001	0.24	0.14	0.69×10^{-3}	1.16×10^{-4}



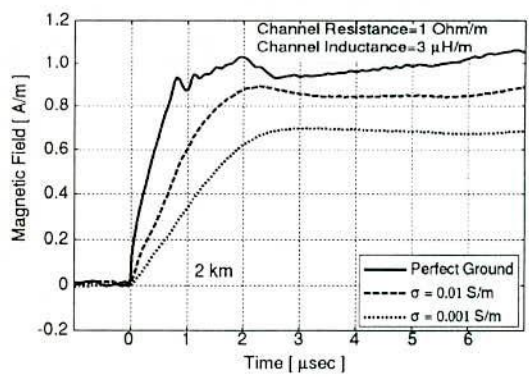
(a)



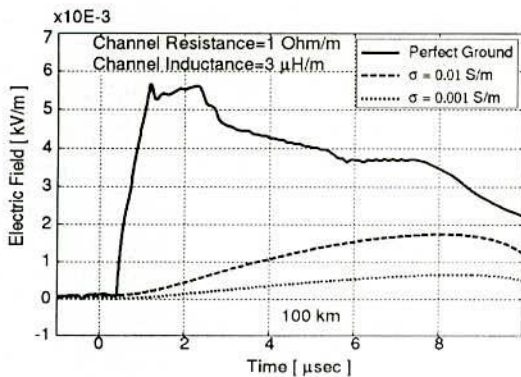
(a)



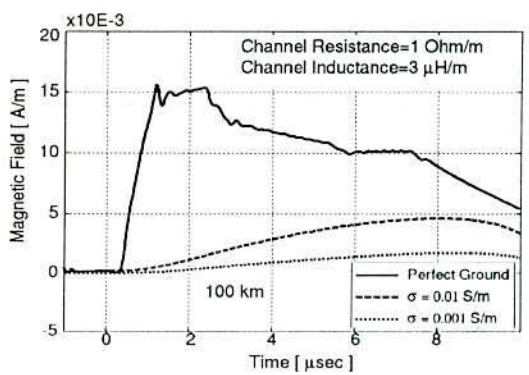
(b)



(b)



(c)



(c)

Fig. 3.18. Vertical electric field at (a) 50 m (b) 2 km and (c) 100 km from the channel in case of lightning strike to ground of perfect conductor (copper), stone and sandy soil.

Fig. 3.19. Azimuthal magnetic field at (a) 50 m (b) 2 km and (c) 100 km from the channel in case of lightning strike to ground of perfect conductor (copper), stone and sandy soil.

3.8 Effect of Subsequent Return Strokes

The subsequent return strokes that are characterized by lower current peaks but higher front steepness and return stroke speeds may be considered as an important source of electromagnetic interferences than first return strokes. To simulate the effects of subsequent return stroke the channel loaded with uniformly distributed resistance of $1 \Omega/\text{m}$ and inductance of $1 \mu\text{H}/\text{m}$ is used and the steep-front waveform as shown in Fig. 3.20 is taken as injected current. Fig. 3.21 shows the computed current propagating along the channel. For convenient comparison with the first stroke, the peak current at the channel base is kept same (20.5 kA) as in the previous analysis. Comparing Figs. 3.9(a) and 3.21, it is observed that except the steepness of the current along the channel and their time to peak, all the parameters are same for both the slow-front and the steep-front injection.

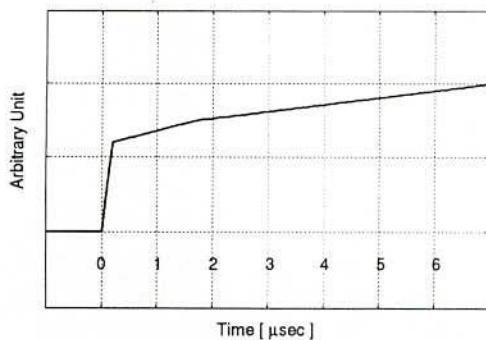


Fig. 3.20. Injected steep-front waveform to simulate the subsequent return stroke.

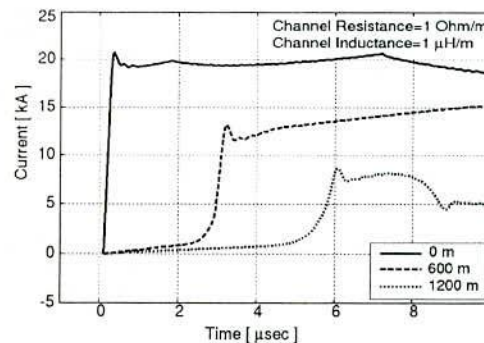
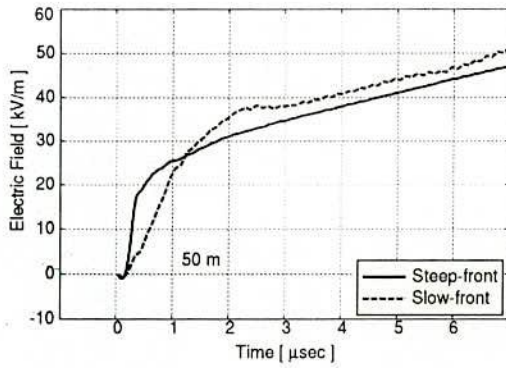
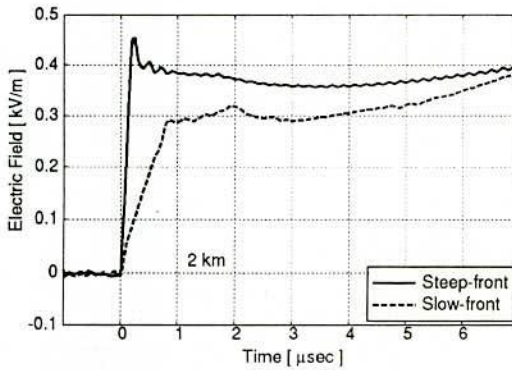


Fig. 3.21. Computed current along the channel for steep-front injection.

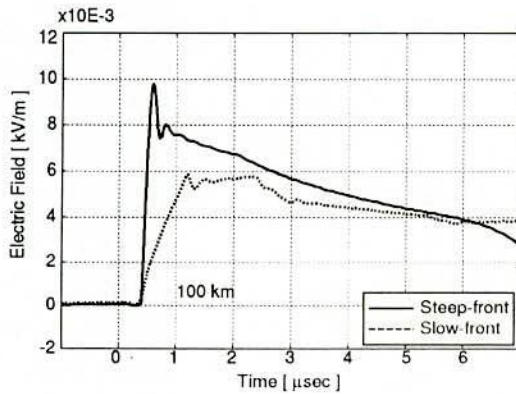
Fig. 3.22 shows the computed waveforms of vertical electric fields for the current pulse in Figs. 3.9(b) and 3.21. Fig. 3.23 shows that of azimuthal magnetic field. It can be observed that the radiated electromagnetic field is larger for the subsequent return stroke though there is a little effect on the field at 50 m except more steepness. Table 3.3 summarizes the significant parameters of lightning current and electromagnetic fields for first and subsequent stroke to ground. It can be calculated that the subsequent-stroke field at 2 km is 1.35 times than first strokes whereas it is 1.66 times at 100 km. Also, the maximum steepness at 100 km is more affected by the subsequent stroke than that at 2 km.



(a)

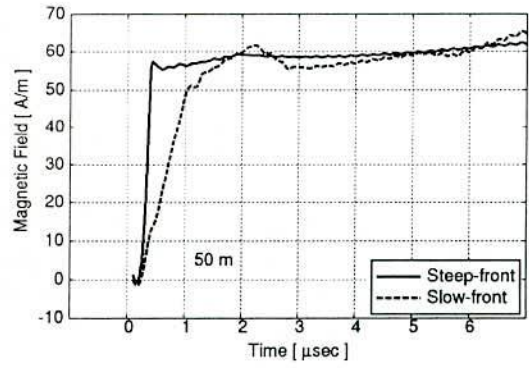


(b)

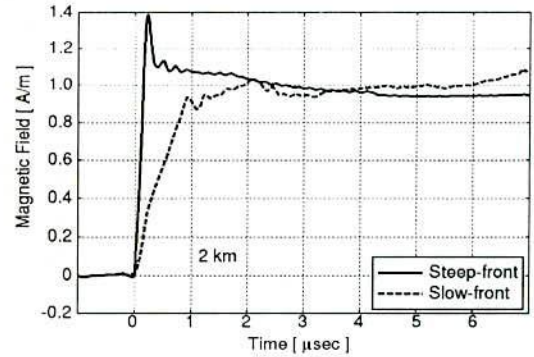


(c)

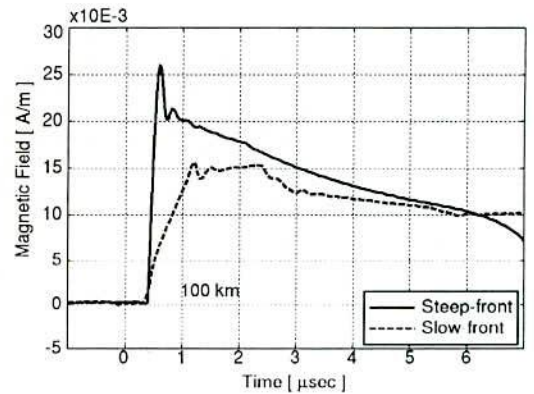
Fig. 3.22. Vertical electric field at (a) 50 m (b) 2 km and (c) 100 km from the lightning channel for first and subsequent stroke in case of lightning return stroke to ground.



(a)



(b)



(c)

Fig. 3.23. Azimuthal magnetic field at (a) 50 m (b) 2 km and (c) 100 km from the channel for first and subsequent stroke in case of lightning return stroke to ground.

Table 3.3

Parameters of lightning return stroke channel base current and the corresponding electric and magnetic field in case of lightning strike to ground.

Waveform		Peak Value			Maximum Steepness			Time to Peak (μ s)	
		Units	First	Subsequent	Units	First	Subsequent	First	Subsequent
Channel Base Current		kA	20.5	20.5	kA/ μ s	20	40	2	0.2
E-Field	2 km	kV/m	0.32	0.456	kV/m/ μ s	0.56	2.4	-	0.2
	100 km		5.91e-3	9.84e-3		9.81e-3	47.2e-3	0.8	0.2
H-Field	2 km	A/m	1.02	1.38	A/m/ μ s	1.64	6.93	-	0.2
	100 km		15.2e-3	25.3e-3		19.3e-3	126e-3	0.8	0.2

If the current is kept constant, the charge per unit length will be decrease with increasing return stroke velocity. Therefore, the amplitude of the static electric field decreases with increasing velocity. The electromagnetic field radiated by the lightning channel depends strongly on the value of the return stroke velocity and a larger return stroke velocity results in a greater electromagnetic field peak. The other factor is the steepness of the current wavefront. The greater steepness of injected current causes greater electromagnetic field peak. To observe the increase in field due to steepness only, compare the solid line of Figs. 3.22 and 3.23 with the dashed line of Figs. 3.10 and 3.11.

It should be mentioned here that the observed fields for subsequent stroke shown in Figs. 3.6 and 3.7 are well reproduced in this work [Figs. 3.22(b) and (c)] for the first few microseconds except the numerical value, because our calculated fields are not corresponding to the currents which causes the observed fields. In fact, this chapter does not try to reproduce the numerical value of the field peaks but the waveshapes. Because, one of the goals of this work is to use the same model to explain the maximum features. The next chapter which explains the lightning return stroke to tall structures is the continuation of the analysis taking this model. On the other hand, the initial fast rising part of the field waveforms is the cause of all disruption. So, the calculation window in this work is limited to few microseconds which also save the computation time.

3.9 Computation Time

The computation is carried out in the frequency range from 19.53 kHz to 10 MHz with the increment step of 19.53 kHz. This corresponds to the time range from 0 to 51.2 μs with 0.1 μs increments. The computation time for the output of NEC-2 block of the flow chart of Fig. 2.5, with 256 MB RAM, Pentium-4 2.8 GHz processor is observed to be 22 seconds in all the cases.

3.10 Summary

Assuming that the representation of the lightning return stroke as a current pulse originating at ground level and traveling along the channel of electrical conductor is valid, the effects of different channel parameters both on the current and electromagnetic fields are investigated. The results show that the introduction of the channel resistance and the inductance will change the model in such a direction that they will come closer to the experimental observations. The ground conductivity has the significant effects on the magnitude and shapes of the electromagnetic fields. The lower ground conductivity reduces the distant electromagnetic field peaks and their derivatives. It can also be observed that the electromagnetic fields are affected by steepness and velocity of the return stroke current.

To simulate the first return stroke, a slow-front current with peak value of 20.5 kA and maximum steepness of 20 kA/ μs is calculated at the base of the channel having resistance of 1 Ω/m and inductance of 3 $\mu\text{H}/\text{m}$. This loading makes the propagation velocity 1.5×10^8 m/s. On the other hand, the subsequent return stroke channel-base current is characterized by a peak value of 20.5 kA and maximum steepness of 40 kA/ μs . For the subsequent return stroke the channel is loaded by uniformly distributed resistance of 1 Ω/m and inductance of 1 $\mu\text{H}/\text{m}$ which make the propagation velocity of 2.1×10^8 m/s.

For the considered case, the subsequent-stroke field at 2 km is 1.35 times than first strokes whereas it is 1.66 times at 100 km. Also, the maximum steepness at 100 km is more affected by the subsequent stroke than that at 2 km.

Chapter 4

Lightning Return Stroke to Tall Structures

4.1 Introduction

The influence of an elevated strike object has recently received considerable attention, since the presence of tall structures such as chimneys of thermal generating stations, telecommunication towers, will affect markedly the lightning return stroke current and the radiated electromagnetic fields. The waveforms of lightning currents measured on such structures show multiple reflections of current waves within the structures and, therefore, the measured electric and magnetic fields also show complex time-varying characteristics [12], [60]-[62].

The problem of lightning return strokes to tall towers was the subject of numerous studies (e.g., [12]-[16], [18], [21], [28]-[31], [54], [63]). Most of the studies about lightning transient have concentrated on extracting information concerning the variation of the current signature along the tower taking the return stroke channel as a perfect conductor and only a few have presented the remote electromagnetic fields predicted by the models.

Motoyama *et al.* proposed the model of electromagnetic field radiation caused by a step current [12]. They used lumped footing resistance and reproduced the observed current waveforms at CN Tower but not the field since transient footing resistance is a nonlinear resistance which depends on the lightning current value. The effect of current reflection within the tower on the remote electromagnetic field has been studied by Rachidi *et al.* using modified transmission line (MTL) model [14]. V. Shostak *et al.* used expanded modified transmission line (EMTL) model and compute the current and magnetic field which are higher than the observed results while the lower value of electric field [15]. Moini *et al.* used Antenna Theory model and the lightning return stroke channel is modeled as a lossy vertical wire antenna [18]. More recently, Y. Baba and M. Ishii applied

electromagnetic model (NEC-2) to reproduce the measured current and electromagnetic field at 2 km distance from CN Tower. They used zero footing resistance and found a reasonably good agreement between computed and experimental results but does not clearly explain the current derivative and field peaks with tower height and at different distances [28].

This work emphasizes on the analysis of the effect of the elevated structures on electromagnetic fields at different distances (50 m, 2 km and 100 km) and their derivatives using NEC-2. One of the major purposes of studies dealing with the lightning electromagnetic field is to provide engineers adequate tools for the evaluation of the effects of this perturbation on realistic equipments which are sensitive to this field.

4.2 Model of Tall Structures Struck by Lightning

Fig. 4.1 illustrates model structure analyzed by NEC-2. An elevated strike object considered by two different height of 200 m and 550 m on perfectly conducting ground, corresponding to the actual height of the high stack in Japan and CN Tower in Canada, respectively. In this work the tower is modeled as a single, uniform and lossless vertical conductor of 0.3 m in radius. Such an assumption does not alter the conclusions of our analysis, although it has been shown that for a more accurate representation of the tower, complex geometries are to be considered [21].

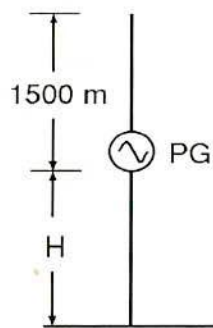


Fig. 4.1. Model for the analysis of lightning return stroke to tall structures of height H (200 m and 550 m).

As the leader descends toward the ground and reaches and attaches to an elevated object, an abrupt potential change generates a wave front (return stroke) that propagates toward the cloud. The current pulse associated with the return stroke phase starts at the top of the elevated object and propagates upward at the return stroke velocity. Simultaneously, a similar current pulse is assumed to be injected by the lightning channel at the top of the object. The return stroke current pulse travels downward the object at the speed of light and is first reflected at the bottom of the object (and part of it is transmitted to ground). The reflected wave travels upward and is reflected at the top of the object (and part of it is transmitted to the lightning channel). This multiple-reflection process along the elevated strike object continues until the energy of the pulse dissipates in the ground and in the lightning channel. A pulse generator (PG) having internal resistance of 400Ω placed at the top of the structure simulates this situation.

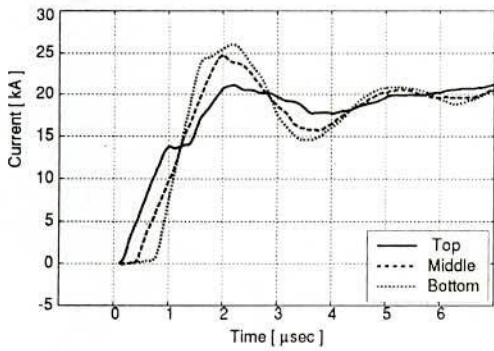
To simulate the lightning first return stroke to a tall tower, the same channel and the injected current which are adopted in the previous chapter to simulate the first return stroke to ground, is used at the top of the tower. Similarly, subsequent stroke current produced by the channel and the injected waveforms in case of ground stroke, is used at the top of the tower to simulate the subsequent stroke. For the numerical analysis, the conductor is divided into cylindrical segments of 25 m in length and 0.3 m in radius.

4.3 Current and Current Derivative along the Tower

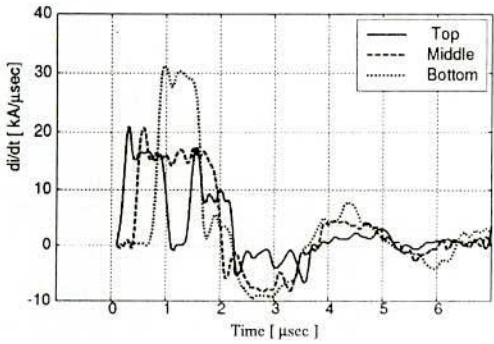
Figs. 4.2 and 4.3 show the waveforms of current and current derivative evaluated at the top, the middle, and the base of 200 m and 550 m tower, respectively for the typical first return stroke current (slow-front injection) presented in Fig. 3.9(b). A comparison of the calculated and measured currents, reveal that despite the simplicity, the tower model is able to reproduce the major reflections that are seen in the measured records [12]. Since the time to current peak is shorter than the wave traveling time along the tower, the current reflections can be clearly distinguished on the waveforms.

It can be seen that moving toward the ground, the current experiences a higher peak value and a shorter time to its peak due to the contribution of the reflected wave at ground level.

From Figs. 4.2(a) and 4.3(a) it can be noticed that the peak current also affected by tower height and it is greater for higher elevated structures. The rise time of peak current increases with the increasing height of elevated structure. The current derivative is higher as moving toward the ground and almost same for both the tower. It can also be seen that [compare Fig. 3.9(b), with Figs. 4.2 and 4.3], both the current and current derivative are more significantly affected by the presence of the tower. The important parameters of the current waveform at various observation points along the tower are summarized in Table 4.1.

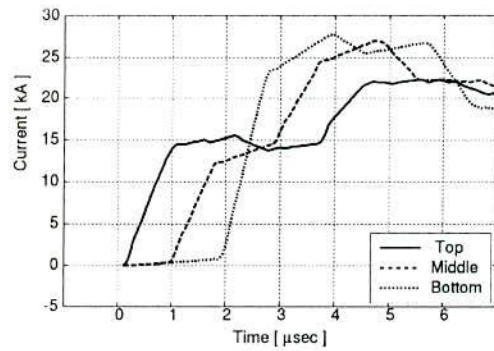


(a)

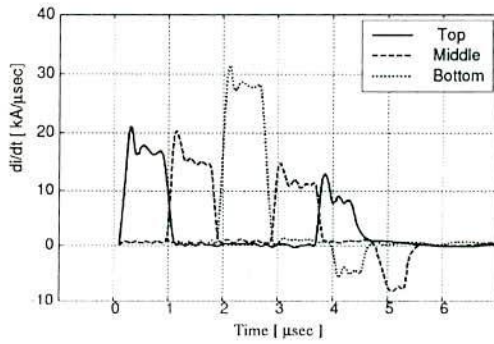


(b)

Fig. 4.2. (a) Current (b) current derivative along the 200 m tall strike object for a typical first return stroke.



(a)



(b)

Fig. 4.3. (a) Current (b) current derivative along the 550 m tall strike object for a typical first return stroke.

It shows that the current peak value at the bottom of the tower are 1.27 times for 200 m tower and 1.33 times for 550 m tower comparing those associated with the stroke initiated at ground level whereas maximum steepness at the bottom of the tower is 1.5 times for both the tower.

Table 4.1

Parameters of lightning current along the tower of height 200 m and 550 m for a typical first return stroke.

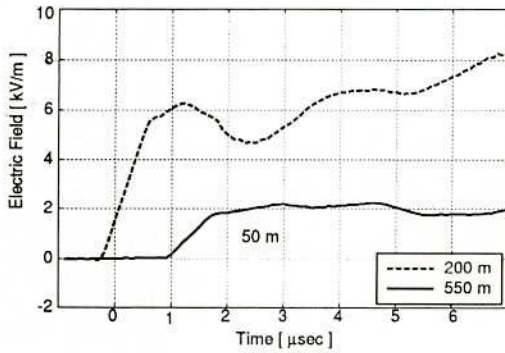
Stroke to	Measured at	Peak Value (kA)	Maximum Steepness (kA/ μ s)	Time to Peak (μ s)
Ground	-	20.5	20	2
200 m Tower	Top	21	20	2.2
	Middle	24.7	20	1.6
	Bottom	26.1	30	1.4
550 m Tower	Top	22.2	20	4.5
	Middle	26.5	20	3.8
	Bottom	27.4	30	2.2

4.4 Electromagnetic Fields

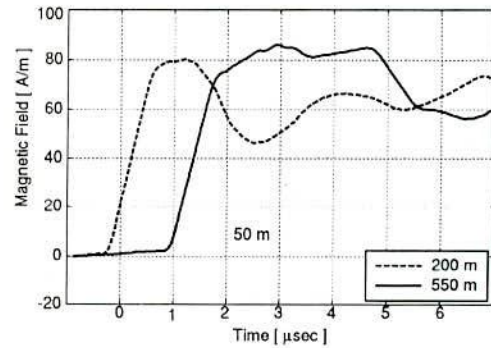
Figs. 4.4 and 4.5 present the waveforms of the vertical electric and azimuthal magnetic field at 50 m, 2 km and 100 km from the tower. A comparison between Figs. 3.10, 3.11 and Figs. 4.4, 4.5 show that, the presence of the tower results in a significant change of the electromagnetic field peaks and also in the appearance of subsidiary peaks. From Figs. 3.10 and 4.4, it can be seen that the static electric field for elevated structure is smaller than that of stroke initiated at ground level and decreases as the height of tower increases. It is due to the increase of charge distribution length with the increasing of tower height. The fields start to rise at different time due to shift in time of the channel's and tower's field contribution.

Since at each segment of the tower current rise time is a function of height, the field start to rise at different time i.e., for different height of tower there is a significant delay in rising the static field and that increases with the height of tower. As the magnetic field has no static component, from Figs. 3.11(a) and 4.5(a), observe that it is larger for elevated structures than that for ground stroke and increases with the height of the tower. Also, in this chapter the field is calculated at the height of 20 m from ground as calculated in the previous chapter. The static electric field at different height for 550 m tower is given in Fig. 4.6. It shows that the field increases as the observation points come closer to the source. There is no significant change of magnetic field at different height.

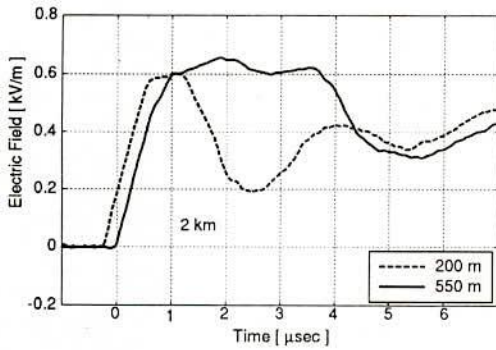
Within first few microseconds, the electric field waveforms in Fig. 4.4(b) typically exhibits a large first peak, followed by a rapid decay to a minimum at a time approximately between 1.5 to 3 μs for 200 m and 3 to 6 μs for 550 m tower, the waveform then slowly rises in an oscillatory manner to a second peak.



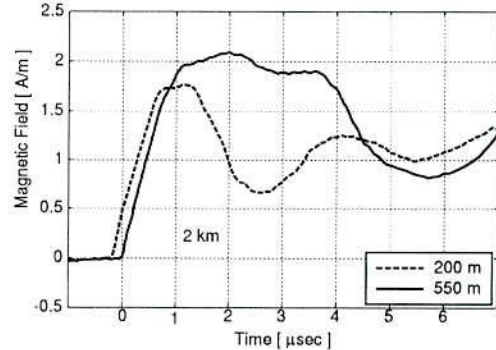
(a)



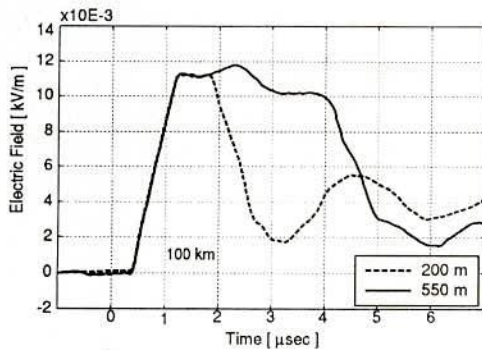
(a)



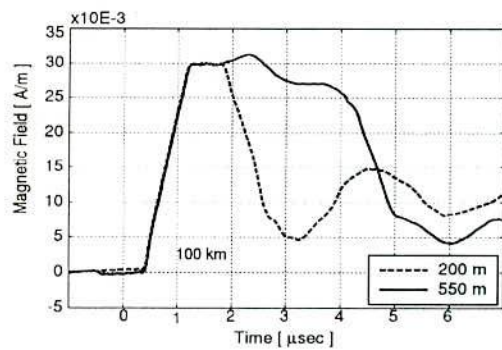
(b)



(b)



(c)



(c)

Fig. 4.4. Vertical electric field at (a) 50 m (b) 2 km and (c) 100 km from the elevated structure of height 200 m and 550 m for a typical first return stroke.

Fig. 4.5. Azimuthal magnetic field at (a) 50 m (b) 2 km and (c) 100 km from the elevated structure of height 200 m and 550 m for a typical first return stroke.

The findings for 550 m tower is in agreement with recent experimental observations of lightning strikes to the CN Tower presented in [12], [15], except the peak field values as the current for which we compute the field was not corresponding to the measured current.

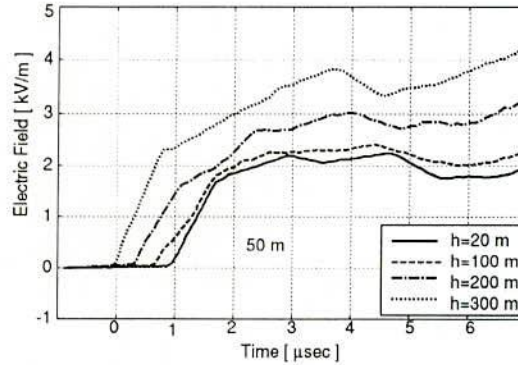


Fig. 4.6. Static electric field at different height in case of lightning strike to 550 m tall tower.

Though the field at 2 km is dominated by radiation component, due to the static component different time to start rising is observed. The magnetic field waveform in Fig. 4.5(b), at the same initial interval of time, has almost the same features as the electric field waveform and both the electric and magnetic field increases with the increasing height of tower. At 100 km, the static and induction field terms vanish and only the radiation term remains. So, the fields for both the 200 m and 550 m in Figs. 4.4(c) and 4.5(c) start to rise at the same time.

Table 4.2 summarizes the significant parameters of the electric field waveforms for both lightning stroke to ground and to the tower. For the considered case, the peak field associated with the strokes at tower top is about 1.9 times to 2.1 times as large as that corresponding to return strokes initiated at ground level. According to Janischewskyj *et al.* the contribution from the CN tower to the electric field at 2 km from the tower is about a factor of two greater than the contribution from the lightning channel [16].

It can be seen from Table 4.2 that the presence of the tower affects also the maximum steepness of field which is about 1.4 times to 2.2 times as large as that corresponding to ground stroke. On the other hand, the increasing height of the tower results in an increase in the time to peak of first stroke field.

Table 4.2

Parameters of lightning (a) electric (b) magnetic fields for a typical first return stroke.
Lightning strike to tall structures of height 200 m and 550 m.

(a) Electric field

Stroke to	Peak Value (kV/m)		Maximum Steepness (kV/m/ μ s)		Time to Peak (μ s)	
	2 km	100 km	2 km	100 km	2 km	100 km
Ground	0.32	5.91e-3	0.56	9.81e-3	-	0.8
200 m Tower	0.6	11.2e-3	0.84	16.4e-3	1.4	1.4
550 m Tower	0.66	11.8e-3	0.87	16.4e-3	2	2

(b) Magnetic field.

Stroke to	Peak Value (A/m)		Maximum Steepness (A/m/ μ s)		Time to Peak (μ s)	
	2 km	100 km	2 km	100 km	2 km	100 km
Ground	1.02	15.0e-3	1.64	19.3e-3	-	0.8
200 m Tower	1.75	30.0e-3	2.27	44.3e-3	1.4	1.4
550 m Tower	2.11	31.4e-3	2.47	44.3e-3	2	2

4.5 First Versus Subsequent Stroke

Fig. 4.7 presents the tower current, using the typical subsequent return stroke current. Comparing Figs. 4.3 and 4.7 it can be seen that in case of subsequent strokes, both the current and current derivative are more significantly affected by the presence of the tower. Table 4.3 shows the comparison of important current parameters for both the first and subsequent stroke in case of lightning stroke to ground [Figs. 3.9(b) and 3.21] and stroke to the 550 m tall tower [Figs. 4.3 and 4.7]. It can be seen that the tower top current is more significantly affected by subsequent stroke (1.22 times) than the first stroke (1.08 times) comparing with the current in case of lightning stroke to ground.

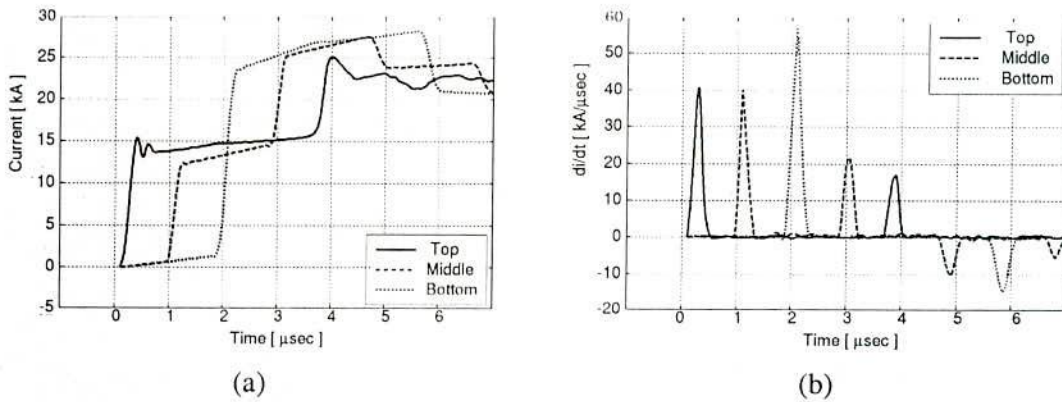


Fig. 4.7. (a) Current (b) current derivative along the 550 m tall strike object for a typical subsequent return stroke.

Table 4.3

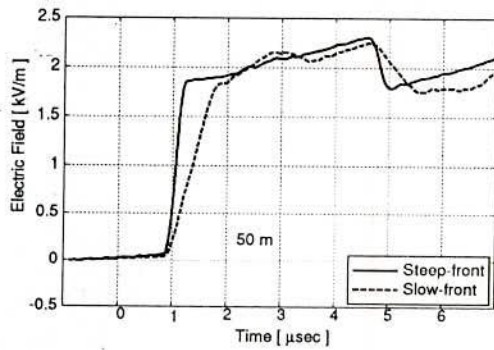
Parameters of lightning current along the 550 m tall tower for typical first and subsequent return stroke.

	Peak Value (kA)		Maximum Steepness (kA/μs)		Time to Peak (μs)	
	First	Subsequent	First	Subsequent	First	Subsequent
Ground	20.5	20.5	20	40	2	0.2
Tower Top	22.2	25	20	40	4.5	3.8
Middle	26.5	27.5	20	40	3.8	3.8
Bottom	27.4	28	30	57	2.2	3.8

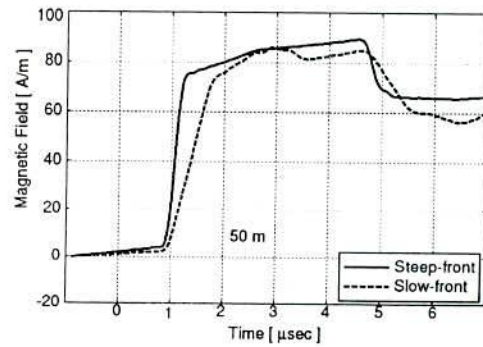
The effect of subsequent stroke current is less as going to the bottom of the tower. Furthermore, for the first stroke the time to current peak decreases as the observation point moves toward the ground while for the subsequent stroke, it remains constant. This result can be explained considering that for the first stroke, the propagation time along the tower is smaller than the rise time of the injected current. This situation is reversed for the subsequent stroke where the propagation time along the tower is larger than the rise time of the injected current.

Figs. 4.8 and 4.9 present the waveforms of the first and subsequent return stroke vertical electric field and azimuthal magnetic field at 50 m, 2 km and 100 km from the tower. A comparison between Figs. 3.22, 3.23 and Figs. 4.8, 4.9 show that, for both first and

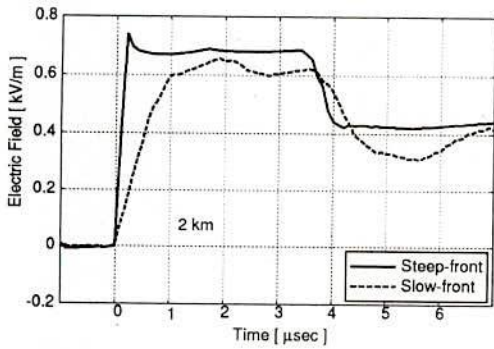
subsequent return strokes, the presence of the tower results in a significant increase of the electromagnetic field peak and maximum steepness at 2 km and 100 km. This increase depends essentially on the wavefront steepness of the input current pulse, and on the return stroke velocity as said in the previous chapter.



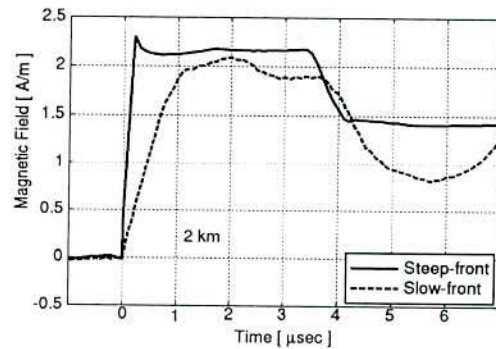
(a)



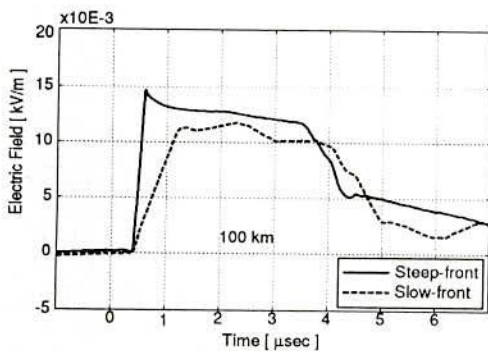
(a)



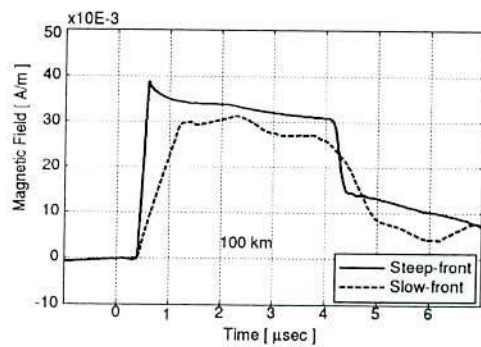
(b)



(b)



(c)



(c)

Fig. 4.8. Vertical electric field at (a) 50 m (b) 2 km and (c) 100 km from the 550 m tall structure for first and subsequent return stroke.

Fig. 4.9. Azimuthal magnetic field at (a) 50 m (b) 2 km and (c) 100 km from the 550 m tall structure for first and subsequent return stroke.

Table 4.4

Parameters of lightning return stroke channel base current and the corresponding electric and magnetic field when lightning strike to 550 m tower.

Waveform		Peak Value			Maximum Steepness			Time to Peak (μs)	
		Units	First	Subsequent	Units	First	Subsequent	First	Subsequent
Channel Base Current		kA	20.5	20.5	kA/ μs	20	40	2	0.2
E-Field	2 km	kV/m	0.66	0.72	kV/m/ μs	0.87	3.46	2	0.2
	100 km		11.8e-3	14.6e-3		16.4e-3	69.9e-3	2	0.2
H-Field	2 km	A/m	2.11	2.32	A/m/ μs	2.47	8.6	2	0.2
	100 km		31.4e-3	38.7e-3		44.3e-3	185e-3	2	0.2

Table 4.4 summarizes the main parameters of the electric and magnetic field waveforms for both the first and subsequent stroke in case of lightning strike to the 550 m tall tower. For the considered case, the peak field associated with tower strokes is about 1.5 times (for the subsequent stroke) to 2 times (for the first stroke) as large as that corresponding to return strokes initiated at ground level [Table 3.3] which are in disagreement with the computed result in ref. [14]. Ref. [14] shows that the increase in field is larger for subsequent stroke than first return stroke. This may be due to the different reflection coefficient considered in their simulation which is the drawback of the TL model. Actually, in the case of ground stroke, only the channel radiate electromagnetic field where the increase in the subsequent stroke fields is due to larger value of the return stroke velocity and also due to the steepness of the current wavefront. On the other hand, in case of stroke to tall structure both the channel and the tower contribute to the radiated electromagnetic fields but the contribution of tower dominate the total field. Since both the first and subsequent stroke current travels along the tower with the same velocity (velocity of light), the increase in the subsequent stroke fields is only due to the steepness of the current wavefront.

It can be calculated that the subsequent stroke fields at 2 km is 1.09 times than first strokes whereas it is 1.24 times at 100 km. The maximum steepness is also more affected by the subsequent stroke at 100 km (4.2 times) than that at 2 km (3.8 times). This is due to the radiation component of the fields is more influenced by the subsequent stroke.

Finally, the mere presence of an elevated strike object increases the electromagnetic field and that influence is greater for currents with steeper wavefronts, as shown by the results obtained in the present study. The values of the average ratio of subsequent-to-first magnetic field peak (at 2 km) to subsequent-to-first current (tower top) peak are reported in Table 4.5. Although the comparison between computed result in this section and experimental data in [12] (shown in the next section) should be considered as only qualitative, it can be seen, however, that the computed values of the ratio of the field peaks to current peaks $(H_S/H_f)/(I_s/I_f) = 1.27$ for 550 m tower, agrees reasonably well with the value 1.24 which is obtained from measured fields and currents. The value of 1.5 is computed by Rachidi *et al.* using MTL model [14] comparing with the measured value of 1.67.

Table 4.5
Ratio of subsequent-to-first magnetic field peak H_S/H_f to subsequent-to-first current peak I_s/I_f , for the field at 2 km.

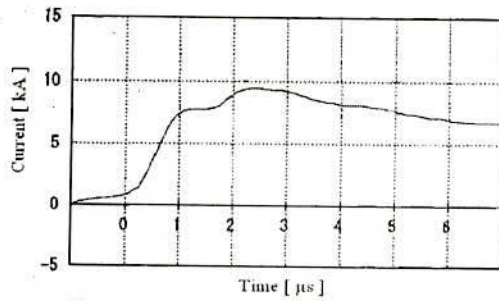
	$(H_S/H_f)/(I_s/I_f)$
Average measured (CN Tower [12])	1.24
Computed, return stroke initiated at ground	1.35
Computed, taking into account the presence of the elevated strike object	1.27

Actually, these results show how the measured fields are closely reproduced in the calculation of this work corresponding with the current for both the first and subsequent return stroke. It is said earlier that the first objective of the lightning analysis is to reproduce the lightning current and associated electromagnetic fields. As it is a random and unpredictable phenomenon, it may have different peaks and waveshapes at different strike. So, the researchers always try to use a simple but common model which can reproduce and explain the maximum features of the measured results. The causes of small difference between the computed and experimental results may include several factors like atmospheric conditions, ground electrical parameters, stepped or dart leader, return stroke velocity etc., on which the lightning electromagnetic fields depend. The sensitivity of measuring system is another important factor which may be the cause for this disagreement.

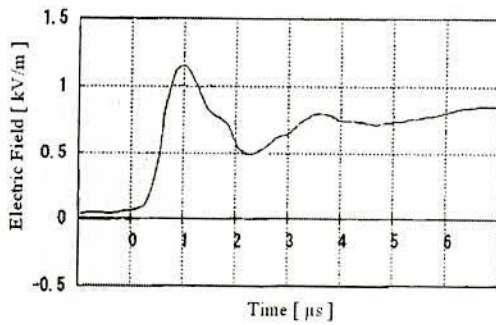
4.6 Comparison with Measured Waveforms

1. 200 m High Stack in Japan

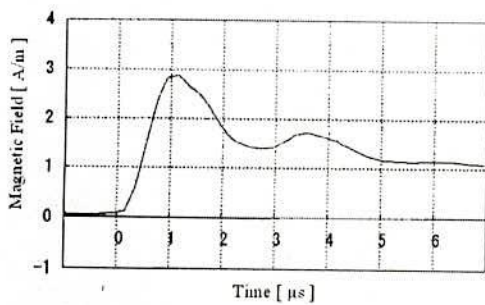
Fig. 4.10 shows the measured [64] and Fig. 4.11 shows the computed waveforms of the current and the fields associated with a lightning stroke hit a 200 m high stack in Japan.



(a) Current at the top of the Stack

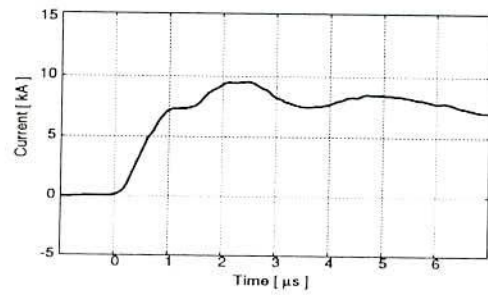


(b) Vertical electric field at 630 m.

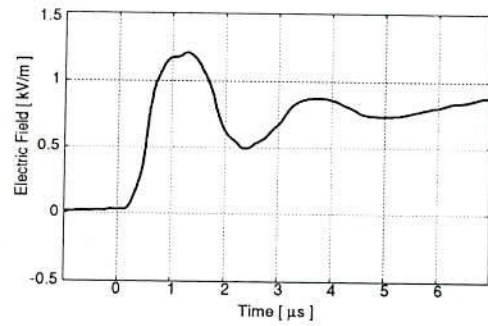


(c) Azimuthal magnetic field at 630 m.

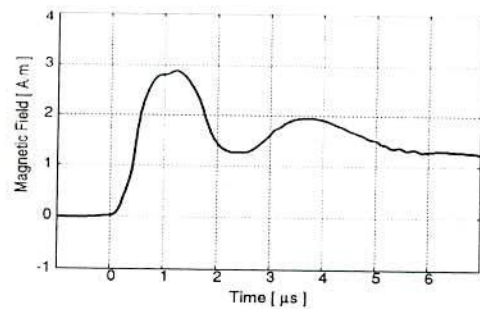
Fig. 4.10. Measured [64] waveforms of lightning current and electromagnetic fields at or around a 200 m high stack.



(a) Current at the top of the Stack



(b) Vertical electric field at 630 m.



(c) Azimuthal magnetic field at 630 m.

Fig. 4.11. Computed waveforms of lightning current and electromagnetic fields at or around a 200 m high stack.

The current is measured at the top of the stack and the fields are measured at a distance of 630 m from the stack. The vertical conductor loaded by resistance of $1 \Omega/\text{m}$ and inductance of $3 \mu\text{H}/\text{m}$ is used as a simulated lightning channel. Fig. 4.12 shows the postulated source voltage waveforms in the simulation to reproduce the measured waveforms.

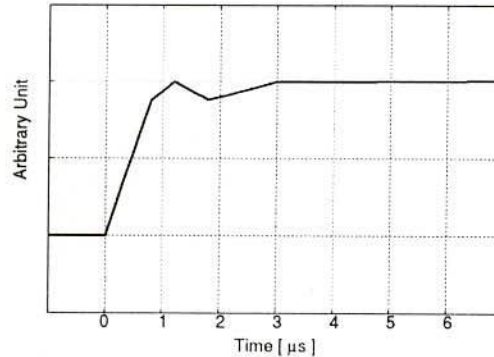


Fig. 4.12. Waveform of voltage source for the computation that produced Fig. 4.11.

The source voltage waveforms were first determined so that the current waveform at the observation point might fit the measured waveform. Then the velocity of the current wave on the simulated lightning channel was adjusted by changing the parameters of loading so that the computed field waveforms might fit the measured ones. The measured waveform of the current is well reproduced by postulating a simple source waveform. The lightning-current waveform is apparently influenced by the tall structure. The increase of the current at about $1.3 \mu\text{s}$ in Fig. 4.10(a) is reflection from the ground. This increment of current is sensitive to the grounding impedance and the discontinuity of impedance between the stack and the lightning channel. The grounding resistance of 30Ω , employed in the present analysis, was determined to reproduce this peak.

Goshima *et al.* [64] postulated 100Ω for the grounding impedance of this stack to reproduce the measured current waveform in the traveling wave analysis, where they represented the stack and the lightning channel by lossless transmission lines whose surge impedance was 300Ω and 1000Ω , respectively. Motoyama *et al.* [12] assumed the grounding impedance of the CN Tower to be 50Ω . Guerrieri *et al.* [13] used about 150Ω as the footing resistance of the Swiss PTT Tower in the similar analysis if the tower surge impedance was assumed to be 300Ω . This tendency, that rather high footing impedance is required in the traveling wave analysis to reproduce measured current waveforms, even at

towers having low footing resistance, was first reported by Chisholm and Janischewskyj [65]. They identified the footing impedance of a model conical tower on a metal plane as 60Ω by the Time-Domain Reflectometry (TDR). The causes of this phenomenon are the distortion of the current wave in the tower due to the intense axial electric field, and the reflection of the spherical electromagnetic wave at the ground plane [66]. Since this apparent high footing impedance is of transient nature, it is prominent only for currents having steep rise. The waveforms of the computed electric field and magnetic field agree well with the measured waveforms when the loaded vertical conductor is used.

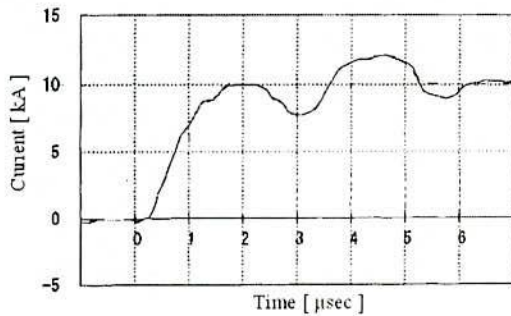
2. CN Tower in Toronto

The observations, showing that the subsequent stroke field peak might be greater than the first stroke peak, have been made on natural lightning in Florida [67]. In ref. [67], electric field waveforms from 46 multiple-stroke flashes were analyzed and it has been found that 15 flashes (33 %) had at least one subsequent stroke whose initial electric field peak was greater than that of the first return stroke.

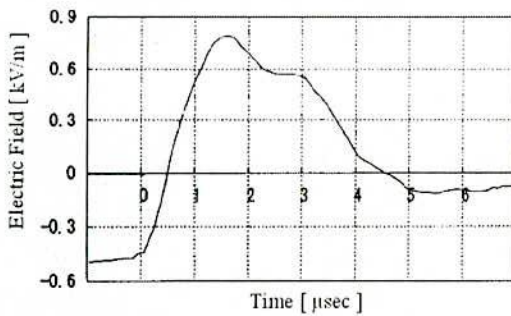
Subsequent stroke field peak greater than the first stroke peak is generally attributed to subsequent stroke current peak greater than the first stroke peak (e.g., [67], [68]). Indeed, although on average first return stroke current peaks are higher than subsequent stroke ones, observed lightning data in Switzerland [69] and in Canada [70] have shown that a nonnegligible number of flashes contain subsequent strokes with higher current peaks than those of their first strokes.

- Five (15 %) of the 33 negative downward multiple stroke flashes striking instrumented towers in Switzerland contained one or two subsequent strikes with return stroke peak currents greater than their respective first stroke peak currents. The percentage of subsequent strokes with greater current peaks than the first stroke peak was about 7 % (8 strokes out of 115) [67], [69].
- Data recorded at the CN Tower in Toronto (about ten times as high as the towers used in Switzerland) have shown that 40 % of subsequent strokes had current peaks ranging from one to four times the value of the first stroke peak [70].

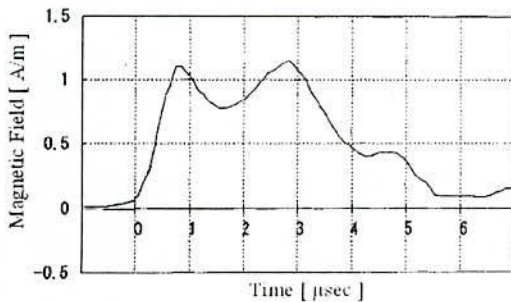
Similar observations [12], showing that subsequent stroke current as well as electric and magnetic fields are larger than those from the first stroke, is illustrated in Figs. 4.13 and 4.14. In figures two sets of simultaneous data (current, E-field, H-field) corresponding to the slow-front (Fig. 4.13) and to the fast-front (Fig. 4.14) to the CN Tower are presented.



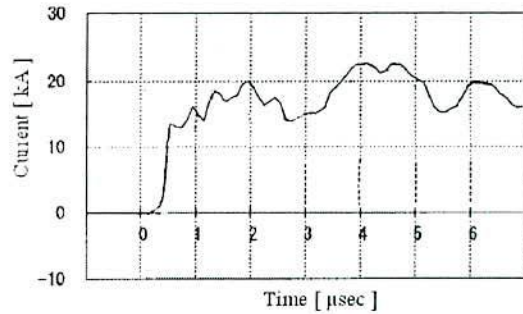
(a) Lightning current at the tower top.



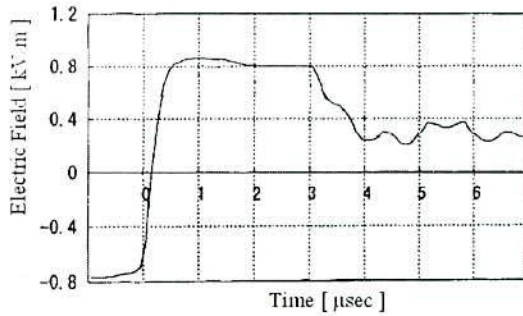
(b) Vertical electric field component



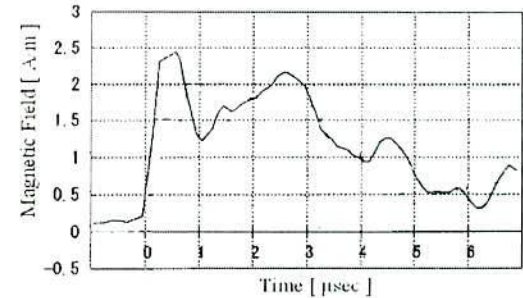
(c) Azimuthal magnetic field component



(a) Lightning current at the tower top.



(b) Vertical electric field component

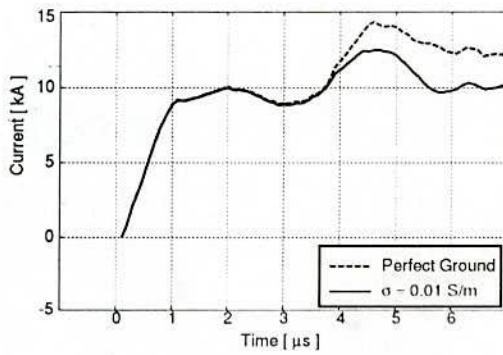


(c) Azimuthal magnetic field component

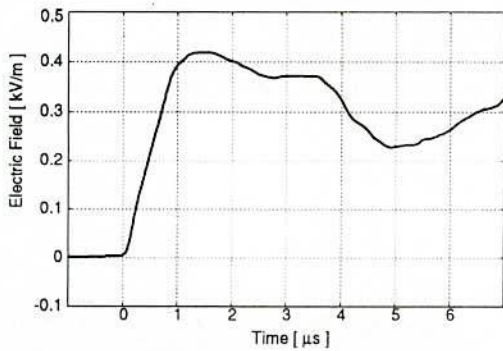
Fig. 4.13. Observation result for slow rise wavefront current of a CN Tower lightning flash recorded on August 17, 1991.

Fig. 4.14. Observation result for fast rise wavefront current of a CN Tower lightning flash recorded on August 17, 1991.

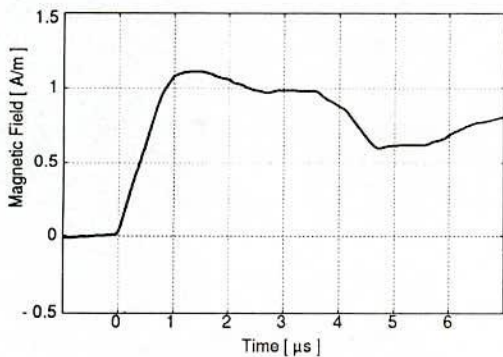
The fields of Figs. 4.13 and 4.14 were measured at a distance of 2 km from the tower. Fig. 4.15 shows the computed waveforms of current and fields associated with a slow-front lightning current injected into the CN Tower. Fig. 4.16 shows those for a steep-front lightning current.



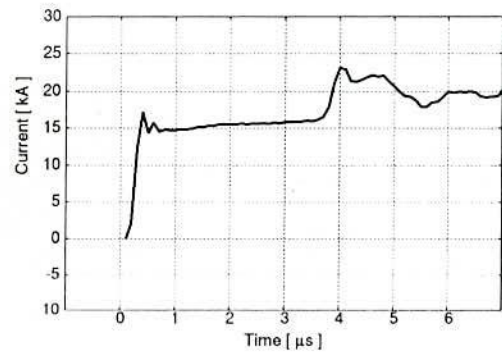
(a) Lightning current waveform



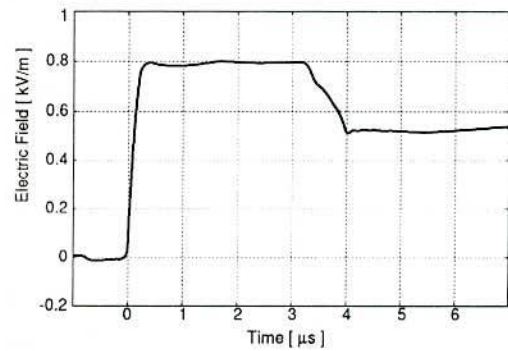
(b) Vertical electric field component



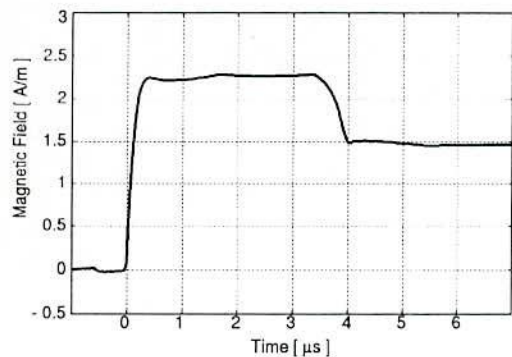
(c) Azimuthal magnetic field component



(a) Lightning current waveform



(b) Vertical electric field component



(c) Azimuthal magnetic field component

Fig. 4.15. Computed waveforms for slow-front injected current at the CN Tower.

Fig. 4.16. Computed waveforms for steep-front injected current at the CN Tower.

The channel loaded by resistance of $1 \Omega/\text{m}$ and inductance of $3 \mu\text{H}/\text{m}$ is used to compute the waveforms of slow-front injection. Similarly, $1 \Omega/\text{m}$ and $1 \mu\text{H}/\text{m}$ are used to compute the waveforms of steep-front injection. The ground conductivity of $0.01 \text{ S}/\text{m}$ is used for both the case. The effect of ground conductivity is shown in Fig. 4.15(a). The grounding resistance is set to 0Ω to reproduce this peak, which is much lower than the value in the analysis based on the transmission line [12]. The reason for this difference was discussed in the preceding section.

The measured waveform of the current is well reproduced by the model, especially in the case of slow-front injection. The increase of the current at about $3.6 \mu\text{s}$ in both the Figs. 4.15(a) and 4.16(a) is reflection from the ground. Due to the simple structure of tower model, multiple reflections is not observed in computed waveforms, which is observed in measured waveforms for complex structure of CN Tower. However, the major reflection is reproduced in the simulation and it does not affect other conclusions.

The computed electric fields [Figs. 4.15(b) and 4.16(b)] do not agree with the measurement [Figs. 4.13(b) and 4.14(b)]. The magnitudes of computed waveforms are only half of the measurement in both cases. Since the analysis by NEC-2 in the fundamental case agrees well with the theory, it is highly probable that the measuring system for the electric field was not properly calibrated. The computed magnetic fields agree with the measurement except for dips appeared in the beginning of the measured waveforms in both cases.

The waveforms and the peak values of fields computed by an equivalent circuit approach [12] and by numerical electromagnetic method [21] are somewhat similar to those of the analysis in this thesis for the slow-front current injection. The initial parts of field waveforms are quite different, however, for the fast-front current injection. This analysis is independent of grounding resistance due to the consideration of finite ground conductivity.

4.7 Computation Time

The computation is carried out in the frequency range from 19.53 kHz to 10 MHz with the increment step of 19.53 kHz . This corresponds to the time range from 0 to $51.2 \mu\text{s}$ with

0.1 μ s increments. The computation time for the output of NEC-2 block of the flow chart of Fig. 2.5, with 256 MB RAM, Pentium-4 2.8 GHz processor is about 25 seconds is observed in all cases.

4.8 Summary

The Numerical Electromagnetic Code is applied to the analysis of the electric and magnetic fields radiated by lightning return strokes to tall tower. Electric and magnetic field waveforms corresponding to typical first and subsequent strokes have been computed and analyzed. The effect of the presence of a tall tower on the magnitude and shape of the fields has been investigated.

According to the simulation, the tower bottom current (1.27 to 1.33 times) and its derivative (1.5 times) are more significantly affected by the presence of the tall objects compared to the ground stroke. The peak field associated with the strokes at tower top is about 1.9 times to 2.1 times as large as that corresponding to return strokes initiated at ground level. The presence of the tower affects also the maximum steepness of field which is about 1.4 times to 2.2 times as large as that corresponding to ground stroke.

For the considered case, the tower top current is more significantly affected by subsequent stroke (1.22 times) than the first stroke (1.08 times) comparing with the current in case of lightning stroke to ground. It can also be seen that the peak field associated with tower strokes is about 1.5 times (for the subsequent stroke) to 2 times (for the first stroke) as large as that corresponding to return strokes initiated at ground level.

The obtained results have been shown to be consistent with experimental observations of lightning strokes to the 200 m high stack in Japan and to the CN Tower. There is a good agreement in both wave-shapes and magnitude between computed and measured results for high stack. On the other hand, in case of CN Tower there are significant discrepancies in terms of electric field magnitude, the computed electric fields being smaller than measured. It is likely that these discrepancies are largely due to calibration errors which resulted in the measured fields being over estimated. The computed magnetic field produces the same peak as measured.

Chapter 5

Simulation by FDTD Method and Comparison with the NEC-2 Results

5.1 Introduction

The most significant analyses which are shown in the previous chapters are also carried out in this chapter by a time domain, FDTD method using VSTL. The advantages of this method are discussed already in chapter 2. Due to the large computation time and storage requirements a reduced scale model is considered in the present analysis. Another limitation of VSTL is that it has no provision to take into account the uniformly distributed channel resistance and inductance. For these limitations, this chapter only tries to explain the most significant observations and contradictory results with other models which were found in the previous analysis. The results of FDTD validate the considered model and NEC-2 results which are presented in this work.

5.2 Simulation by FDTD Method

In the analysis of VSTL, the analysis space is defined as a rectangular-parallelepiped space. Arbitrary number of thin-wire conductors, rectangular-parallelepiped conductors, and localized voltage and current sources are arbitrarily placed in the analysis space, and transient electric and magnetic fields are calculated. The bottom of the analysis space can be defined as an imperfectly-conducting medium such as earth, and each boundary of the analysis space can independently be defined as a perfectly-conducting plane or an absorbing plane which simulates the effect of free space beyond the boundary forever. The waveform of a localized voltage or current at an arbitrary position is outputted as specified.

Since FDTD is a time domain technique which finds the electromagnetic fields everywhere in the computational domain, it lends itself to provide animation displays of

the electromagnetic field distributions throughout the analysis space by transferring data to MATLAB. This type of display is extremely useful to understand exactly about the presence of electromagnetic fields and their distribution along the channel and computational domain.

5.2.1 Lightning Return Stroke to Ground

The same model [Fig. 3.1] but the channel length of 20 m and the radius of 3 cm is considered for reduced scale simulation. In the simulation with FDTD, the dimensions of the analysis space were 8.1 m \times 40.05 m \times 26.1 m with space step $\Delta s = 15$ cm. The time step was determined by (2.41) with $\alpha = 0.001$ and all the six boundaries of the cell were treated as the second-order Liao's absorbing boundary. The thickness and the resistivity of the earth were set to 2.7 m and $1.69 \times 10^{-8} \Omega\text{m}$, respectively. A pulse generator (PG) with internal resistance of 10 Ω is used as the source of lightning current. The rise time of the current pulse is set at 20 ns for slow-front and 5 ns for steep-front [Fig. 5.1] with pulse duration of 110 ns which covers the round trip time for the traveling wave in the vertical conductor system.

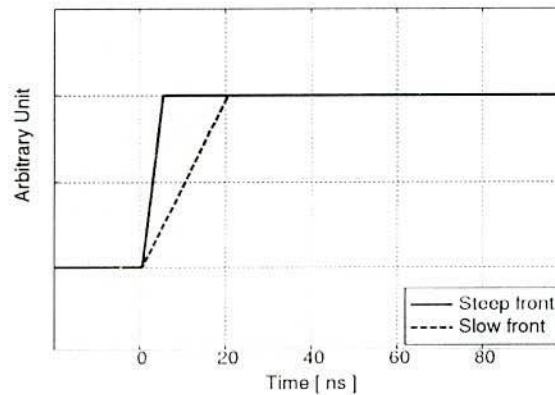


Fig. 5.1. Injected voltage waveforms for the reduced scale model.

Fig 5.2 shows the computed current along the channel for slow-front [Fig. 5.2(a)] and steep-front [Fig. 5.2(b)] injection. The observation indicates that the peak current of the return stroke decreases with height while its rise time increases. The ground conductivity is set to copper conductivity 5.89×10^7 S/m.

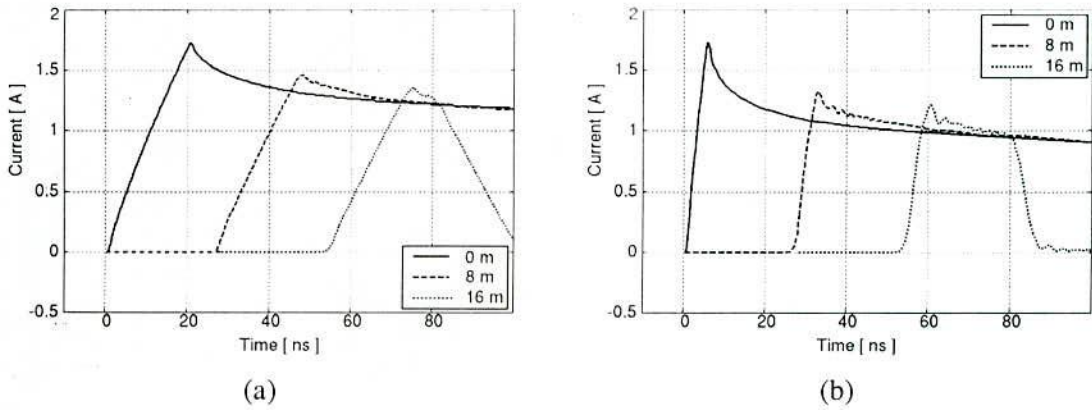


Fig. 5.2. (a) Slow-front (b) steep-front current along the channel. Computed by the FDTD method on reduced scale model.

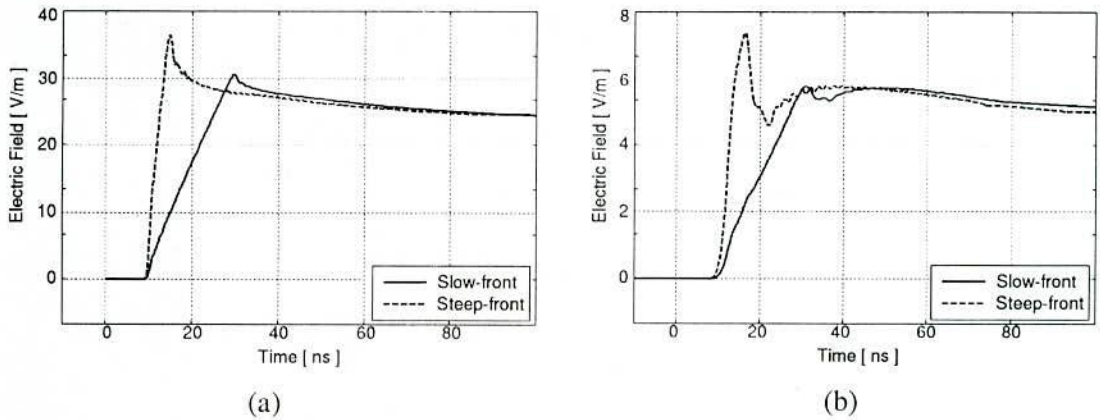


Fig. 5.3. Vertical electric field at (a) 2 m and (b) 20 m from the channel for the current shown in Fig. 5.2. Computed by the FDTD method.

Fig. 5.3 shows the electric field at different distances for the current shown in Fig. 5.2. It is found that the waveforms of electric field at 2 m resemble the current waveforms and the fields at 20 m show a slow ramp followed by a fast rising peak and then decay to the same value. In both figures the electric field for steep-front injection is 1.2 times greater than that of slow-front. The magnetic field distributions corresponding to the ground stroke at different times are shown in Appendix H.

Figs. 5.4 and 5.5 show the current waveforms for different ground conductivity and their associated electric fields, respectively. To observe the effect of ground electrical parameter steep-front current is chosen for injection and three different grounds whose conductivity

are 5.89×10^7 S/m, 0.01 S/m and 0.001 S/m are taken. It can be observed that the electric fields and its derivatives decrease with decreasing the ground conductivity.

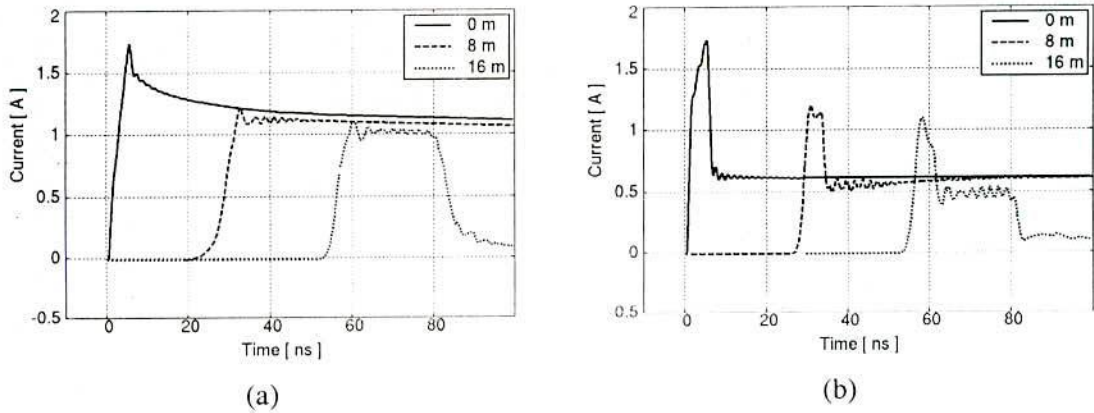


Fig. 5.4. Current along the channel for ground conductivity (a) 0.01 S/m and (b) 0.001 S/m. Computed by the FDTD method on reduced scale model.

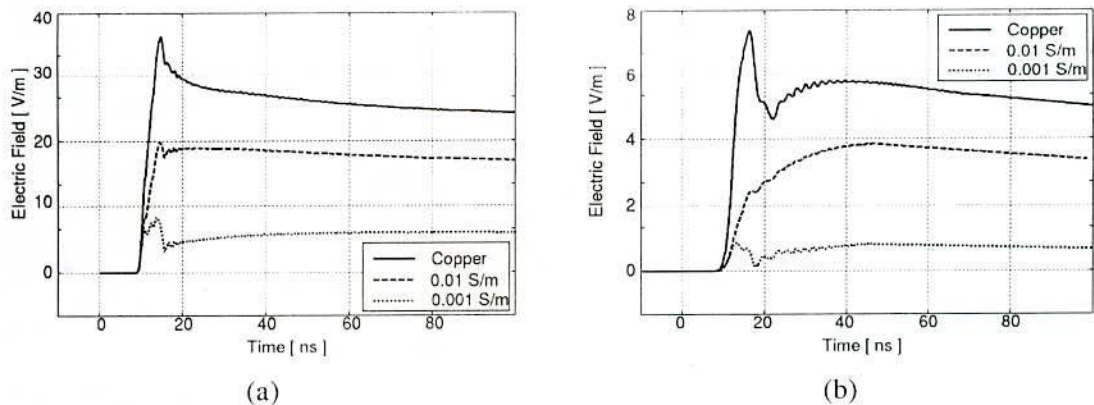


Fig. 5.5. Vertical electric field for different ground conductivities at (a) 2 m and (b) 20 m from the channel. Computed by the FDTD method.

5.2.2 Lightning Return Stroke to Tall Structures

In this case of reduced scale simulation, the model used in Chapter 4 [Fig. 4.1] but the channel length of 20 m, tower height of 6 m and both the radius of 3 cm are considered. The dimensions of the analysis space were 8.1 m \times 40.05 m \times 30.0 m with space step $\Delta s = 15$ cm. The PG with internal resistance of 10 Ω is placed at the top of the tower.

Fig 5.6 shows the computed current along the tower for (a) slow-front and (b) steep-front injection. The time to travel the current along the tower from top to ground and then reaches to top in form of the reflected wave is 40 ns. This indicates that the wave travels at the velocity of light. It is shown that the tower current increases as one go from top to bottom. These currents are larger than that for lightning stroke to ground [compare Figs. 5.2 and 5.6] and the effect is greater for the steep-front injection. The vertical electric fields at different distances corresponding to these currents are shown in Fig. 5.7. It is found that the field for steep-front is 1.05 to 1.09 times larger than the fields of slow-front. The magnetic field distributions corresponding to the lightning stroke to tall object at different times are shown in Appendix H.

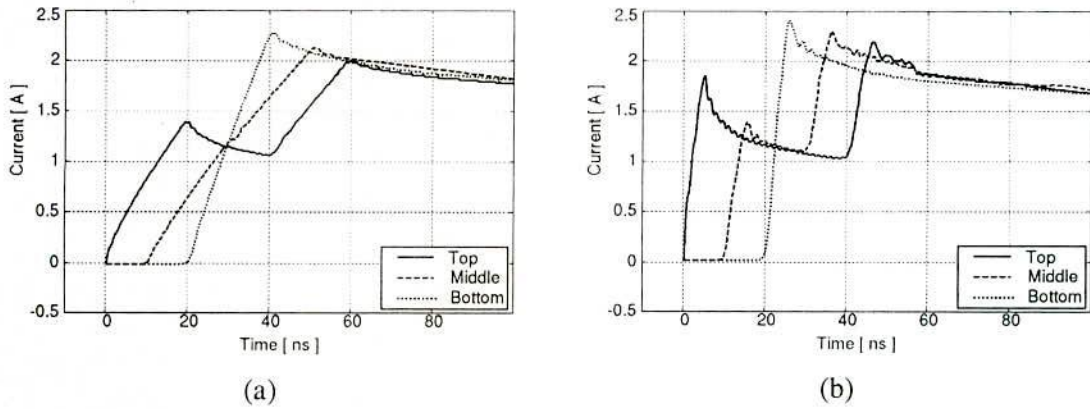


Fig. 5.6. (a) Slow-front (b) steep-front current along the tower. Computed by the FDTD method on reduced scale model.

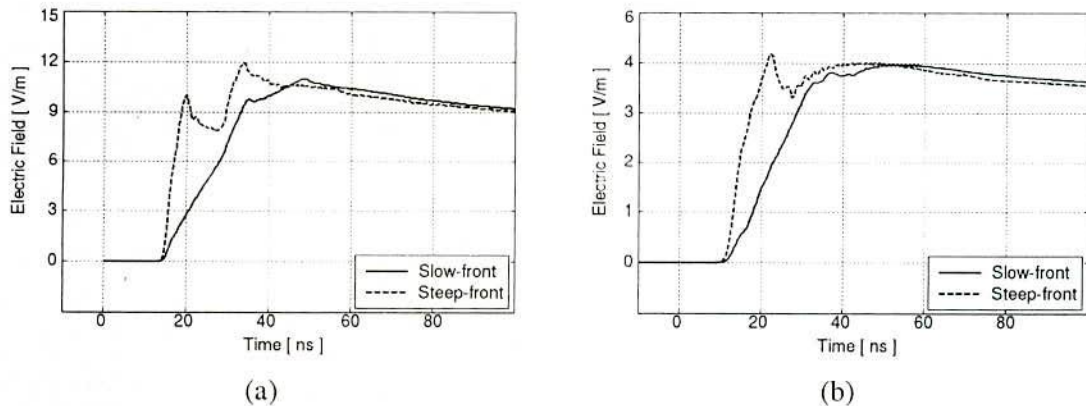


Fig. 5.7. Vertical electric field at (a) 2 m (b) 20 m from the tower for different input current. Computed by the FDTD method on reduced scale model.

From Figs. 5.3 and 5.7 it is observed that the electric field at 20 m for the lightning stroke to reduced scale tower is less than that of ground stroke. It leads to examine further the field at far distances. But in FDTD, it is very time consuming. The electric fields at 35 m for both the ground stroke and stroke to tall object (6 m) are shown in Fig. 5.8. It shows similar overall field wave shapes. This result is in agreement with the ref. [13] which takes the tower of height 10 m. It is also shown that the tall strike object affects the current distribution and, consequently, the radiated electric fields only for objects heights of some hundreds of meters.

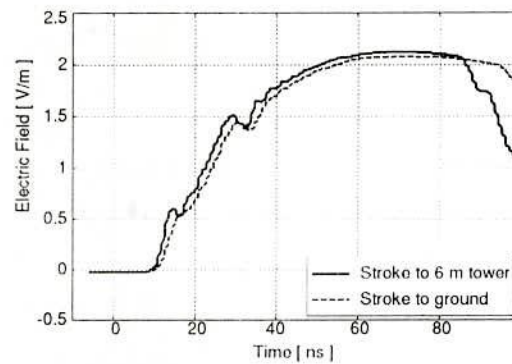


Fig. 5.8. Vertical electric field at 35 m for slow-front injection.

The effect of ground electrical parameters on the tower top current is shown in Fig. 5.9. The peak of the reflected current decreases as the ground conductivity decreases. The steep-front injection is considered in this case and the ground conductivity is taken as 5.89×10^7 S/m, 0.1 S/m and 0.01 S/m.

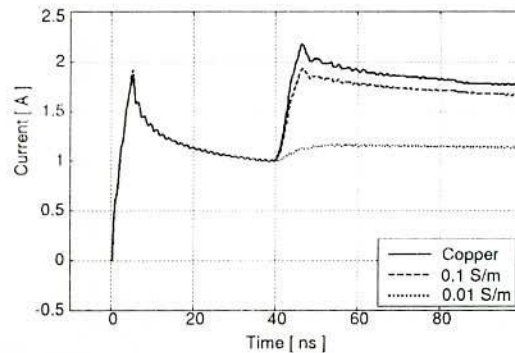


Fig. 5.9. Tower top current for different ground parameters. Computed by the FDTD method.

5.2.3 Computation Time

It might be believed that the FDTD method is a time consuming method. But, the progress of computers in speed and memory is considerable, and a recent personal computer can be used for the FDTD calculations. Actually, the simulations presented in this paper were performed by a personal computer with Pentium IV, 2.8 GHz CPU and 256 MB RAM. The computation time of the ground stroke case in section 5.2.1 was 11 minutes and 35 seconds, and in case of stroke to tall structures in section 5.2.2 was 13 minutes and 22 seconds. This time drastically increases for the computation of field at 35 m distant and takes 1 hour and 46 minutes.

5.3 NEC-2 Results of Reduced Scale Model

As like the model used in the FDTD simulation, the channel length of 20 m and the radius of 3 cm is considered in case of lightning stroke to ground. For the numerical analysis, the conductor is divided into cylindrical segments of 20 cm in length. The computation is carried out in the frequency range from 1.953 MHz to 1000 MHz with the increment step of 1.953 MHz. This corresponds to the time range from 0 to 0.512 μ s with 1 ns increments. PG with internal resistance of 10 Ω is used for current source. The current waveform shown in Fig. 5.1 is injected in this case also.

5.3.1 Lightning Return Stroke to Ground

Fig 5.10 shows the computed current along the channel for slow-front [Fig. 5.10(a)] and steep-front [Fig. 5.10(b)] injection. Fig. 5.11 shows the electric field at different distances for the current shown in Fig. 5.10.

Figs. 5.12 and 5.13 show the current for different ground conductivity and their associated electric fields, respectively. It is found that all the results of NEC-2 simulation on reduced scale model produced the same phenomenon as the work produced in the full scale in the previous chapters.

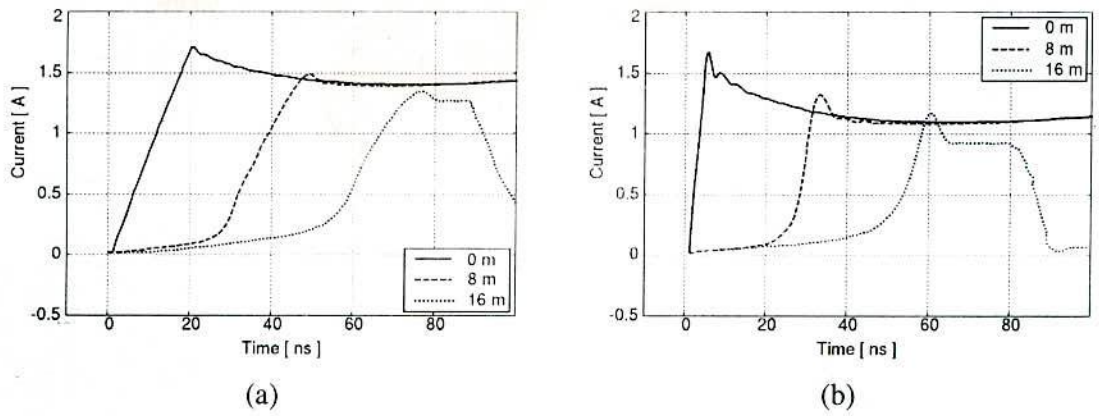


Fig. 5.10. (a) Slow-front (b) steep-front current along the channel. Computed by NEC-2 on reduced scale model.

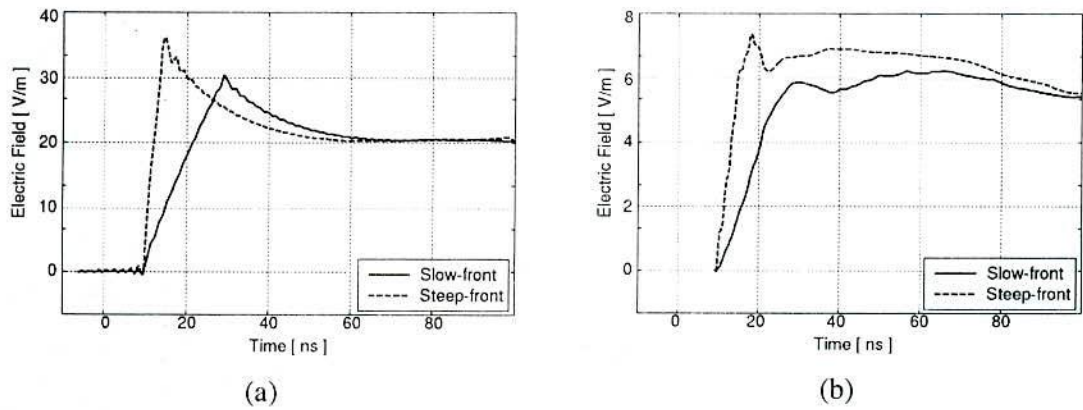


Fig. 5.11. Vertical electric field at (a) 2 m and (b) 20 m from the channel for the current shown in Fig. 5.10. Computed by NEC-2.

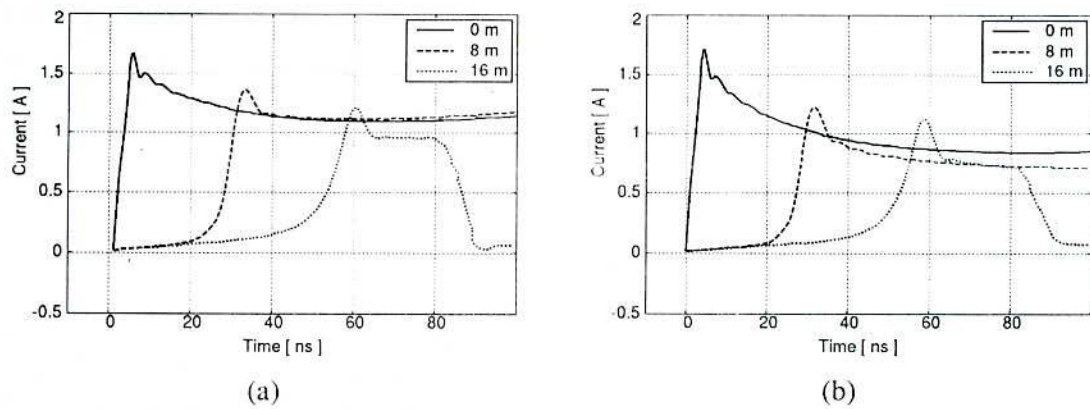


Fig. 5.12. Current along the channel for ground conductivity (a) 0.01 S/m and (b) 0.001 S/m. Computed by NEC-2 on reduced scale model.

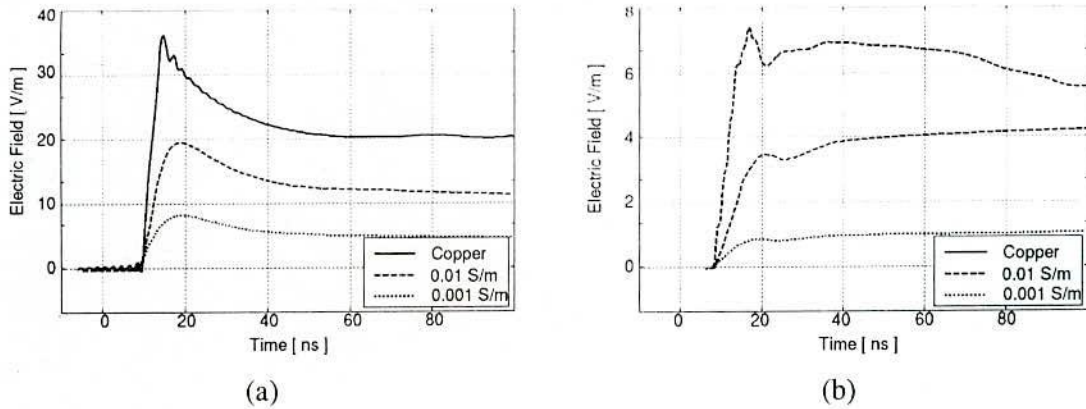


Fig. 5.13. Vertical electric field for different ground conductivities at (a) 2 m and (b) 20 m from the channel. Computed by NEC-2 on reduced scale model.

5.3.2 Lightning Return Stroke to Tall Structures

A uniform, lossless vertical conductor of length 6 m is taken as the tower. Fig 5.14 shows the computed current along the tower for (a) slow-front and (b) steep-front injection.

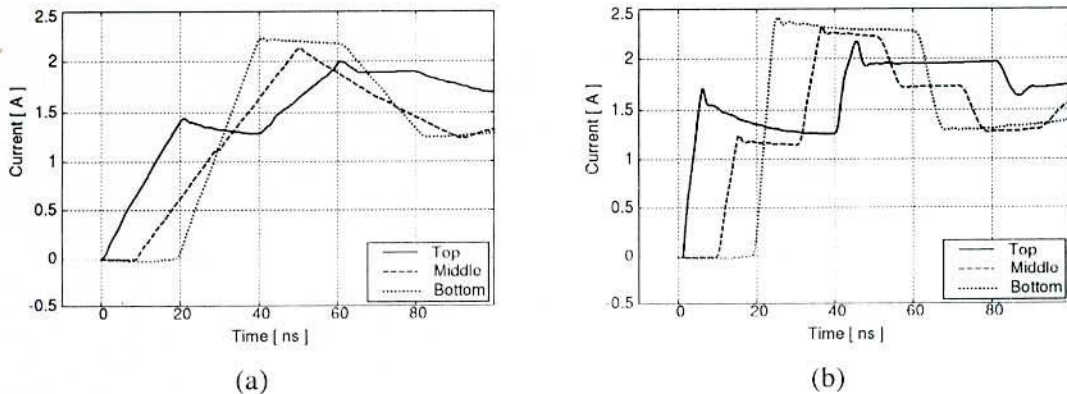


Fig. 5.14. (a) Slow-front (b) steep-front current along the tower. Computed by NEC-2 on reduced scale model.

It can be seen that the current peak value at the bottom of the tower is 1.31 times for slow-front injection and 1.39 times for steep-front injection comparing those associated with the stroke initiated at ground level. It can also be seen that the tower top current is more significantly affected by steep-front injection (1.28 times) than the slow-front injection

(1.14 times) comparing with the current in case of lightning stroke to ground. The effect of steep-front injected current is less as going to the bottom of the tower. The vertical electric fields at different distances corresponding to these currents are shown in Fig. 5.15. It is found that the field at 2 m and 20 m for steep-front is 1.05 to 1.09 times larger than the fields of slow-front.

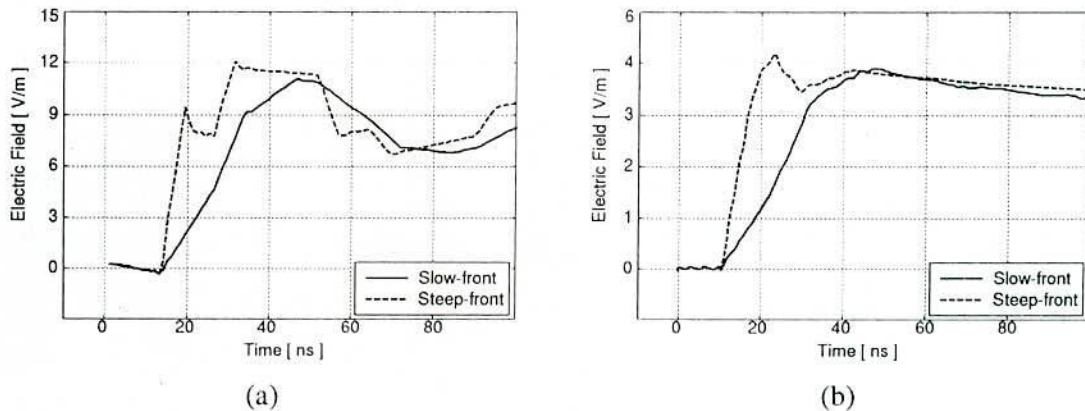


Fig. 5.15. Vertical electric field at (a) 2 m (b) 20 m for different input current. Computed by NEC-2 on reduced scale model.

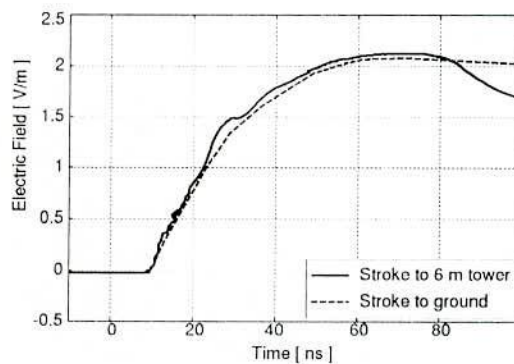


Fig. 5.16. Vertical electric field at 35 m for slow-front injection. Computed by NEC-2 on reduced scale model.

The electric fields at 35 m for both the ground stroke and stroke to tall object (6 m) [Fig. 5.16] show similar overall field wave shapes. The effect of ground electrical parameters on the tower top current is shown in Fig. 5.17. The peak of the reflected current decreases as the ground conductivity decreases. The perfect ground with copper and finite ground with conductivity of 0.1 S/m and 0.01 S/m are taken also here with the steep-front injection.

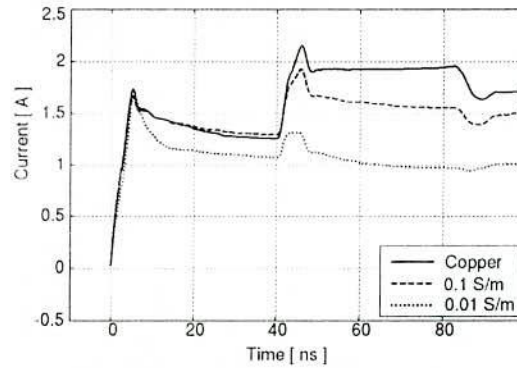


Fig. 5.17. Tower top current for different ground parameters. Computed by NEC-2 on reduced scale model.

5.3.3 Computation Time

The computation is carried out in the frequency range from 1.953 MHz to 1000 MHz with the increment step of 1.953 MHz. This corresponds to the time range from 0 to 0.512 μ s with 1 ns increments. The computation time for the output of NEC-2 block of the flow chart of Fig. 2.5, with 256 MB RAM, Pentium-4 2.8 GHz processor is about 2 seconds is observed in all cases.

5.4 Comparison of the FDTD and NEC-2 Results

Comparing the FDTD results [Figs. 5.2 - 5.9] with the corresponding NEC-2 results [Figs. 5.10 - 5.17] it can be concluded that there is no noticeable difference between them, especially in the peak of the waveforms. If some discrepancies are observed somewhere in the peak, it is mentioned that those are not more than 2.5 %. Some dissimilarity is also observed in the wave tail [compare Figs. 5.6 and 5.14, Figs. 5.7 and 5.15] due to different computation method. Another reason is that the NEC-2 considered the multiple reflection (actual) phenomenon of current when lightning strikes to tall structures which is produced in Fig. 5.14, whereas, the VSTL may not incorporate this feature. In fact, all the lightning analyses concentrate on the transient currents and fields; hence the tails are less significant.

Considering both the FDTD and NEC-2 results in reduced scale model, some significant observations are listed below.

1. Lightning return stroke current propagates along the channel with constant velocity (velocity of light) and its value decreases with height while its rise time increases [Figs. 5.2 and 5.10].
2. The peak current along the channel and its rise time does not change with ground conductivities but significant change is observed at the wave tail [Figs. 5.4 and 5.12].
3. Remote electromagnetic field peak and its derivative decreases as the ground conductivity decrease [Figs. 5.5 and 5.13].
4. Lightning current along the tall structures is significantly affected by the height of the structure [compare Figs. 5.2 and 5.6, Figs. 5.10 and 5.14].
5. Tower top current is more affected by the subsequent stroke (1.28 times) than the first stroke (1.14 times) compared with the ground stroke current [compare Figs. 5.2(b) and 5.6(b), Figs. 5.10(b) and 5.14(b)].
6. For the considered case, the electric field obtained for the ground stroke is essentially identical to that calculated considering the presence of the tall object [Figs. 5.8 and 5.16].
7. Subsequent stroke fields are larger (1.05 to 1.09 times) than that of first stroke [Figs. 5.3, 5.7 and Figs. 5.11 and 5.15].
8. The computation by VSTL based on FDTD method takes more time and space than the computation by NEC-2.

5.5 Summary

The simulation by VSTL and NEC-2, for the considered case of reduced scale model, produces the same result, specifically, with the difference of less than 2.5 %. Though the current amplitude appreciably affected by the small strike objects, it produce essentially identical field at 35 m as produced by the ground stroke current. The computation of field at larger distance increases the analysis space of FDTD. Small increments of length in one axis increases the analysis volume significantly and hence, drastically increases the computation time.

Chapter 6

Discussions and Conclusions

6.1 Discussions

The Numerical Electromagnetic Code (NEC-2) is applied to the analysis of the electric and magnetic fields radiated by lightning return strokes. Electric and magnetic field waveforms corresponding to typical first strokes have been computed and analyzed considering the lightning channel as a vertical conductor loaded by series inductance and resistance so as to simulate the slower propagation velocity of the current wave and the lossy channel. The effect of the presence of a tall tower on the magnitude and shape of the fields has been investigated. It was shown in particular that the presence of the tower tends, in general, to increase substantially electromagnetic field peaks and their derivatives. This increase is mainly caused by the presence of two oppositely propagating current wave fronts originating from the tower top and by the very high velocity (practically speed of light) of current propagation within the tower, and depends essentially on the wavefronts steepness of the current pulse.

On the other hand, it is important to realize that even a subsequent return stroke with a lower current peak than the first, could result in a greater field peak. This might be ascribed several factors. One of those, is the fact that the subsequent return stroke velocity is in general greater than the first return stroke velocity [71]. The electromagnetic field radiated by the lightning return stroke depends strongly on the value of the return stroke velocity and a larger value of the return stroke velocity results in a greater electromagnetic field peak. The other factor is the steepness of the current wavefront. Since subsequent strokes are associated with shorter rise times than first return strokes, their increased steepness will make a larger contribution to the electromagnetic field. Finally, the presence of an elevated strike object increases the electromagnetic field and the effect is larger for currents with steeper wavefronts, as shown by the results obtained in the present study.

Three approaches to the testing of electromagnetic models have been used. The first approach involves the initial field peak (at 2 km and 100 km) and the initial current peak is reasonably well related by the transmission line formula. The second approach involves the comparison of the computed fields with typical observed fields. Although the comparison between computed results and experimental observations should be considered as only qualitative, it can be seen, there exists a good agreement between the measured and calculated waveforms. The third approach involves the comparison of the results computed by FDTD method on reduced scale model. The NEC-2 based on MoM and the VSTL based on FDTD method produce same results. The advantage of the analysis using NEC-2 is that it can accurately compute the current distribution along a wire structure with far smaller amount of postulation than the approaches based on the traveling wave analysis and with less time and memory than FDTD method.

6.2 Conclusions

Electromagnetic field analysis of lightning return stroke current requires both the return stroke models to create the electromagnetic environment and the computation of the fields at different distances, the ground properties and their influences and the response of the tall structures on those fields. The thesis combines all these features taking a single model that can be utilized in the analysis of the interaction of electromagnetic fields with various circuits and systems. In this work, lightning electric and magnetic fields measured at the distance of 50 m, 2 km and 100 km are characterized and discussed.

Results of the analysis may be useful for interpretation of electromagnetic field waveforms, in lightning protection, for operation of Lightning Location and Protection (LLP) systems and for EMC applications.

6.3 Scopes for Future Work

The future studies will be concentrated on the following aspects:

1. For an improvement in modeling and for a more close comparison to experimental records, one may consider the use of more accurate parameters

(return stroke velocity, attenuation factors, input waveforms), of a more sophisticated model of the tower, and of actual channel geometry.

2. The present society relies highly on advanced electronic and telecommunication systems that regulate power distribution systems. The power network could provide several pathways for the transients to come into the distribution substations and affect their communication system. Indeed, the modern electronic equipment is highly sensitive to voltage fluctuations. However, there is a lack of information concerning the way in which these systems respond to nearby lightning strikes. There is a need to include full system configuration in over voltage calculations so that the transients entering into different parts of the network can be evaluated.
3. Mobile communication is rapidly growing technology in our country. Because of high altitude of placing radio transmission antennas, lightning strokes to the structures supporting the antennas are relatively frequent. There might be often limited possibilities of applying the lightning protection elements on towers or specific conditions or requirements for grounding systems. Another danger of destruction due to the lightning strikes comes from a new application that has been introduced in recent years, the installation of GSM antennas for mobile phones on HV power-line towers. Besides the direct effects on grounding system, the induced current may flow through the cabling systems into the radio-transmission equipment and the same lightning current creates strong electromagnetic pulse which can generate large over voltages and over currents in wires of electric and electronic systems. With the modeling of instrumented tower, the computed fields can be used as an input to the analysis of lightning effects in base station of Global Systems for Mobile Communication.
4. Lightning electromagnetic fields may affect biomedical equipment significantly. Especially it may be a cause of misleading results during measuring records. Hence, it requires proper modeling and analysis of such effects.

Bibliography

- [1] V. Cooray, "*The Lightning Flash*," IEE power and energy series 34, pp. 127-131, first edition, 2003.
- [2] Martin A. Uman, "*Lightning*," Dover publications, Inc. New York, c. 1984, ISBN 0-486-64575-4.
- [3] V. A. Rakov, "Lightning Electromagnetic Fields: Modeling and Measurements," in *Proc. 12th Int. Zurich Symp. on Electromagn. Compat.*, Zurich, Switzerland, February 1997, pp. 59-64.
- [4] V. A. Rakov, "Some inferences on the propagation mechanism of dart leaders and return strokes," *J. of Geophys. Res.*, vol. 103, pp. 1879-1887, 1998.
- [5] M. A. Uman and D. K. McLain, "Magnetic Field of Lightning Return Stroke," *Journal of Geophysical Research*, vol. 74, 1969.
- [6] F. Heidler, "Traveling Current Source Model for LEMP Calculation," in *Proc. 6th Int. Zurich Symp. on Electromagn. Compat.*, Zurich, Switzerland, March 1985, pp. 157-162.
- [7] C. A. Nucci, C. Mazzetti, F. Rachidi and M. Ianoz, "On Lightning Return Stroke Models for LEMP Calculations," in *Proc. 19th Int. Conf. on Lightning protection*, Graz, Austria, April 1988, pp. 463-469.
- [8] C. A. Nucci and F. Rachidi, "Experimental Validation of a Modification to the Transmission Line Model for LEMP Calculations," in *Proc. 8th Int. Symp. and Technical Exhibition on Electromagn. Compat.*, Zurich, Switzerland, 1989.
- [9] V. A. Rakov and A. A. Dulzon, "A Modified Transmission Line Model for Lightning Return Stroke Field Calculations," in *Proc. 9th Int. Symp. and Technical Exhibition on Electromagn. Compat.*, Zurich, Switzerland, 1991, pp. 229-235.
- [10] G. Diendorfer and M. A. Uman, "An Improved Return Stroke Model with Specified Channel-Base Current," *J. of Geoph. Res.*, vol. 95, no. D9, pp. 13621-13644, August 1990.
- [11] R. Thotappilil, D. K. McLain, M. A. Uman and G. Diendorfer, "Extension of the Diendorfer-Uman Lightning Return Stroke Model to the Case of a Variable Upward Return Stroke Speed and a Variable Downward Discharge Current Speed," *J. of Geoph. Res.*, vol. 96, no. D9, pp. 17143-17150, September 1991.

- [12] H. Motoyama, W. Janischewskyj, A. M. Hussein, R. Rusan, W. A. Chosholm, and J-S. Chang, "Electromagnetic field radiation model for lightning strokes to tall structures," *IEEE Trans. Power Delivery*, vol. 11, no. 3, pp. 1624-1632, July 1996.
- [13] S. Guerrieri, C. A. Nucci, F. Rachidi, and M. Rubinstein, "On the influence of elevated strike objects on directly measured and indirectly estimated lightning currents," *IEEE Trans. Power Delivery*, vol. 13, no. 4, pp. 1543-1551, Oct. 1998.
- [14] F. Rachidi, W. Janischewskyj, A. M. Hussein, C. A. Nucci, S. Guerrieri, B. Kordi, and J-S. Chang, "Current and electromagnetic field associated with lightning-return strokes to tall towers" *IEEE Trans. Electromagn. Compat.*, vol. 43, no. 3, pp. 356-367, Aug. 2001.
- [15] V. Shostak, W. Janischewskyj, A. M. Hussein, and B. Kordi, "Electromagnetic fields of lightning strikes to a tall tower: A model that accounts for upward-connecting discharges", in *Proc. of the 25th Int. Conf. on Lightning Protection*, Greece, Sept. 2000.
- [16] W. Janischewskyj, V. Shostak, and A. M. Hussein, "Lightning electric field characteristics of first and subsequent return strokes to a tall Tower," *Proc. of 11th Int. Symp. on High Voltage Engineering*, London, U. K., 1999.
- [17] A. S. Podgorski, and J. A. Landt, "Three dimensional time domain modelling of lightning," *IEEE Trans. Power Delivery*, vol. 2, pp. 931-938, 1987.
- [18] R. Moini, V. A. Rakov, M. A. Uman, and B. Kordi, "An antenna theory model for the lightning return stroke," in *Proc. 12th Int. Zurich Symp. on Electromagn. Compat.*, Zurich, Switzerland, Feb. 1997, pp. 149-152.
- [19] M. N. O. Sadiku, "Elements of Electromagnetics." Orlando, Florida: Sounders College, p. 821, 1994.
- [20] C. R. Paul, "Analysis of multiconductor transmission lines," New York: Wiley-Interscience, 1994.
- [21] M. Ishii and Y. Baba, "Numerical electromagnetic field analysis of tower surge response," *IEEE Trans. Power Delivery*, vol. 12, no. 1, pp. 483-488, Jan. 1997.
- [22] R. F. Harrington, *Field Computation by Moment Methods*, NY: Macmillan Company, 1968.
- [23] M. Van Blaricum and E. K. Miller, "TWTD—A computer program for time-domain analysis of thin-wire structures," Lawrence Livermore Laboratory, Rept. UCRL-51 277, 1972.

- [24] G. J. Burke and A. J. Poggio, "Numerical electromagnetic code (NEC) - method of moments," Naval Ocean Systems Center, San Diego, Technical Document 116, Jan. 1980.
- [25] F. Heidler and K. Muller, "LEMP calculations with traveling current source model," in *Proc. 1989 Int. Conf. on Lightning and Static Electricity*, Bath, U.K., Sept. 1989, 7B.2.1.
- [26] S. Cristina and A. Orlandi, "Lightning channel's influence on currents and electromagnetic fields in a building struck by lightning," in *Proc. 1990 IEEE Int. Symp. on Electromagn. Compa*, Washington DC, Aug. 1990, pp. 338-342.
- [27] J. C. Chai, H. A. Heritage, and R. Briet, "Electromagnetic effects of the four-tower supported catenary wires array lightning protection system," in *Proc. 16th Int. Aerospace and Ground Conf. Lightning and Static Electricity*, Mannheim, May 1994, pp. 377-386.
- [28] Y. Baba and M. Ishii, "Numerical electromagnetic field analysis of lightning current in tall structures," *IEEE Trans. Power Delivery*, vol. 16, no. 2, pp. 324-328, Apr. 2001.
- [29] Md. Osman Goni, Md. Faruque Hossain, Md. Salah Uddin Yusuf, Md. Mostafizur Rahaman, E. Kaneko and H. Takahashi, "Simulation and experimental analysis of transient behavior of lightning surge on vertical conductors", *IEEE Trans. Power Delivery*, (To be published).
- [30] Md. Faruque Hossain, Md. Salah Uddin Yusuf, Md. Osman Goni and Md. A. K. Azad, "Numerical analysis of current and electromagnetic field associated with lightning strokes to a tall tower", *J. of Institution of Engineers of Bangladesh (IEB)*, (To be published).
- [31] Md. Faruque Hossain, Md. Salah Uddin Yusuf, Md. Osman Goni and M. M. Rahman, "Numerical electromagnetic field analysis of lightning return strokes to tall towers," *J. of Institution of Engineers of Bangladesh (IEB)*, (To be published).
- [32] Md. Salah Uddin Yusuf, Md. Faruque Hossain and Md. Osman Goni, "Electromagnetic simulation of a lightning surge on a vertical conductor model," *J. of Institution of Engineer of Bangladesh (IEB)*, (To be published).
- [33] Md. Salah Uddin Yusuf, Md. Faruque Hossain and Md. Osman Goni, "Electromagnetic simulation of a lightning surge on a vertical conductor model,"

- in *Proc. 3rd Int. Conf. on Electrical & Computer Engineering, ICECE 2004*, December 28-30, 2004, Dhaka, Bangladesh, pp.163-166.
- [34] Md. Osman Goni, Md. Salah Uddin Yusuf, Md. Faruque Hossain, Md. Mostafizur Rahaman, E. Kaneko and H. Takahashi, "Theoretical simulation and experimental investigation of the surge response of a tower model of vertical conductor," *Int. Journal of power and energy system*, ACTA Press, USA, (To be published).
- [35] K. Tanabe, "Novel method for analyzing the transient behavior of grounding systems based on the FDTD method," in *Proc. IEEE Power Engineering Society Winter Meeting*, Vol. 3, 2001, pp. 1128 – 1132.
- [36] K. S. Yee, "Numerical solution of initial boundary value problems involving Maxwell's equations in isotropic media," *IEEE Trans. Antennas & Propag.*, Vol. AP-14, No. 3, pp. 302 – 307, 1966.
- [37] J. Moore Ed. And R. Pizer Ed., "*Moment Methods in Electromagnetics: Techniques and Applications*," Research Studies Press Ltd., England, 1984.
- [38] Johnson J. H. Wang, "*Generalized Moment Methods in Electromagnetics: Formulation and Computer Solution of Integral Equations*," John Wiley & Sons, Inc., New York, 1991.
- [39] T. Noda and S. Yokoyama, "Development of a general surge analysis program based on the FDTD method," *Trans. IEE of Japan*, vol. 121-B, no. 5, pp. 625-632, 2001.
- [40] A. Ralston, "*A First Course in Numerical Analysis*," McGraw-Hill, New York, 1965.
- [41] G. J. Burke, "Numerical electromagnetic code (NEC-4) - method of moments," *Lawrence Livermore National Laboratory*, UCRL-MA-109338 pt. II, Jan. 1992.
- [42] K. S. Kunz and R. J. Luebbers, "*The finite difference time domain method for electromagnetics*," Boca Raton, FL., *CRC Press*, 1993.
- [43] G. J. Burke and E. K. Miller, "Modeling antennas near to and penetrating a lossy interface," *IEEE Trans. Antennas & Propag.*, Vol. AP-32, No. 10, pp. 1040 – 1049, 1984.
- [44] K. R. Umashankar, et al., "Calculation and experimental validation of induced currents on coupled wires in an arbitrary shaped cavity," *IEEE Trans. Antennas & Propag.*, AP-35, No. 11, pp. 1248 – 1257, 1987.

- [45] T. Kashiwa, S. Tanaka and I. Fukai, "Time domain analysis of Yagi-Uda antennas using the FDTD method." *IEICE Trans.*, B-II, Vol. J76-B-II, No. 11, pp. 872-879, 1993.
- [46] T. Noda and S. Yokoyama, "Thin wire representation in finite difference time domain surge simulation," *IEEE Trans. power Delivery*, vol. 17, no. 3, pp. 840-847, 2002.
- [47] Z. P. Liao, H. L. Wong, B.-P. Yang and Y.-F. Yuan, "A transmitting boundary for transient wave analysis," *Science Sinica, Series A*, 27, 10, pp. 1063 - 1076, 1984.
- [48] D. M. Mach, and W. D. Rust, "Two-dimensional velocity, optical risetime, and peak current estimates for natural positive lightning return strokes" *J. Geophys. Res.*, vol. 98, 2635-2638, 1993.
- [49] V. P. Idone, R. E. Orville, D. M. Mach, and W.D. Rust, "The propagation speed of a positive lightning return stroke" *Geophys. Res. Lett.*, vol. 14, 1150-1153, 1987.
- [50] M. A. O. Schroeder, A. Soares Jr., S. F. Visacro, L. C. L. Cherchiglia, V. J. Souza, J. H. Diniz, and A. M. Carvalho, "Evaluation of directly measured lightning parameters," in *Proc. 1999 Int. Symp. Lightning Protection (V SIPDA)*, pp. 7-11.
- [51] C. Gomes and V. Cooray, "Correlation between the optical signatures and current waveforms of long sparks: application in lightning research," *J. Electrostatics*, vol. 43, pp. 267-274, 1998.
- [52] D. M. Jordan and M. A. Uman, "Variation in light intensity with height and time from subsequent return strokes," *J. Geophys. Res.*, vol. 88, pp. 6555-6562, 1983.
- [53] Y. T. Lin, M. A. Uman, J. A. Tiller, R. D. Brantley, W. H. Beasley, E. P. Krider, and C. D. Weidman, "Characterization of lightning return stroke electric and magnetic fields from simultaneous two-station measurements", *J. of Geophys. Res.*, vol. 84, pp. 6307-6314, 1979.
- [54] V. Rakov, "Lightning discharges triggered using rocket- and wire techniques," *Recent Res. Devel. Geophys.*, vol. 2, pp. 141-171, 1999.
- [55] M. A. Uman, D. K. McLain, and E. P. Krider, "The electromagnetic radiation from a finite antenna," *Amer. J. of Phys.*, vol. 43, pp. 33-38, Jan. 1975.
- [56] C. D. Weidman and E. P. Krider, "The fine structure of lightning return stroke wave forms," *J. of Geophys. Res.*, vol. 83, pp. 6239-6247, 1978.

- [57] J. C. Willett, J. C. Bailey, V. P. Idone, A. Eyebert-Berard, and L. Barret, "Submicrosecond intercomparison of radiation fields and currents an triggered lightning return strokes based on the transmission line model," *J. of Geophys. Res.*, vol. 94, pp. 13 275–13 286, 1989.
- [58] Nelson Theethayi and Veron Cooray, "On the representation of the lightning return stroke process as a current pulse propagating along a transmission line," *IEEE Trans. Power Delivery*, vol. 20, no. 2, pp. 823–837, Apr. 2005.
- [59] A. Soares, M. A. O. Schroeder, and S. Visacro, "Transient voltages in transmission lines caused by direct lightning strikes," *IEEE Trans. Power Delivery*, vol. 20, no. 2, pp. 1447–1452, Apr. 2005.
- [60] O. Beierl, "Front shape parameters of negative subsequent strokes measured at the Peissenberg tower", in *Proc. 21th Int. Conf. on Lightning Protection*, Berlin, Sept. 21-25, 1992.
- [61] W. Janischewskyj, A. M. Hussein, and V. Shostak, "Propagation of lightning current within the CN tower," in *Proc. Int. CIGRE Colloq. Insulation Coordination*, Toronto, Canada, Sept. 1997, paper 33-2.10.
- [62] E. Montandon, B. Beyeler, "The lightning measuring equipment on the Swiss PTT telecommunications tower at St. Chrischona, Switzerland", in *Proc. 22nd Int. Conf. on Lightning Protection*, Budapest, Hungary, Sept. 19-23, 1994.
- [63] M. O. Goni and H. Takahashi, "Theoretical and Experimental investigations of the surge response of a vertical conductor," *The Applied Computational Electromagnetic Society (ACES) Journal*, vol. 19, no. 1a, pp. 55-64, Mar. 2004.
- [64] H. Goshima, H. Motoyama, A. Asakawa, A. Wada, T. Shindo, and S. Yokoyama, "Characteristics of electromagnetic fields due to lightning stroke current to a high stack in winter lightning," *Trans. IEE Japan*, vol. 120-B, no. 1, pp. 44-49, Jan. 2000.
- [65] W. A. Chisholm and W. Janischewskyj, "Lightning surge response of ground electrodes," *IEEE Trans. Power Delivery*, vol. 4, no. 2, pp. 1329–1337, Apr. 1989.
- [66] Y. Baba and M. Ishii, "Numerical electromagnetic field analysis on lightning surge response of tower with shield wire," *IEEE Trans. Power Delivery*, vol. 15, no. 3, pp. 1010–1015, Jul. 2000.
- [67] R. Thotappilil, V. A. Rakov, and M. A. Uman, "Lightning subsequent-stroke electric field peak greater than the first stroke peak and multiple ground

- terminations," *J. of Geophys. Res.*, vol. 97, no. D7, pp. 7503-7509, September 20, 1991.
- [68] K. L. Cummins, E. P. Krider, and M. D. Malone, "The US national lightning detection network and applications to cloud-to-ground lightning data by electric power utilities," *IEEE Trans. Electromagn. Compat.*, vol. 40, pp. 465-480, Nov. 1980.
- [69] K. Berger, "Methoden und resultate der Blitzforschung auf dem Monte San Salvatore bei Lugano in den Jahren 1963-1971," *Bull. SEV*, vol. 63, pp. 1403-1422, 1972.
- [70] W. Janischewskyj, A. M. Hussein, and J-S. Chang, "Characteristics of CN Tower multistroke flashes," in *Proc. 10th Int. Symp. on High Voltage Engineering*, Montreal, Canada, pp. 29-34, Aug. 1997.
- [71] D. M. Mach, and W. D. Rust, "Photoelectric return stroke velocity, and peak current estimates in natural and triggered lightning," *J. of Geophys. Res.*, vol. 94, no. D11, 13237-13247, 1989.
- [72] "RCS computer program BRACKT, log-periodic scattering array program II," MBAssociates report, no. MB-R-69/46, Contact no. F04801-68-C-0188, 1969.
- [73] "Antenna modeling program," MBAssociates report, no. MB-R-74/46, 74/62, 1974.

Appendix A

Electric Field Integral Equation

The first step in developing the solution for the current on a wire antenna is determining the appropriate integral equation. The starting point in deriving the electric field integral equation (EFIE) is Maxwell's equations in the frequency domain. Assuming a linear, isotropic, and non-dispersive media, Maxwell's equations are:

$$\nabla \times \bar{E} = -j\omega\mu\bar{H} \quad \text{A.1}$$

$$\nabla \times \bar{H} = j\omega\epsilon\bar{E} + \bar{J} \quad \text{A.2}$$

$$\nabla \cdot \bar{E} = \frac{\rho_e}{\epsilon} \quad \text{A.3}$$

$$\nabla \cdot \bar{H} = 0 \quad \text{A.4}$$

If medium 1 is a perfect electrical conductor (PEC), the fields inside the surface will become zero and the boundary condition on the electric field becomes

$$\hat{n} \times (\bar{E}_2) = 0 \quad \text{A.5}$$

The electric field outside of S , \bar{E}_2 may be written as the sum of an incident electric field, \bar{E}_i , and a scattered electric field, \bar{E}_s . The incident electric field induces the surface current \bar{J}_s which in turn creates the scattered field \bar{E}_s . The Equivalence Principle can be used to remove the PEC giving a homogeneous free space problem. For the PEC case, the equivalent current equals the induced current, \bar{J}_s .

When the divergence of \bar{H} is zero, the magnetic field may be defined as the curl of an auxiliary vector, $\bar{H} = \nabla \times \bar{A}$, A.6

where \bar{A} is called the magnetic vector potential. After substituting (A.6) into (A.1) and noting that curl of \bar{E} is proportional to the curl of \bar{A} , the electric scalar potential, Φ , is defined in terms of \bar{E} and \bar{A} as

$$-\nabla\Phi = \bar{E} + j\omega\mu\bar{A} \quad \text{A.7}$$

The electric scalar potential and the magnetic vector potential allow for the solution of the electric and magnetic fields by one uncoupled equation, called the wave equation, rather than the two coupled curl equations (A.1) and (A.2). After substituting (A.6) and (A.7) into (A.2) and making use of a vector identity and the Lorentz gauge,

$$\nabla \cdot \bar{A} = -j\omega\epsilon\Phi \quad \text{A.8}$$

the vector wave equation is found to be

$$\nabla^2 \bar{A} + k^2 \bar{A} = -\bar{J} \quad \text{A.9}$$

Solving the vector wave equation for the magnetic vector potential due to \bar{J}_s , the free space solution is found to be

$$\bar{A}(\bar{r}) = \iint_s \bar{J}_s(\bar{r}') G(R) ds' \quad \text{A.10}$$

where the free space Green's function, G , is given by

$$G(R) = \frac{e^{-jkR}}{4\pi R}, \quad R = |\bar{r} - \bar{r}'|. \quad \text{A.11}$$

The primed vector, \bar{r}' , defines the source coordinates, \bar{r} defines the observation coordinates, and the wave number is $k = \omega\sqrt{\epsilon_0\mu_0}$. The scattered electric field is then found from combining (A.7) and (A.8) to give

$$\bar{E}_s = -j\omega\mu_0 \bar{A} - j \frac{1}{\omega\epsilon_0} \nabla(\nabla \cdot \bar{A}) \quad \text{A.12}$$

where ϵ_0 and μ_0 are the permittivity and permeability of free space.

The final step in determining the EFIE is to combine (A.5) and (A.12) to relate the scattered and incident fields, giving

$$\hat{n} \times \frac{j}{\omega\epsilon_0} (k^2 \bar{A} + \nabla(\nabla \cdot \bar{A})) = \hat{n} \times \bar{E}_i \quad \text{A.13}$$

If \bar{A} is replaced by (A.10), then (A.13) may be written as

$$\hat{n} \times \frac{j}{\omega\epsilon_0} \left[\iint_s k^2 \bar{J}_s(\bar{r}') G(R) ds' + \nabla \left(\nabla \cdot \iint_s \bar{J}_s(\bar{r}') G(R) ds' \right) \right] = \hat{n} \times \bar{E}_i \quad \text{A.14}$$

After simplifying, (A.14) reduces to

$$\hat{n} \times \frac{j}{\omega\epsilon_0} \iint_s \left[k^2 \bar{J}_s(\bar{r}') G(R) + (\nabla' \cdot \bar{J}_s(\bar{r}')) \nabla G(R) \right] ds' = \hat{n} \times \bar{E}_i \quad \text{A.15}$$

where ∇' means that the "del" operator now works on the source coordinates, \bar{r}' .

Finally we get the form

$$\frac{j\eta}{4\pi k} \iint_s \left[\bar{J}_s(\bar{r}') \left\{ k^2 G(R) + \nabla' \nabla G(R) \right\} \right] ds' \quad \text{A.16}$$

Equation (A.16) is the general electric field integral equation which will be used for the straight wire formulation.

Appendix B

History and Availability of NEC-2

The first in a series of NEC-MoM codes was BRACK [72] developed at MBAssociates in San Ramon, California. BRACK solved Pocklington's integral equation for thin wires with a three-term sinusoidal current expansion and point matching of the boundary condition. This code could model wire antennas including the effect of interaction with a finitely conducting ground through the Fresnel reflection-coefficient approximation. However, BRACK was used mainly by its developers.

The Antenna Modeling Program (AMP) [73] was the first code released for use by public users. AMP also solved Pocklington's integral equation for thin wires with a three term sinusoidal current expansion and point matching. The current expansion was chosen so that the current on a segment, with the form $A_i + B_i \sin ks + C_i \cos ks$, when extrapolated to the centers of the adjacent segments would coincide with the values of current on those segments. At a junction of several wires, the current was extrapolated to the center of a "phantom segment" whose length was the average of the connected segments. This extrapolation procedure smoothed the current distribution along wires, but still left discontinuities in current and charge density. AMP included options to model lumped or distributed loading on wires, transmission lines and networks.

AMP-2 included a magnetic field integral equation model for surfaces while the previous version was restricted to modeling thin wires.

NEC-1 was developed from AMP-2. It included a new way of implementing the three-term sinusoidal current expansion so that current and charge density exactly satisfied continuity conditions imposed at the junctions. The current was forced to satisfy Kirchhoff's current law at the junction, and the charge densities on wires were related to a function of the log of wire radius to provide approximate continuity of potential.

NEC-2 added a solution for wires over a lossy ground by implementing the rigorous Sommerfeld-integral approach.

NEC-3 extended the Sommerfeld-Integral ground model to wires buried in the ground or penetrating from air into ground.

NEC-4 [41] retains all of the capabilities of NEC-3, with changes and additions to improve the accuracy for stepped-radius wires and electrically small segments, and to add end caps and insulated wires.

The author employs NEC-2 in the present study, since later versions, NEC-3 and NEC-4, are available only to the citizens of the United States and Canada, or to the users who are licensed from Lawrence Livermore National Laboratory.

The documentation for NEC-2 is officially available from the National Technical Information Service, U.S. Department of Commerce.

National Technical Information Service

U.S. Department of Commerce

Springfield, Virginia 22161

Phone: + 1- 703- 487- 4650

It consists of three volumes; the theory, the source code in Fortran and the user's guide. The current price is about 200 dollars. The volumes of the theory and the user's guide are also obtained on a WWW site at

<http://members.home.net/nec2/>

The information's on the free executables of NEC-2 and commercial programs sold by vendors are also available on the above site.

Recent materials on the MoM theory and its applications contain detailed descriptions of the MoM, and they are useful for persons who wish to learn to use NEC-MoM codes.

Appendix C

FDTD Formulation

Maxwell's Equations and Initial Value Problem:

For simplicity suppose a three-dimensional (3D) model with linear, isotropic, non-dispersive medium and there is no magnetic charge and magnetic current. Also assume that initially all field components and sources are zero. Thus the Maxwell's equations which describe the initial value problem (IVP) for the model are as follows:

$$\nabla \times \bar{E} = -\frac{\partial \bar{B}}{\partial t} \quad \text{C.1}$$

$$\nabla \times \bar{H} = \bar{J} + \frac{\partial \bar{D}}{\partial t} \quad \text{C.2}$$

$$\nabla \cdot \bar{D} = \rho_e \quad \text{C.3}$$

$$\nabla \cdot \bar{B} = 0 \quad \text{C.4}$$

$$\bar{E}(x, y, z, t)|_{t=0} = \bar{H}(x, y, z, t)|_{t=0} = \bar{J}(x, y, z, t)|_{t=0} = 0 \text{ and } \rho_e(x, y, z, t)|_{t=0} = 0 \quad \text{C.5}$$

for all $(x, y, z) \in R^3$ and $t > 0$.

From (C.1):

$$\nabla \cdot (\nabla \times \bar{E}) = -\nabla \cdot \left(\frac{\partial \bar{B}}{\partial t} \right) = 0 \Rightarrow \frac{\partial}{\partial t} (\nabla \cdot \bar{B}) = 0$$

Using the initial condition (C.5), $\nabla \cdot \bar{B}|_{t=0} = \mu \nabla \cdot \bar{H}|_{t=0} = 0$, this implies that:

$$\nabla \cdot \bar{B}|_{t>0} = \nabla \cdot \bar{B}|_{t=0} = 0$$

Note that the vector identity $\nabla \cdot \nabla \times \bar{A} = 0$ is used.

Therefore the divergence equation for \bar{B} is implicit in (C.1).

Now consider (C.2),

$$\nabla \cdot (\nabla \times \bar{H}) = \nabla \cdot \bar{J} + \nabla \cdot \left(\frac{\partial \bar{D}}{\partial t} \right) = 0 \Rightarrow -\nabla \cdot \bar{J} = \frac{\partial}{\partial t} (\nabla \cdot \bar{D})$$

$$\nabla \cdot \bar{D} = -\int_0^t \nabla \cdot \bar{J} d\tau + C_2$$

Using the initial condition (C.5), $\nabla \cdot \bar{D}|_{t=0} = \epsilon \nabla \cdot \bar{E}|_{t=0} = 0$, this implies that $C_2 = 0$ and

$$\nabla \cdot \bar{D} = \int_0^t \nabla \cdot \bar{J} d\tau = \rho_e$$

Again this shows that divergence equation for \bar{D} is implicit in (C.2) provided initial conditions (C.5) applies. From this argument, we see that the divergence equations (C.2) and (C.3) are redundant, thus allowing for conduction electric current density $\bar{J} = \sigma \bar{E}$, the IVP of (C.1)-(C.5) can be reduced to:

$$\nabla \times \bar{E} = -\mu \frac{\partial \bar{H}}{\partial t} \quad \text{C.6}$$

$$\nabla \times \bar{H} = \epsilon \frac{\partial \bar{E}}{\partial t} + \sigma \bar{E} \quad \text{C.7}$$

$$\bar{E}(x, y, z, t)|_{t=0} = \bar{H}(x, y, z, t)|_{t=0} = \bar{J}(x, y, z, t)|_{t=0} = 0, \rho_e(x, y, z, t)|_{t=0} = 0 \quad \text{C.8}$$

In general this is also true when the medium is dispersive and nonlinear, as long as the initial conditions for magnetic and electric flux densities fulfill $\nabla \cdot \bar{D}|_{t=0} = \nabla \cdot \bar{B}|_{t=0} = 0$.

Yee's FDTD Formulation:

Equations (C.6)-(C.7) can be written as:

$$\frac{\partial \bar{E}}{\partial t} = \frac{1}{\epsilon} \nabla \times \bar{H} - \frac{\sigma}{\epsilon} \bar{E}$$

$$\frac{\partial \bar{H}}{\partial t} = -\frac{1}{\mu} \nabla \times \bar{E}$$

Under Cartesian coordinate system, these can be further expanded as:

$$\frac{\partial H_x}{\partial t} = -\frac{1}{\mu} \left(\frac{\partial E_z}{\partial y} - \frac{\partial E_y}{\partial z} \right) \quad \text{C.9}$$

$$\frac{\partial H_y}{\partial t} = -\frac{1}{\mu} \left(\frac{\partial E_x}{\partial z} - \frac{\partial E_z}{\partial x} \right) \quad \text{C.10}$$

$$\frac{\partial H_z}{\partial t} = -\frac{1}{\mu} \left(\frac{\partial E_y}{\partial x} - \frac{\partial E_x}{\partial y} \right) \quad \text{C.11}$$

$$\frac{\partial E_x}{\partial t} = \frac{1}{\epsilon} \left(\frac{\partial H_z}{\partial y} - \frac{\partial H_y}{\partial z} - \sigma E_x \right) \quad \text{C.12}$$

$$\frac{\partial E_y}{\partial t} = \frac{1}{\epsilon} \left(\frac{\partial H_x}{\partial z} - \frac{\partial H_z}{\partial x} - \sigma E_y \right) \quad \text{C.13}$$

$$\frac{\partial E_z}{\partial t} = \frac{1}{\epsilon} \left(\frac{\partial H_y}{\partial x} - \frac{\partial H_x}{\partial y} - \sigma E_z \right) \quad \text{C.14}$$

Let us introduce the notation:

$$E_{x(i,j,k)}^n = E_x(i\Delta x, j\Delta y, k\Delta z, n\Delta t) \quad \text{C.15}$$

and so on for E_y, E_z, H_x, H_y and H_z components. In Yee's scheme [36], the model is first divided into many small cubes. The edges of each cube will form the three-dimensional space grid. The position of the \mathbf{E} and \mathbf{H} field components in the space grid is shown in Fig. C.1.

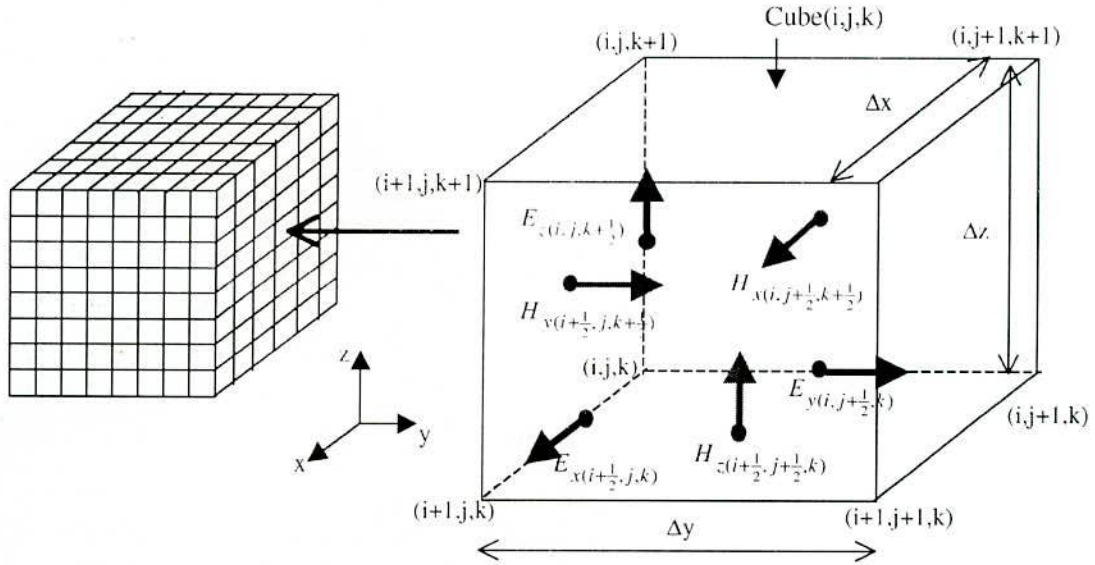


Fig. C.1 – Discretization of the model into cubes and the position of field components on the grid.

From Fig. C.1, it is observed that each \mathbf{E} field component is surrounded by four \mathbf{H} field components; similarly each \mathbf{H} field component is surrounded by four \mathbf{E} field components. For example, the component $H_{x(i,j+\frac{1}{2},k+\frac{1}{2})}$ is surrounded by $E_{z(i,j,k+\frac{1}{2})}$, $E_{z(i,j,k+\frac{1}{2})}$, $E_{y(i,j+\frac{1}{2},k)}$ and $E_{y(i,j+\frac{1}{2},k+1)}$. Using the center difference operator to replace the time and space

derivatives at time-step n and space lattice point $\left(i\Delta x, (j + \frac{1}{2})\Delta y, (k + \frac{1}{2})\Delta z \right)$ on (C.9):

$$\begin{aligned}
 & \frac{1}{\Delta t} \left(H_{x(i,j+\frac{1}{2},k+\frac{1}{2})}^{n+\frac{1}{2}} - H_{x(i,j+\frac{1}{2},k+\frac{1}{2})}^{n-\frac{1}{2}} \right) = \frac{1}{\mu} \left(\frac{1}{\Delta y} \left(E_{z(i,j+1,k+\frac{1}{2})}^n - E_{z(i,j,k+\frac{1}{2})}^n \right) \right. \\
 & \left. - \frac{1}{\Delta z} \left(E_{y(i,j+\frac{1}{2},k+1)}^n - E_{y(i,j+\frac{1}{2},k)}^n \right) \right) \\
 \Rightarrow H_{x(i,j+\frac{1}{2},k+\frac{1}{2})}^{n+\frac{1}{2}} &= H_{x(i,j+\frac{1}{2},k+\frac{1}{2})}^{n-\frac{1}{2}} - \frac{\Delta t}{\mu} \left(\frac{E_{z(i,j+1,k+\frac{1}{2})}^n - E_{z(i,j,k+\frac{1}{2})}^n}{\Delta y} - \frac{E_{y(i,j+\frac{1}{2},k+1)}^n - E_{y(i,j+\frac{1}{2},k)}^n}{\Delta z} \right) \quad \text{C.16}
 \end{aligned}$$

Repeating this procedure for (C.12) at time step $n + \frac{1}{2}$ and space lattice point $\left((i + \frac{1}{2})\Delta x, j\Delta y, k\Delta z \right)$:

$$\begin{aligned}
 \frac{1}{\Delta t} \left(E_{x(i+\frac{1}{2},j,k)}^{n+1} - E_{x(i+\frac{1}{2},j,k)}^n \right) &= \frac{1}{\epsilon \Delta y} \left(H_{z(i+\frac{1}{2},j+\frac{1}{2},k)}^{n+\frac{1}{2}} - H_{z(i+\frac{1}{2},j-\frac{1}{2},k)}^{n+\frac{1}{2}} \right) \\
 & - \frac{1}{\epsilon \Delta z} \left(H_{y(i+\frac{1}{2},j,k+\frac{1}{2})}^{n+\frac{1}{2}} - H_{y(i+\frac{1}{2},j,k-\frac{1}{2})}^{n+\frac{1}{2}} \right) - \frac{1}{\epsilon} \sigma E_{x(i+\frac{1}{2},j,k)}^{n+\frac{1}{2}}
 \end{aligned}$$

Substituting $E_{x(i,j,k)}^{n+\frac{1}{2}}$ with the average between time-step n and $n+1$:

$$\begin{aligned}
 \frac{1}{\Delta t} \left(E_{x(i+\frac{1}{2},j,k)}^{n+1} - E_{x(i+\frac{1}{2},j,k)}^n \right) &= \frac{1}{\epsilon \Delta y} \left(H_{z(i+\frac{1}{2},j+\frac{1}{2},k)}^{n+\frac{1}{2}} - H_{z(i+\frac{1}{2},j-\frac{1}{2},k)}^{n+\frac{1}{2}} \right) \\
 & - \frac{1}{\epsilon \Delta z} \left(H_{y(i+\frac{1}{2},j,k+\frac{1}{2})}^{n+\frac{1}{2}} - H_{y(i+\frac{1}{2},j,k-\frac{1}{2})}^{n+\frac{1}{2}} \right) - \frac{1}{\epsilon} \sigma \cdot \frac{1}{2} \left(E_{x(i+\frac{1}{2},j,k)}^{n+1} + E_{x(i+\frac{1}{2},j,k)}^n \right)
 \end{aligned}$$

After some algebraic manipulation, we obtained:

$$\begin{aligned}
 E_{x(i+\frac{1}{2},j,k)}^{n+1} &= \left(\frac{1 - \frac{\sigma \Delta t}{2\epsilon}}{1 + \frac{\sigma \Delta t}{2\epsilon}} \right) E_{x(i+\frac{1}{2},j,k)}^{n+1} \\
 & + \frac{\Delta t}{\epsilon} \left(\frac{H_{z(i+\frac{1}{2},j+\frac{1}{2},k)}^{n+\frac{1}{2}} - H_{z(i+\frac{1}{2},j-\frac{1}{2},k)}^{n+\frac{1}{2}}}{\Delta y} - \frac{H_{y(i+\frac{1}{2},j,k+\frac{1}{2})}^{n+\frac{1}{2}} - H_{y(i+\frac{1}{2},j,k-\frac{1}{2})}^{n+\frac{1}{2}}}{\Delta z} \right) \quad \text{C.17}
 \end{aligned}$$

By the same token, the update equations for the other field components can be derived:

$$H_{y(i+\frac{1}{2},j,k+\frac{1}{2})}^{n+\frac{1}{2}} = H_{y(i+\frac{1}{2},j,k+\frac{1}{2})}^{n-\frac{1}{2}} - \frac{\Delta t}{\mu} \left(\frac{E_{x(i+\frac{1}{2},j,k+1)}^n - E_{x(i+\frac{1}{2},j,k)}^n}{\Delta z} - \frac{E_{z(i+1,j,k+\frac{1}{2})}^n - E_{z(i,j,k+\frac{1}{2})}^n}{\Delta x} \right) \quad \text{C.18}$$

$$H_{z(i+\frac{1}{2},j+\frac{1}{2},k)}^{n+\frac{1}{2}} = H_{z(i+\frac{1}{2},j+\frac{1}{2},k)}^{n-\frac{1}{2}} - \frac{\Delta t}{\mu} \left(\frac{E_{y(i+1,j+1,k)}^n - E_{y(i,j+\frac{1}{2},k)}^n}{\Delta x} - \frac{E_{x(i+\frac{1}{2},j+1,k)}^n - E_{x(i+\frac{1}{2},j,k)}^n}{\Delta y} \right) \quad \text{C.19}$$

$$E_{y(i,j+\frac{1}{2},k)}^{n+1} = \left(\frac{1 - \frac{\sigma \Delta t}{2\epsilon}}{1 + \frac{\sigma \Delta t}{2\epsilon}} \right) E_{y(i,j+\frac{1}{2},k)}^{n+1} + \frac{\Delta t}{\epsilon} \left(\frac{H_{x(i,j+\frac{1}{2},k+\frac{1}{2})}^{n+\frac{1}{2}} - H_{x(i,j+\frac{1}{2},k-\frac{1}{2})}^{n+\frac{1}{2}}}{\Delta z} - \frac{H_{z(i+\frac{1}{2},j+\frac{1}{2},k)}^{n+\frac{1}{2}} - H_{z(i-\frac{1}{2},j+\frac{1}{2},k)}^{n+\frac{1}{2}}}{\Delta x} \right) \quad \text{C.20}$$

$$E_{z(i,j,k+\frac{1}{2})}^{n+1} = \left(\frac{1 - \frac{\sigma \Delta t}{2\epsilon}}{1 + \frac{\sigma \Delta t}{2\epsilon}} \right) E_{z(i,j,k+\frac{1}{2})}^{n+1} + \frac{\Delta t}{\epsilon} \left(\frac{H_{y(i+\frac{1}{2},j,k+\frac{1}{2})}^{n+\frac{1}{2}} - H_{y(i-\frac{1}{2},j,k+\frac{1}{2})}^{n+\frac{1}{2}}}{\Delta x} - \frac{H_{x(i,j+\frac{1}{2},k+\frac{1}{2})}^{n+\frac{1}{2}} - H_{x(i,j-\frac{1}{2},k+\frac{1}{2})}^{n+\frac{1}{2}}}{\Delta y} \right) \quad \text{C.21}$$

Equations (C.16)-(C.21) are explicit in nature, thus computer implementation does not require solving for determinant or inverse of a large matrix. To facilitate the implementation in digital computer, the indexes of the field components are renamed as shown in Fig. C.2, so that all the indexes become integers. This allows the value of each field component to be stored in a three-dimensional array in the software, with the array indexes correspond to the spatial indexes of Fig. C.2. In the figure additional field components are drawn to improve the clarity of the convention.

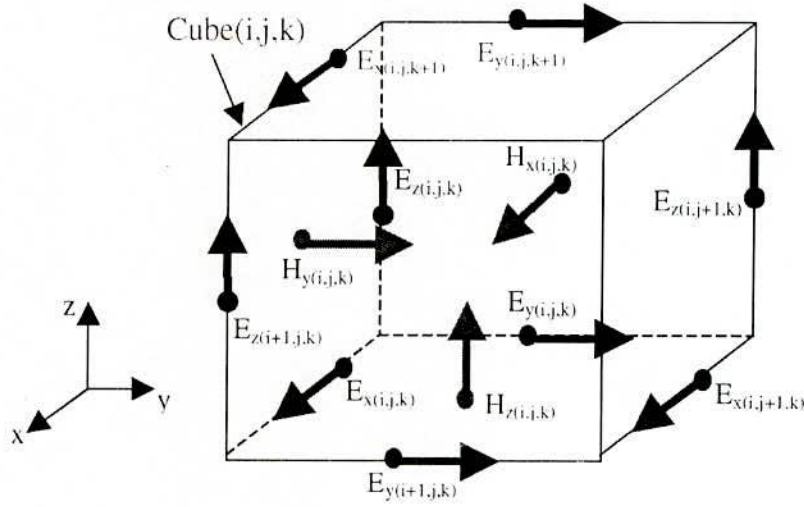


Fig. C.2– Renaming the indexes of E and H field components corresponding to cube (i,j,k).

Using the new spatial indexes for field components as in Fig. C.2, (C.16)-(C.21) becomes:

$$H_{x(i,j,k)}^{n+\frac{1}{2}} = H_{x(i,j,k)}^{n-\frac{1}{2}} - K_3[\{E_{z(i,j+1,k)}^n - E_{z(i,j,k)}^n\} - \{E_{y(i,j,k+1)}^n - E_{y(i,j,k)}^n\}] \quad \text{C.22}$$

$$H_{y(i,j,k)}^{n+\frac{1}{2}} = H_{y(i,j,k)}^{n-\frac{1}{2}} - K_3[\{E_{x(i,j,k+1)}^n - E_{x(i,j,k)}^n\} - \{E_{z(i+1,j,k)}^n - E_{z(i,j,k)}^n\}] \quad \text{C.23}$$

$$H_{z(i,j,k)}^{n+\frac{1}{2}} = H_{z(i,j,k)}^{n-\frac{1}{2}} - K_3[\{E_{y(i+1,j,k)}^n - E_{y(i,j,k)}^n\} - \{E_{x(i,j+1,k)}^n - E_{x(i,j,k)}^n\}] \quad \text{C.24}$$

$$E_{x(i,j,k)}^{n+1} = K_1 E_{x(i,j,k)}^n + K_2[\{H_{z(i,j,k)}^{n+\frac{1}{2}} - H_{z(i,j-1,k)}^{n+\frac{1}{2}}\} - \{H_{y(i,j,k)}^{n+\frac{1}{2}} - H_{y(i,j,k-1)}^{n+\frac{1}{2}}\}] \quad \text{C.25}$$

$$E_{y(i,j,k)}^{n+1} = K_1 E_{y(i,j,k)}^n + K_2[\{H_{x(i,j,k)}^{n+\frac{1}{2}} - H_{x(i,j,k-1)}^{n+\frac{1}{2}}\} - \{H_{z(i,j,k)}^{n+\frac{1}{2}} - H_{z(i-1,j,k)}^{n+\frac{1}{2}}\}] \quad \text{C.26}$$

$$E_{z(i,j,k)}^{n+1} = K_1 E_{z(i,j,k)}^n + K_2[\{H_{y(i,j,k)}^{n+\frac{1}{2}} - H_{y(i-1,j,k)}^{n+\frac{1}{2}}\} - \{H_{x(i,j,k)}^{n+\frac{1}{2}} - H_{x(i,j-1,k)}^{n+\frac{1}{2}}\}] \quad \text{C.27}$$

In the derivation of the above equations, an approximation $\sigma \mathbf{E}^{n-1/2} \cong \sigma \{\mathbf{E}^{n-1} + \mathbf{E}^n\} / 2$ is used and for simplicity the cubes are assumed to be same size, and coefficients K_1 , K_2 , and K_3 are given by the following equations.

$$K_1 = \frac{1 - \frac{\sigma \Delta t}{2\varepsilon}}{1 + \frac{\sigma \Delta t}{2\varepsilon}}, \quad K_2 = \frac{\Delta t}{\varepsilon \Delta s} \frac{1}{1 + \frac{\sigma \Delta t}{2\varepsilon}}, \quad K_3 = \frac{\Delta t}{\mu \Delta s} \quad \text{C.28}$$

Appendix D

Sample Input Data to NEC-2 for Stroke to Ground

```
CM CURRENT AT THE BASE OF THE CHANNEL IN CASE OF GROUND STROKE
CM Lightning Channel of Perfect Electrical Conductor
CM N=512 DT= 0.1E-06 SEC DL= 25 m
CE PERFECTLY CONDUCTING GROUND
GW 1 60 0.0 0.0 1500.0 0.0 0.0 0.0 0.3
GE 1
GN 1
LD 4 1 60 4.0E+02
FR 0 257 0.01953 0.01953
EX 0 1 60 00 22.0E+03 0.0
PT 0 1 60
XQ
EN
```

```
CM CURRENT AT 600 m HEIGHT OF THE CHANNEL IN CASE OF GROUND STROKE
CM Lightning Channel of Perfect Electrical Conductor
CM N=512 DT= 0.1E-06 SEC DL= 25 m
CE PERFECTLY CONDUCTING GROUND
GW 1 60 0.0 0.0 1500.0 0.0 0.0 0.0 0.3
GE 1
GN 1
LD 4 1 60 4.0E+02
FR 0 257 0.01953 0.01953
EX 0 1 60 00 22.0E+03 0.0
PT 0 1 36
XQ
EN
```

```
CM CURRENT AT 1200 m HEIGHT OF THE CHANNEL IN CASE OF GROUND STROKE
CM Lightning Channel of Perfect Electrical Conductor
CM N=512 DT= 0.1E-06 SEC DL= 25 m
CE PERFECTLY CONDUCTING GROUND
GW 1 60 0.0 0.0 1500.0 0.0 0.0 0.0 0.3
GE 1
GN 1
LD 4 1 60 4.0E+02
FR 0 257 0.01953 0.01953
EX 0 1 60 00 22.0E+03 0.0
PT 0 1 12
XQ
EN
```

Appendix D: Sample Input Data to NEC-2 for Stroke to Ground

```

CM ELECTRIC FIELD AT 50 m FROM THE CHANNEL IN CASE OF GROUND STROKE
CM Lightning Channel of Perfect Electrical Conductor
CM N=512 DT= 0.1E-06 SEC DL= 25 m
CE PERFECTLY CONDUCTING GROUND
GW 1 60 0.0 0.0 1500.0 0.0 0.0 0.0 0.3
GE 1
GN 1
LD 4 1 60 4.0E+02
FR 0 257 0.01953 0.01953
EX 0 1 60 00 22.0E+03 0.0
NE 0 1 1 1 50.0 0.0 20.0 0.0 0.0 0.0
XQ
EN

```

```

CM ELECTRIC FIELD AT 2 Km FROM THE CHANNEL IN CASE OF GROUND STROKE
CM Lightning Channel of Perfect Electrical Conductor
CM N=512 DT= 0.1E-06 SEC DL= 25 m
CE PERFECTLY CONDUCTING GROUND
GW 1 60 0.0 0.0 1500.0 0.0 0.0 0.0 0.3
GE 1
GN 1
LD 4 1 60 4.0E+02
FR 0 257 0.01953 0.01953
EX 0 1 60 00 22.0E+03 0.0
NE 0 1 1 1 2000.0 0.0 20.0 0.0 0.0 0.0
XQ
EN

```

```

CM MAGNETIC FIELD AT 50 m DISTANCE IN CASE OF STROKE TO GROUND
CM Lightning Channel of Perfect Electrical Conductor
CM N=512 DT= 0.1E-06 SEC DL= 25 m
CE PERFECTLY CONDUCTING GROUND
GW 1 60 0.0 0.0 1500.0 0.0 0.0 0.0 0.3
GE 1
GN 1
LD 4 1 60 4.0E+02
FR 0 257 0.01953 0.01953
EX 0 1 60 00 22.0E+03 0.0
NH 0 1 1 1 50.0 0.0 20.0 0.0 0.0 0.0
XQ
EN

```

```

CM CURRENT AT THE BASE OF THE CHANNEL IN CASE OF GROUND STROKE
CM Lightning Channel With Resistance of 1 Ω/m and Zero Inductance
CM N=512 DT= 0.1E-06 SEC DL= 25 m
CE PERFECTLY CONDUCTING GROUND
GW 1 60 0.0 0.0 1500.0 0.0 0.0 0.0 0.3
GE 1
GN 1
LD 2 1 1 59 1.0 0.0 0.0
LD 4 1 60 4.0E+02
FR 0 257 0.01953 0.01953
EX 0 1 60 00 24.5E+03 0.0
PT 0 1 60
XQ
EN

```


Appendix D: Sample Input Data to NEC-2 for Stroke to Ground

```

CM CURRENT AT THE BASE OF THE CHANNEL IN CASE OF GROUND STROKE
CM Lightning Channel With Resistance of 3 Ω/m and Zero Inductance
CM N=512 DT= 0.1E-06 SEC DL= 25 m
CE PERFECTLY CONDUCTING GROUND
GW 1 60 0.0 0.0 1500.0 0.0 0.0 0.0 0.3
GE 1
GN 1
LD 2 1 1 59 3.0 0.0 0.0
LD 4 1 60 4.0E+02
FR 0 257 0.01953 0.01953
EX 0 1 60 00 27.5E+03 0.0
PT 0 1 60
XQ
EN
    
```

```

CM CURRENT AT THE BASE OF THE CHANNEL IN CASE OF GROUND STROKE
CM Lightning Channel With Resistance of 1 Ω/m and Inductance of 1 μH/m
CM N=512 DT= 0.1E-06 SEC DL= 25 m
CE PERFECTLY CONDUCTING GROUND
GW 1 60 0.0 0.0 1500.0 0.0 0.0 0.0 0.3
GE 1
GN 1
LD 2 1 1 59 1.0 1.0E-06 0.0
LD 4 1 60 4.0E+02
FR 0 257 0.01953 0.01953
EX 0 1 60 00 26.5E+03 0.0
PT 0 1 60
XQ
EN
    
```

```

CM ELECTRIC FIELD AT 2 km FROM THE CHANNEL IN CASE OF GROUND STROKE
CM Lightning Channel With Resistance of 1 Ω/m and Inductance of 1 μH/m
CM N=512 DT= 0.1E-06 SEC DL= 25 m
CE PERFECTLY CONDUCTING GROUND
GW 1 60 0.0 0.0 1500.0 0.0 0.0 0.0 0.3
GE 1
GN 1
LD 2 1 1 59 1.0 1.0E-06 0.0
LD 4 1 60 4.0E+02
FR 0 257 0.01953 0.01953
EX 0 1 60 00 26.5E+03 0.0
NE 0 1 1 1 2000.0 0.0 20.0 0.0 0.0
XQ
EN
    
```

```

CM CURRENT AT THE BASE OF THE CHANNEL IN CASE OF GROUND STROKE
CM Lightning Channel With Resistance of 1 Ω/m and Inductance of 3 μH/m
CM N=512 DT= 0.1E-06 SEC DL= 25 m
CE PERFECTLY CONDUCTING GROUND
GW 1 60 0.0 0.0 1500.0 0.0 0.0 0.0 0.3
GE 1
GN 1
LD 2 1 1 59 1.0 3.0E-06 0.0
LD 4 1 60 4.0E+02
FR 0 257 0.01953 0.01953
EX 0 1 60 00 29.6E+03 0.0
PT 0 1 60
XQ
EN
    
```

Appendix D: Sample Input Data to NEC-2 for Stroke to Ground

```

CM E-FIELD AT 50 m DISTANCE AND AT THE HEIGHT OF 40 m FROM GROUND
CM Lightning Channel With Resistance of 1 Ω/m and Inductance of 3 μH/m
CM N=512 DT= 0.1E-06 SEC DL= 25 m
CE PERFECTLY CONDUCTING GROUND
GW 1 60 0.0 0.0 1500.0 0.0 0.0 0.0 0.3
GE 1
GN 1
LD 2 1 1 59 1.0 3.0E-06 0.0
LD 4 1 60 4.0E+02
FR 0 257 0.01953 0.01953
EX 0 1 60 00 29.6E+03 0.0
NE 0 1 1 1 50.0 0.0 40.0 0.0 0.0 0.0
XQ
EN

```

```

CM ELECTRIC FIELD AT 2 km FROM THE CHANNEL IN CASE OF GROUND STROKE
CM Lightning Channel With Resistance of 1 Ω/m and Inductance of 3 μH/m
CM N=512 DT= 0.1E-06 SEC DL= 25 m
CE PERFECTLY CONDUCTING GROUND
GW 1 60 0.0 0.0 1500.0 0.0 0.0 0.0 0.3
GE 1
GN 1
LD 2 1 1 59 1.0 3.0E-06 0.0
LD 4 1 60 4.0E+02
FR 0 257 0.01953 0.01953
EX 0 1 60 00 29.6E+03 0.0
NE 0 1 1 1 2000.0 0.0 20.0 0.0 0.0 0.0
XQ
EN

```

```

CM CURRENT AT THE BASE OF THE CHANNEL IN CASE OF GROUND STROKE
CM Lightning Channel With Resistance of 1 Ω/m and Inductance of 3 μH/m
CM N=512 DT= 0.1E-06 SEC DL= 25 m
CE GROUND CONDUCTIVITY 0.01 S/m
GW 1 60 0.0 0.0 1500.0 0.0 0.0 0.0 0.3
GE 1
GN 0 0.01
LD 2 1 1 59 1.0 3.0E-06 0.0
LD 4 1 60 4.0E+02
FR 0 257 0.01953 0.01953
EX 0 1 60 00 32.7E+03 0.0
PT 0 1 60
XQ
EN

```

```

CM CURRENT AT THE BASE OF THE CHANNEL IN CASE OF GROUND STROKE
CM Lightning Channel With Resistance of 1 Ω/m and Inductance of 3 μH/m
CM N=512 DT= 0.1E-06 SEC DL= 25 m
CE GROUND CONDUCTIVITY 0.001 S/m
GW 1 60 0.0 0.0 1500.0 0.0 0.0 0.0 0.3
GE 1
GN 0 0.001
LD 2 1 1 59 1.0 3.0E-06 0.0
LD 4 1 60 4.0E+02
FR 0 257 0.01953 0.01953
EX 0 1 60 00 39.5E+03 0.0
PT 0 1 60
XQ
EN

```

Appendix E

Sample Input Data to NEC-2 for Stroke to Tall Tower

CM CURRENT AT THE TOP OF 200 m TOWER IN CASE OF STROKE TO TALL STRUCTURE
CM Lightning Channel With Resistance of 1 Ω /m and Inductance of 3 μ H/m
CM N=512 DT= 0.1E-06 SEC DL= 25 m
CE PERFECTLY CONDUCTING GROUND
GW 1 8 0.0 0.0 200.0 0.0 0.0 0.0 0.3
GW 2 60 0.0 0.0 1700.0 0.0 0.0 200.0 0.3
GE 1
GN 1
LD 2 2 1 59 1.0 3.0E-06 0.0
LD 4 2 60 4.0E+02
FR 0 257 0.01953 0.01953
EX 0 2 60 00 29.6E+03 0.0
PT 0 1 1
XQ
EN

CM CURRENT AT THE TOP OF 550 m TOWER IN CASE OF STROKE TO TALL STRUCTURE
CM Lightning Channel With Resistance of 1 Ω /m and Inductance of 3 μ H/m
CM N=512 DT= 0.1E-06 SEC DL= 25 m
CE PERFECTLY CONDUCTING GROUND
GW 1 22 0.0 0.0 550.0 0.0 0.0 0.0 0.3
GW 2 60 0.0 0.0 2050.0 0.0 0.0 550.0 0.3
GE 1
GN 1
LD 2 2 1 59 1.0 3.0E-06 0.0
LD 4 2 60 4.0E+02
FR 0 257 0.01953 0.01953
EX 0 2 60 00 29.6E+03 0.0
PT 0 1 1
XQ
EN

CM CURRENT AT MIDDLE OF 550 m TOWER IN CASE OF STROKE TO TALL STRUCTURE
CM Lightning Channel With Resistance of 1 Ω /m and Inductance of 3 μ H/m
CM N=512 DT= 0.1E-06 SEC DL= 25 m
CE PERFECTLY CONDUCTING GROUND
GW 1 22 0.0 0.0 550.0 0.0 0.0 0.0 0.3
GW 2 60 0.0 0.0 2050.0 0.0 0.0 550.0 0.3
GE 1
GN 1
LD 2 2 1 59 1.0 3.0E-06 0.0
LD 4 2 60 4.0E+02
FR 0 257 0.01953 0.01953
EX 0 2 60 00 29.6E+03 0.0
PT 0 1 11
XQ
EN

Appendix E: Sample Input Data to NEC-2 for Stroke to Tall Tower

CM CURRENT AT BOTTOM OF 550 m TOWER IN CASE OF STROKE TO TALL STRUCTURE
 CM Lightning Channel With Resistance of 1 Ω /m and Inductance of 3 μ H/m
 CM N=512 DT= 0.1E-06 SEC DL= 25 m
 CE PERFECTLY CONDUCTING GROUND
 GW 1 22 0.0 0.0 550.0 0.0 0.0 0.0 0.3
 GW 2 60 0.0 0.0 2050.0 0.0 0.0 550.0 0.3
 GE 1
 GN 1
 LD 2 2 1 59 1.0 3.0E-06 0.0
 LD 4 2 60 4.0E+02
 FR 0 257 0.01953 0.01953
 EX 0 2 60 00 29.6E+03 0.0
 PT 0 1 22
 XQ
 EN

CM ELECTRIC FIELD AT 50 m DISTANCE IN CASE OF STROKE TO TALL STRUCTURE
 CM Lightning Channel With Resistance of 1 Ω /m and Inductance of 3 μ H/m
 CM N=512 DT= 0.1E-06 SEC DL= 25 m
 CE PERFECTLY CONDUCTING GROUND
 GW 1 22 0.0 0.0 550.0 0.0 0.0 0.0 0.3
 GW 2 60 0.0 0.0 2050.0 0.0 0.0 550.0 0.3
 GE 1
 GN 1
 LD 2 2 1 59 1.0 3.0E-06 0.0
 LD 4 2 60 4.0E+02
 FR 0 257 0.01953 0.01953
 EX 0 2 60 00 29.6E+03 0.0
 NE 0 1 1 1 50.0 0.0 20.0 0.0 0.0 0.0
 XQ
 EN

CM MAGNETIC FIELD AT 2 km DISTANCE IN CASE OF STROKE TO TALL STRUCTURE
 CM Lightning Channel With Resistance of 1 Ω /m and Inductance of 3 μ H/m
 CM N=512 DT= 0.1E-06 SEC DL= 25 m
 CE PERFECTLY CONDUCTING GROUND
 GW 1 22 0.0 0.0 550.0 0.0 0.0 0.0 0.3
 GW 2 60 0.0 0.0 2050.0 0.0 0.0 550.0 0.3
 GE 1
 GN 1
 LD 2 2 1 59 1.0 3.0E-06
 LD 4 2 60 4.0E+02
 FR 0 257 0.01953 0.01953
 EX 0 2 60 00 29.6E+03 0.0
 NH 0 1 1 1 2000.00 0.0 20.00 0.0 0.0 0.0
 XQ
 EN

CM TO REPRODUCE THE SLOW-FRONT CURRENT OBSERVED AT TOP OF 550 m CN TOWER
 CM Lightning Channel With Resistance of 1 Ω /m and Inductance of 3 μ H/m
 CM N=512 DT= 0.1E-06 SEC DL= 25 m
 CE GROUND CONDUCTIVITY 0.01 S/m
 GW 1 22 0.0 0.0 550.0 0.0 0.0 0.0 0.3
 GW 2 60 0.0 0.0 2050.0 0.0 0.0 550.0 0.3
 GE 1
 GN 0 0.01

Appendix E: Sample Input Data to NEC-2 for Stroke to Tall Tower

```
LD 2 2 1 59 1.0 3.0E-06 0.0
LD 4 2 60 4.0E+02
FR 0 257 0.01953 0.01953
EX 0 2 60 00 19.5E+03 0.0
PT 0 1 1
XQ
EN
```

CM TO REPRODUCE THE SLOW-FRONT E-FIELD OBSERVED AT 2 km FROM CN TOWER
 CM Lightning Channel With Resistance of 1 Ω/m and Inductance of 3 μH/m
 CM N=512 DT= 0.1E-06 SEC DL= 25 m

CE PERFECTLY CONDUCTING GROUND

```
GW 1 22 0.0 0.0 550.0 0.0 0.0 0.0 0.3
GW 2 60 0.0 0.0 2050.0 0.0 0.0 550.0 0.3
```

GE 1

GN 1

```
LD 2 2 1 59 1.0 3.0E-06
LD 4 2 60 4.0E+02
FR 0 257 0.01953 0.01953
EX 0 2 60 00 19.5E+03 0.0
NE 0 1 1 1 2000.0 0.0 20.0 0.0 0.0 0.0
XQ
EN
```

CM TO REPRODUCE STEEP-FRONT CURRENT OBSERVED AT TOP OF 550 m CN TOWER
 CM Lightning Channel With Resistance of 1 Ω/m and Inductance of 1 μH/m
 CM N=512 DT= 0.1E-06 SEC DL= 25 m

CE GROUND CONDUCTIVITY 0.01 S/m

```
GW 1 22 0.0 0.0 550.0 0.0 0.0 0.0 0.3
GW 2 60 0.0 0.0 2050.0 0.0 0.0 550.0 0.3
```

GE 1

GN 0

```
LD 2 2 1 59 1.0 1.0E-06 0.0
LD 4 2 60 4.0E+02
FR 0 257 0.01953 0.01953
EX 0 2 60 00 29.0E+03 0.0
PT 0 1 1
XQ
EN
```

CM TO REPRODUCE STEEP-FRONT H-FIELD OBSERVED AT 2 km FROM CN TOWER
 CM Lightning Channel With Resistance of 1 Ω/m and Inductance of 1 μH/m
 CM N=512 DT= 0.1E-06 SEC DL= 25 m

CE PERFECTLY CONDUCTING GROUND

```
GW 1 22 0.0 0.0 550.0 0.0 0.0 0.0 0.3
GW 2 60 0.0 0.0 2050.0 0.0 0.0 550.0 0.3
```

GE 1

GN 1

```
LD 2 2 1 59 1.0 1.0E-06
LD 4 2 60 4.0E+02
FR 0 257 0.01953 0.01953
EX 0 2 60 00 29.0E+03 0.0
NH 0 1 1 1 2000.00 0.0 20.00 0.0 0.0 0.0
XQ
EN
```

Appendix E: Sample Input Data to NEC-2 for Stroke to Tall Tower

CM TO REPRODUCE THE CURRENT OBSERVED AT TOP OF 200 m HIGH STACK IN JAPAN
 CM Lightning Channel With Resistance of 1 Ω /m and Inductance of 3 μ H/m
 CM N=512 DT= 0.1E-06 SEC DL= 25 m
 CE PERFECTLY CONDUCTING GROUND
 GW 1 8 0.0 0.0 200.0 0.0 0.0 0.0 0.3
 GW 2 60 0.0 0.0 1700.0 0.0 0.0 200.0 0.3
 GE 1
 GN 1
 LD 2 2 1 59 1.0 3.0E-06 0.0
 LD 4 2 60 4.0E+02
 LD 4 1 8 30.0
 FR 0 257 0.01953 0.01953
 EX 0 2 60 00 12.5E+03 0.0
 PT 0 1 1
 XQ
 EN

CM TO REPRODUCE THE E-FIELD OBSERVED AT 630 m FROM HIGH STACK IN JAPAN
 CM Lightning Channel With Resistance of 1 Ω /m and Inductance of 3 μ H/m
 CM N=512 DT= 0.1E-06 SEC DL= 25 m
 CE PERFECTLY CONDUCTING GROUND
 GW 1 8 0.0 0.0 200.0 0.0 0.0 0.0 0.3
 GW 2 60 0.0 0.0 1700.0 0.0 0.0 200.0 0.3
 GE 1
 GN 1
 LD 2 2 1 59 1.0 3.0E-06 0.0
 LD 4 2 60 4.0E+02
 LD 4 1 8 30.0
 FR 0 257 0.01953 0.01953
 EX 0 2 60 00 12.5E+03 0.0
 NE 0 1 1 1 630.0 0.0 50.0 0.0 0.0 0.0
 XQ
 EN

CM TO REPRODUCE THE H-FIELD OBSERVED AT 630 m FROM HIGH STACK IN JAPAN
 CM Lightning Channel With Resistance of 1 Ω /m and Inductance of 3 μ H/m
 CM N=512 DT= 0.1E-06 SEC DL= 25 m
 CE PERFECTLY CONDUCTING GROUND
 GW 1 8 0.0 0.0 200.0 0.0 0.0 0.0 0.3
 GW 2 60 0.0 0.0 1700.0 0.0 0.0 200.0 0.3
 GE 1
 GN 1
 LD 2 2 1 59 1.0 3.0E-06 0.0
 LD 4 2 60 4.0E+02
 LD 4 1 8 30.0
 FR 0 257 0.01953 0.01953
 EX 0 2 60 00 12.5E+03 0.0
 NH 0 1 1 1 630.00 0.0 50.00 0.0 0.0 0.0
 XQ
 EN

Appendix F

Sample Input Data to FDTD for Reduced Scale Model

Input Data For Stroke to Perfect Ground (Slow-front Current)

```
# SIMULATION PARAMETERS
#   DS      NX      NY      NZ      TMAX      NOUT      ALPHA
#   0.15    54     267    174    1.1E-7    4         1.0E-3
#
# BOUNDARY TYPE
#   TXMIN    TXMAX    TYMIN    TYMAX    TZMIN    TZMAX
#   LIAO2    LIAO2    LIAO2    LIAO2    LIAO2    LIAO2
#
# EARTH PARAMETERS
#   ZGND      RHOE
#   2.70      1.69E-8
#   If ZGND < 0, no earth is presented.
#   If ZGND >= NZ*DS, the analyzed area is filled with earth soil.
#
# WIRES
#   R      X      Y      Z      DIR      LEN
#   0.03   4.0    20.0   2.85   ZDIR     20.0
#
# RECT. OBJECTS
#   X      Y      Z      XLEN    YLEN    ZLEN
#
# VOLTAGE SOURCES
#   TYPE      X      Y      Z      DIR      R0
#   RAMP      4.0    20.0   2.70   ZDIR     10.0
#   0.0      20.0E-9  500    1.1E-7  500
#
# CURRENT SOURCES
#   TYPE      X      Y      Z      DIR      R0
#
# VOLTAGE PROBES
#   X      Y      Z      DIR
#   4.000  18.00  4.85   ZDIR
#   4.000  2.000  4.85   ZDIR
#
# CURRENT PROBES
#   X      Y      Z      DIR
#   4.000  20.00  2.85   ZDIR
#   4.000  20.00  10.85  ZDIR
#   4.000  20.00  18.85  ZDIR
#
# OUTPUT TYPE
#   OPLANE    PLPOS    OTYPE
#   YZ        1.000    HNRM
#
# OUTPUT FILE NAME
ch20pg1.m
#
# GRAPHIC CONTROLS
colorbar('horiz'); caxis([ 0.0 0.1 ]); shading interp; axis equal; pause;
#
# To use the following line instead of the above line creating jpg files
```

Appendix F: Sample Input Data to FDTD for Reduced Scale Model

```
# for animation, type "n = 0" at first in MATLAB.
caxis( [ 0.0 0.1 ] ); shading interp; axis equal; saveas( 1,
num2str(n, '%03d.jpg' ) ); n = n + 1; pause(0.1);
```

Input Data For Stroke to Finite Ground (Steep-front Current)

```
# SIMULATION PARAMETERS
#      DS      NX      NY      NZ      TMAX      NOUT      ALPHA
#      0.15     54     267     174     1.1E-7     4         1.0E-3
#
# BOUNDARY TYPE
#      TXMIN    TXMAX    TYMIN    TYMAX    TZMIN    TZMAX
#      LIAO2     LIAO2     LIAO2     LIAO2     LIAO2     LIAO2
#
# EARTH PARAMETERS
#      ZGND      RHOE
#      2.70      100.0
#      If ZGND < 0, no earth is presented.
#      If ZGND >= NZ*DS, the analyzed area is filled with earth soil.
#
# WIRES
#      R      X      Y      Z      DIR      LEN
#      0.03    4.0    20.0    2.85    ZDIR     20.0
#
# RECT. OBJECTS
#      X      Y      Z      XLEN    YLEN    ZLEN
#
# VOLTAGE SOURCES
#      TYPE      X      Y      Z      DIR      R0
#      RAMP     4.0    20.0    2.70    ZDIR     10.0
#      0.0     5.0E-9    500    1.1E-7    500
#
# CURRENT SOURCES
#      TYPE      X      Y      Z      DIR      R0
#
# VOLTAGE PROBES
#      X      Y      Z      DIR
#      4.000    18.00    4.85    ZDIR
#      4.000    2.000    4.85    ZDIR
#
# CURRENT PROBES
#      X      Y      Z      DIR
#      4.000    20.00    2.85    ZDIR
#      4.000    20.00    10.85    ZDIR
#      4.000    20.00    18.85    ZDIR
#
# OUTPUT TYPE
#      OPLANE    PLPOS    OTYPE
#      YZ        1.000    HNRM
#
# OUTPUT FILE NAME
ch20fg1.m
#
# GRAPHIC CONTROLS
colorbar('horiz'); caxis([ 0.0 0.1 ] ); shading interp; axis equal; pause;
#
# To use the following line instead of the above line creating jpg files
# for animation, type "n = 0" at first in MATLAB.
caxis( [ 0.0 0.1 ] ); shading interp; axis equal; saveas( 1,
num2str(n, '%03d.jpg' ) ); n = n + 1; pause(0.1);
```

Input Data For Lightning Stroke to Tall Object

```

# SIMULATION PARAMETERS
#   DS      NX      NY      NZ      TMAX      NOUT      ALPHA
#   0.15    54     267    200    1.1E-7    4         1.0E-3
#
# BOUNDARY TYPE
#   TXMIN    TXMAX    TYMIN    TYMAX    TZMIN    TZMAX
#   LIAO2    LIAO2    LIAO2    LIAO2    LIAO2    LIAO2
#
# EARTH PARAMETERS
#   ZGND      RHOE
#   2.70     1.69E-8
#   If ZGND < 0, no earth is presented.
#   If ZGND >= NZ*DS, the analyzed area is filled with earth soil.
#
# WIRES
#   R      X      Y      Z      DIR      LEN
#   0.03   4.0    20.0   2.70   ZDIR     6.0
#   0.03   4.0    20.0   8.85   ZDIR     20.0
#
# RECT. OBJECTS
#   X      Y      Z      XLEN    YLEN    ZLEN
#
# VOLTAGE SOURCES
#   TYPE      X      Y      Z      DIR      R0
#   RAMP     4.0    20.0   8.70   ZDIR     10.0
#   0.0     5.0E-9  500    1.1E-7  500
#
# CURRENT SOURCES
#   TYPE      X      Y      Z      DIR      R0
#
# VOLTAGE PROBES
#   X      Y      Z      DIR
#   4.000  18.00  4.85   ZDIR
#   4.000  2.000  4.85   ZDIR
#
# CURRENT PROBES
#   X      Y      Z      DIR
#   4.000  20.00  2.70   ZDIR
#   4.000  20.00  5.70   ZDIR
#   4.000  20.00  8.70   ZDIR
#
# OUTPUT TYPE
#   OPLANE    PLPOS    OTYPE
#   YZ        1.000    HNRM
#
# OUTPUT FILE NAME
t6mpg1.m
#
# GRAPHIC CONTROLS
#colorbar('horiz'); caxis([ 0.0 0.1 ] ); shading interp; axis equal; pause;
#
# To use the following line instead of the above line creating jpg files
# for animation, type "n = 0" at first in MATLAB.
caxis( [ 0.0 0.1 ] ); shading interp; axis equal; saveas( 1,
num2str(n, '%03d.jpg' ) ); n = n + 1; pause(0.1);

```


E-field at 35m For Lightning Stroke to Tall Object

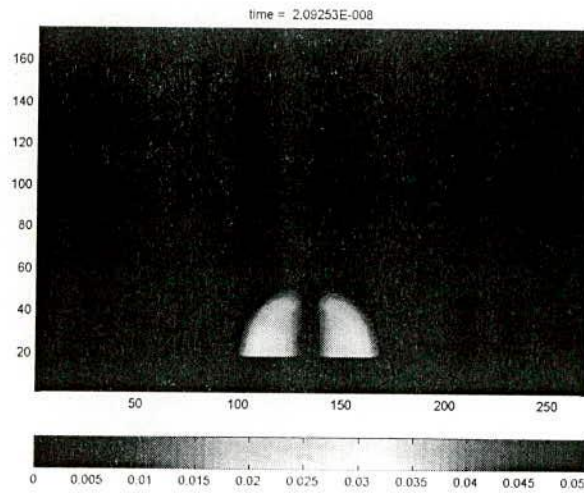
```

# SIMULATION PARAMETERS
#   DS      NX      NY      NZ      TMAX      NOUT      ALPHA
#   0.15    54     267    200    2.5E-7    4         1.0E-3
#
# BOUNDARY TYPE
#   TXMIN   TXMAX   TYMIN   TYMAX   TZMIN   TZMAX
#   LIAO2   LIAO2   LIAO2   LIAO2   LIAO2   LIAO2
#
# EARTH PARAMETERS
#   ZGND     RHOE
#   2.70     1.69E-8
#   If ZGND < 0, no earth is presented.
#   If ZGND >= NZ*DS, the analyzed area is filled with earth soil.
#
# WIRES
#   R      X      Y      Z      DIR      LEN
#   0.03   4.0    3.0    2.70   ZDIR     6.0
#   0.03   4.0    3.0    8.85   ZDIR     20.0
#
# RECT. OBJECTS
#   X      Y      Z      XLEN   YLEN   ZLEN
#
# VOLTAGE SOURCES
#   TYPE   X      Y      Z      DIR      R0
#   RAMP   4.0    3.0    8.70   ZDIR     10.0
#   0.0    20.0E-9  500    2.5E-7  500
#
# CURRENT SOURCES
#   TYPE   X      Y      Z      DIR      R0
#
# VOLTAGE PROBES
#   X      Y      Z      DIR
#   4.000  38.00  4.85   ZDIR
#   4.000  23.00  4.85   ZDIR
#   4.000  5.000  4.85   ZDIR
#
# CURRENT PROBES
#   X      Y      Z      DIR
#   4.000  20.00  2.70   ZDIR
#   4.000  20.00  5.70   ZDIR
#   4.000  20.00  8.70   ZDIR
#
# OUTPUT TYPE
#   OPLANE  PLPOS  OTYPE
#   YZ      1.000  HNRM
#
# OUTPUT FILE NAME
t6mpg2.m'
#
# GRAPHIC CONTROLS
#colorbar('horiz'); caxis([ 0.0 0.1 ] ); shading interp; axis equal; pause;
#
# To use the following line instead of the above line creating jpg files
# for animation, type "n = 0" at first in MATLAB.
caxis( [ 0.0 0.1 ] ); shading interp; axis equal; saveas( 1,
num2str(n, '%03d.jpg' ) ); n = n + 1; pause(0.1);

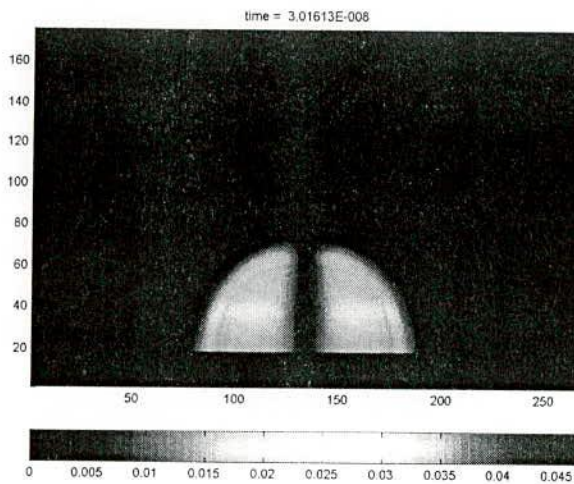
```

Appendix G

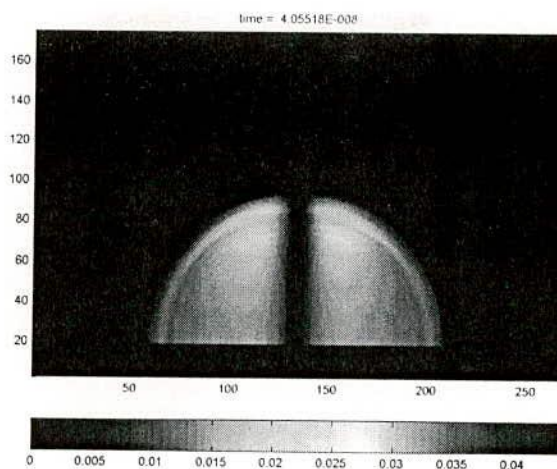
Magnetic Field Distributions



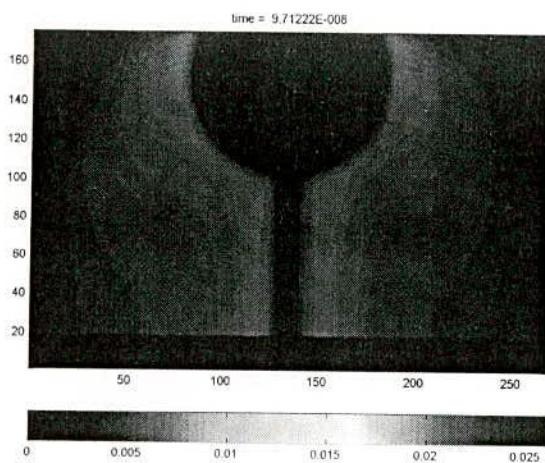
(a) $t = 20$ ns



(b) $t = 30$ ns

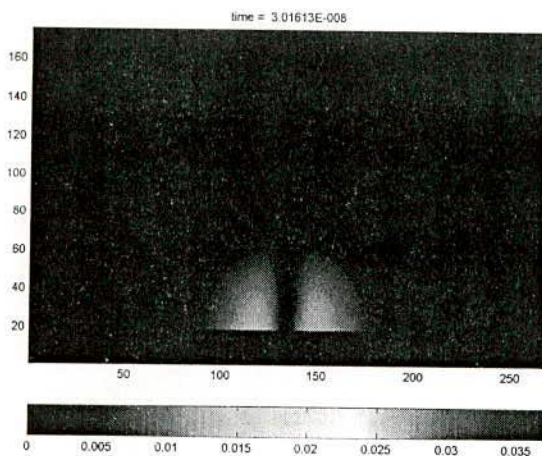


(c) $t = 40$ ns

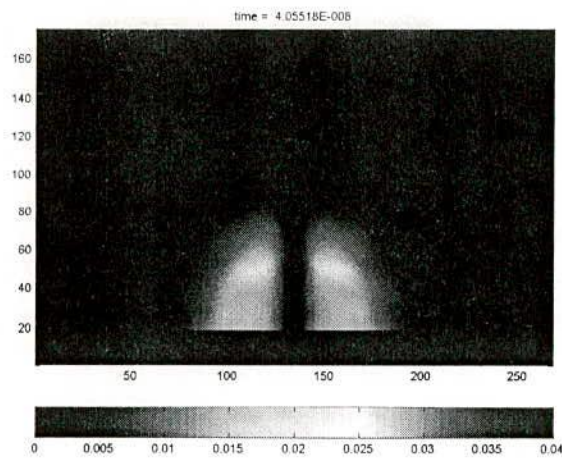


(d) $t = 97$ ns

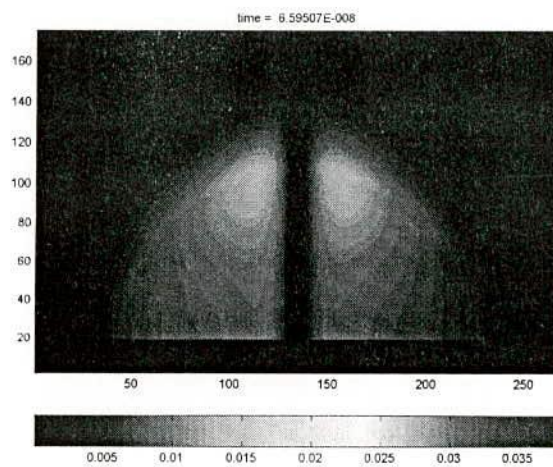
Fig. H.1. Magnetic field strength at different times for lightning strike to perfect ground (steep-front current); unit of vertical and horizontal axes is in cells ($\Delta s = 15$ cm).



(a) $t = 30$ ns

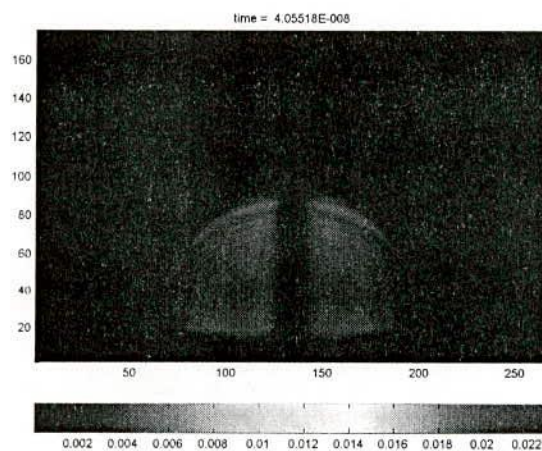


(b) $t = 40 \text{ ns}$

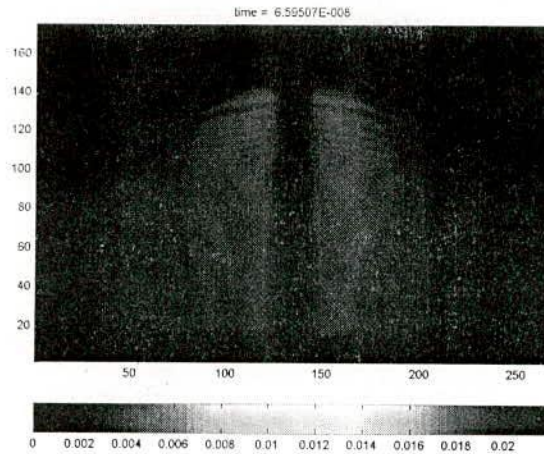


(c) $t = 66 \text{ ns}$

Fig. H.2. Magnetic field strength at different times for lightning strike to perfect ground (slow-front current); unit of vertical and horizontal axes is in cells ($\Delta s = 15 \text{ cm}$).

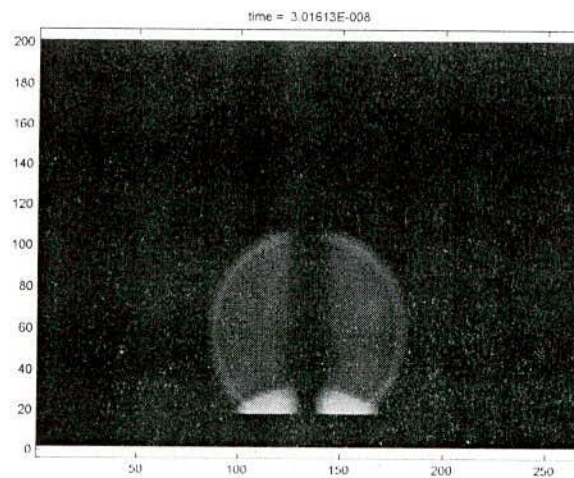


(a) $t = 40 \text{ ns}$

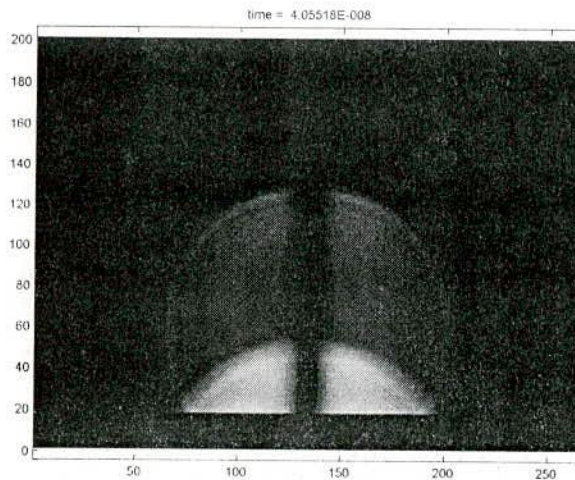


(b) $t = 66 \text{ ns}$

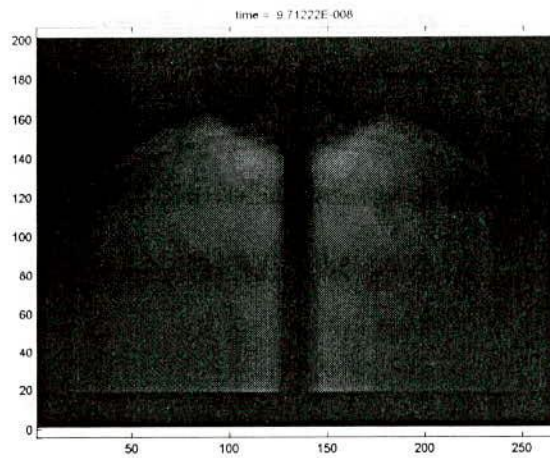
Fig. H.3. Magnetic field strength at different times for lightning strike to finite (0.01 S/m) ground (steep-front injection); unit of vertical and horizontal axes is in cells ($\Delta s = 15 \text{ cm}$).



(a) $t = 30 \text{ ns}$

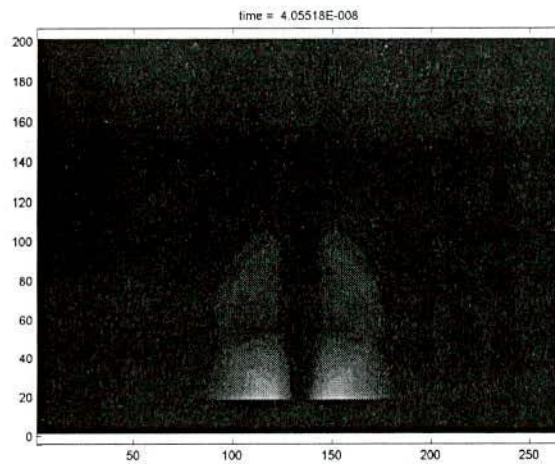


(b) $t = 40 \text{ ns}$

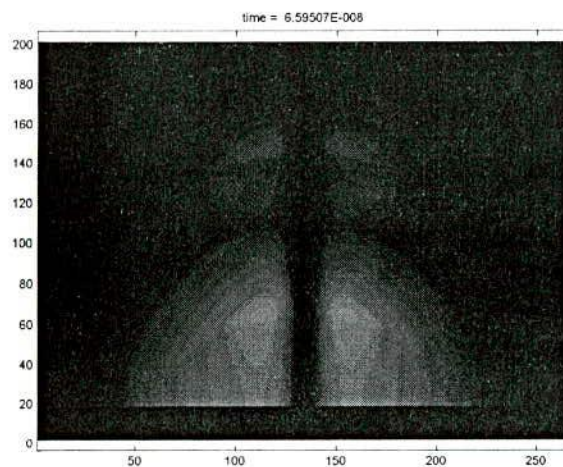


(c) $t = 97 \text{ ns}$

Fig. H.4. Magnetic field strength at different times for lightning strike to tall object (steep-front injection); unit of vertical and horizontal axes is in cells ($\Delta s = 15 \text{ cm}$).



(a) $t = 40 \text{ ns}$



(b) $t = 66 \text{ ns}$

Fig. H.5. Magnetic field strength at different times for lightning strike to tall object (slow-front injection); unit of vertical and horizontal axes is in cells ($\Delta s = 15 \text{ cm}$).

Publications

1. Md. Osman Goni, **Md. Faruque Hossain**, Md. Salah Uddin Yusuf, Md. Mostafizur Rahaman, E. Kaneko, and H. Takahashi, "Simulation and Experimental Analysis of Transient Behavior of Lightning Surge on Vertical Conductors," *IEEE Transaction, Power Delivery*, accepted for publication.
2. **Md. Faruque Hossain**, Md. Salah Uddin Yusuf, Md. Osman Goni, and Md. A. K. Azad, "Numerical Analysis of Current and Electromagnetic Field Associated with Lightning Strokes to a Tall Tower," *Journal of Institution of Engineer of Bangladesh (IEB)*, Vol. EE32, No. I-II, Paper no. IEB/EE/05/16, accepted for publication.
3. **Md. Faruque Hossain**, Md. Salah Uddin Yusuf, Md. Osman Goni, and M. M. Rahman, "Numerical Electromagnetic Field Analysis of Lightning Return Strokes to Tall Towers," *Journal of Institution of Engineer of Bangladesh (IEB)*, Vol. EE32, No. I-II, Paper no. IEB/EE/05/19, accepted for publication.
4. Md. Salah Uddin Yusuf, **Md. Faruque Hossain**, and Md. Osman Goni, "Electromagnetic Simulation of a Lightning Surge on a Vertical conductor Model," *Journal of Institution of Engineer of Bangladesh (IEB)*, accepted for publication.
5. Md. Salah Uddin Yusuf, **Md. Faruque Hossain**, and Md. Osman Goni, "Electromagnetic Simulation of a Lightning Surge on a Vertical Conductor Model," in *Proc. of the 3rd International Conference on Electrical & Computer Engineering, ICECE 2004*, pp.163-166, 28-30 December 2004, Dhaka, Bangladesh.